



**national accelerator laboratory**

FN-264  
8000.000

**CRYOGENIC ENERGY STORAGE SYSTEM DESIGN REPORT**

**Fermi National Accelerator Laboratory**

**In Collaboration With**

**The University of Wisconsin**

**October 1974**



FERMI NATIONAL ACCELERATOR LABORATORY  
PULSED ENERGY STORAGE SYSTEM DESIGN

Feasibility Study Group

Mills, F. E., Chairman	Reardon, P. J.
Biallis, G.	Snowden, S. C.
Cassel, R. L.	Strauss, B. P.
Fowler, W. B.	Teng, L. C.
Livdahl, P. V.	Winje, R. A.
Palmer, M. L.	

University of Wisconsin

Ballou, J. K.	McIntosh, G. E.
Boom, R. W.	Mohan, N.
Dreifuerst, G. R.	Moses, R. W.
Hartmann, D. P.	Peterson, H. A.
Hartwig, K. T.	Richard, T. G.
Hilal, M. A.	Sviatoslavsky, I.
Ibrahim, E. A.	Winkelman, J. R.
Kuchnir, M.	Yadavalli, S. R.
	Young, W. C.

## PREFACE

The study of pulsed superconductive energy storage was initiated in collaboration with the University of Wisconsin in August, 1973. Since then about 3 man years aggregate effort by Fermi National Accelerator Laboratory staff has been provided on this study. During the same period \$84,000 was expended on the joint effort at the University of Wisconsin, with 73% funding by the University.

This joint effort and joint funding is in recognition of the mutual interest in pulsed superconductive energy storage. A substantial amount of information used in this pulsed storage study was adapted from a parallel superconductive energy storage project for electric utility systems at the University of Wisconsin.

## TABLE OF CONTENTS

	<u>Page No.</u>
Author Page	ii
Preface	iii
Table of Contents	iv
Table of Figures	vi
List of Tables	ix
Summary	x
Overview	xi
Chapter I. Introduction	I-1
II. D. C. Magnet Design	II-1
A. Constraints	II-1
B. Analytic Model	II-1
C. Numeric Model and Comparison	II-4
D. External Fields	II-5
E. Virial Theorem and Present Design	II-6
F. Conclusions	II-7
G. References	II-8
III. Superconductor Shielding	III-1
A. Shield Current Distribution	III-1
B. Shield Hoop Coupling	III-2
C. Resistive Heating in the Shield and Hoop	III-4
1. Theory	III-4
2. Examples	III-5
D. Compensation of Shield Resistance	III-7
1. Reduction of Hoop Losses	III-8
2. Room Temperature Shields	III-9
E. References	III-10

	Page No.
III-A. Conductor Location in the Shield	III-A-1
III-B. Shield Resistance	III-B-1
III-C. Scaling Laws	III-C-1
IV. Cryogenics	IV-1
A. Shield Cryogenic Design	IV-1
1. Choice of Operating Temperature	IV-1
2. Refrigeration Power Required	IV-3
3. Heat Transfer Calculations and Cooling Scheme	IV-4
4. Pressure Drop Calculations	IV-7
B. Superconductive Magnet, Cryogenic Design	IV-8
1. Composite Conductor Design	IV-8
2. Heat Load Calculations	IV-12
3. Helium Requirement and Flow	IV-14
IV-A. A. C. Losses in the Normal Metal	IV-A-1
IV-B. A. C. Twist Losses	IV-B-1
IV-C. Hysteresis Losses	IV-C-1
IV-D. Helium Vapor Flow in the Superconducting Magnet	IV-D-1
V. Real and Reactive Power Compensation	V-1
V-A. Reactive Power Control	V-A-1
VI. System Design	VI-1
A. D. C. Magnet Design	VI-1
B. Shield Design	VI-7
VI-A. Power System Specification	VI-A-1
VII. Conclusions	VII-1

TABLE OF FIGURES

	Page No.
1. N. A. L. 500 BEV pulsed power compensation.	xiii
I-1. Superconducting magnet stored energy system.	I-7
I-2. Power supply-inductor configuration.	I-8
II-1. Analytic model.	II-10
II-2. Distribution of radial force in the layer of conductor nearest the midplane of the hoop.	II-11
III-1. Converter-inductor system.	III-11
III-2. Isometric view of N.A.L.-U.W. pulsed energy storage.	III-12
III-3. Inductor-cross section.	III-13
III-4. Converter-inductor system with resistance compensation.	III-14
III-A-1. Initial shield model with uniformly separated conductors having variable currents.	III-A-4
III-A-2. Lines of constant magnetic flux produced by a current in the shield.	III-A-5
III-A-3. Shield conductors with equal currents and variable separations.	III-A-6
IV-1. Carnot cycle for helium in shield.	IV-16
IV-2. Coefficient of performance including pressure drop losses.	IV-17
IV-3. Helium and conductor temperature in shield.	IV-18
IV-4. Composite conductor cross-section.	IV-19
IV-5. Stability curve for Purcell type conduction with 10:1 height to width ratio and copper stabilizer at 4.2 K.	IV-20
V-1. Equivalent representation of the superconductive inductor and the N.A.L. pulsed load connected to the source.	V-4
V-2. N.A.L. proposed four converter series arrangement with bypass thyristors.	V-5

	Page No.
V-A-1. N.A.L. proposed four converter series arrangement with bypass thyristors.	V-A-4
V-A-2. Reactive power control by converter bridge with the bypass thyristor on.	V-A-5
V-A-3. Operating characteristics of four series converter units and pulsed load line.	V-A-6
V-A-4. N.A.L. pulsed real power and the converter-inductor power requirement at 400 GeV.	V-A-7
V-A-5. Reactive power drawn by N.A.L. pulsed load and converter inductor.	V-A-8
V-A-6. Real and reactive power requirements on converter 1 at 400 GeV.	V-A-9
V-A-7. Real and reactive power requirements on converter 2 at 400 GeV.	V-A-10
V-A-8. Real and reactive power requirements on converter 3 at 400 GeV.	V-A-11
V-A-9. Real and reactive power requirements on converter 4 at 400 GeV.	V-A-12
VI-1. Conductor details.	VI-14
VI-2. Overall cross-section. N.A.L.-U.W. pulsed energy storage.	VI-15
VI-3. Possible winding scheme-top view.	VI-16
VI-4. Cross-over electrical connection between layers.	VI-17
VI-5. Magnetic field strength and stresses as functions of radial distance along median plane.	VI-18
VI-6. Isometric view of N.A.L.-U.W. pulsed energy storage.	VI-19
VI-7. Banding detail.	VI-20
VI-8. Inner dewar section.	VI-21
VI-9. Shield support reinforcing ring.	VI-22
VI-10. 40 K helium gas routing scheme.	VI-23

	Page No.
VI-A-1. Pulsed energy storage system electrical network.	VI-A-7
VI-A-2. 12.5 MW converter.	VI-A-8

LIST OF TABLES

	<u>Page No.</u>
II-1. Comparison of several 1MWh storage hoops.	II-9
III-1. Fourier coefficients for complete load leveling of the N.A.L. accelerator demand at 400 GeV.	III-7
IV-1. Refrigeration power as a function of shield temperature.	IV-2
IV-2. Coefficient of performance as a function of shield inlet temperature.	IV-4
IV-D-1. Helium vapor flow in the superconducting magnet.	IV-D-3
V-1. Comparison of converter operation under the two operating philosophies for reactive power control.	V-2
VI-A-1. 12.5 MW power supply operating parameters.	VI-A-5
VI-A-2. P.E.S. operating parameters.	VI-A-6

## Summary

A superconductive energy storage magnet which is connected to the three phase power system could be designed, constructed, and placed in operation at Fermilab which would essentially eliminate the large repetitive power pulses now required from the power system. In addition to the power pulses, voltage flicker is also caused due to the reactive power pulsation.

Specifically, a one megawatt hour superconductive energy storage magnet and a 200 megawatt thyristorized converter can achieve nullification of these power pulses up to 400 GEV synchrotron operation. Above 400 GEV, operation should be possible up to 500 GEV with appreciable less power pulsing requirements from the system than are now considered permissible. Carried to successful completion, this project would serve to advance applied superconductivity to a highly significant degree. The effect would be of world wide importance to both high energy physics and to the electric power industry.

The preliminary magnet design is a 1 MWh dipole composed of cryogenically stable composite conductors connected in parallel with aluminum shield windings. The shield windings carry impressed pulsed currents while eliminating pulsed currents from the dc superconductive windings. Without pulsed currents or pulsed magnetic fields there are no ac losses in standard helium. The major radius of the dipole is 8.85 m; the minor radius is 0.69m; there are 188 turns at 80,000 A and each turn is 4 conductors wound in parallel. The 20,000 A TiNb-copper composite conductor is 10x 1.12 cm in cross section similar to but larger than the NAL bubble chamber conductor.

The shield is 188 turns (equal number of turns is a shielding condition) of hollow aluminum conductor cooled via circulated cold helium gas at 40K. The turns are spaced around the minor circumference according to a cosine distribution which produces zero internal field.

In use the shield loss converted to room temperature power is about .8 MW when .1 MWh is used from a 1 MWh storage dipole. The 0.1 MWh is sufficient to provide complete load leveling for 400 GEV pulses, and operation at 500 GEV with lower power transients than are presently experienced.

## OVERVIEW

The synchrotron pulsed power requirements at NAL are repetitive at a frequency of about 0.1 Hz and of such magnitude (several hundred megawatts) as to be a source of grave concern, even though the power company (Commonwealth Edison) is one of the largest in the United States. The average power requirements are no problem. It is the pulsed power requirement, especially looking to the likelihood of operating at up to 500 GEV, that is the cause of concern (see Figure 1).

What is needed at NAL to offset the pulsed power load requirements is some means for storing energy during the portion of time when load is less than average and alternately releasing energy when load is above average. Full compensation would completely mask the pulsed power nature of the load so that viewed from the power system, only the steady average power would be supplied.

There are many instances one can think of wherein a stored energy device would be helpful. One of the most important involves the electric power industry. Load on our power systems is not constant but fluctuates markedly from hour to hour. In the course of a typical day, the peak load during the day may be on the order of twice the minimum night time load. Since generators must be installed at present day costs of about \$500 per kW to meet the peak load anticipated, it is clear that some means of alternately storing and releasing energy and thus serving as a load leveling device is a very important need. It is the major reason for the relatively sudden acceleration of research funding in areas of energy storage, such as storage batteries, fuel cells, compressed air and even flywheels. Pumped storage hydro is the only means currently employed by the electric power industry to achieve a small degree of load leveling. Pumped storage sites are limited in number and capacity so that this approach has very limited potential. Incentive for development of other means of accomplishing load leveling is therefore very high.

The NAL requirement differs from the general electric power industry requirement in that the cycle of energy storage and retrieval is about 10 seconds (0.1 Hz) instead of 24 hours. The energy storage requirement is much less because of the shorter cycling period. A superconductive magnet rated at one megawatt hour would be adequate at NAL. To be economically

competitive, units of much larger size up to 10,000 MWh would be most desirable for general electric power system load leveling use. Power rating requirements are large in either case. A 200 MW thyristorized Graetz bridge converter is contemplated for the NAL project. Such converters are readily available and used increasingly by the electric power industry in numerous installations around the world.

The NAL project therefore should serve not only to satisfy a specific need, important as that need may be. It will also serve to advance energy storage and applied superconductivity technology very significantly. The broader objective of load leveling in bulk transmission of electric power systems is of tremendous importance as we evaluate all options likely to be available on the energy scene now and looking to the future.

N. A. L. 500 PEV PULSED POWER COMPENSATION

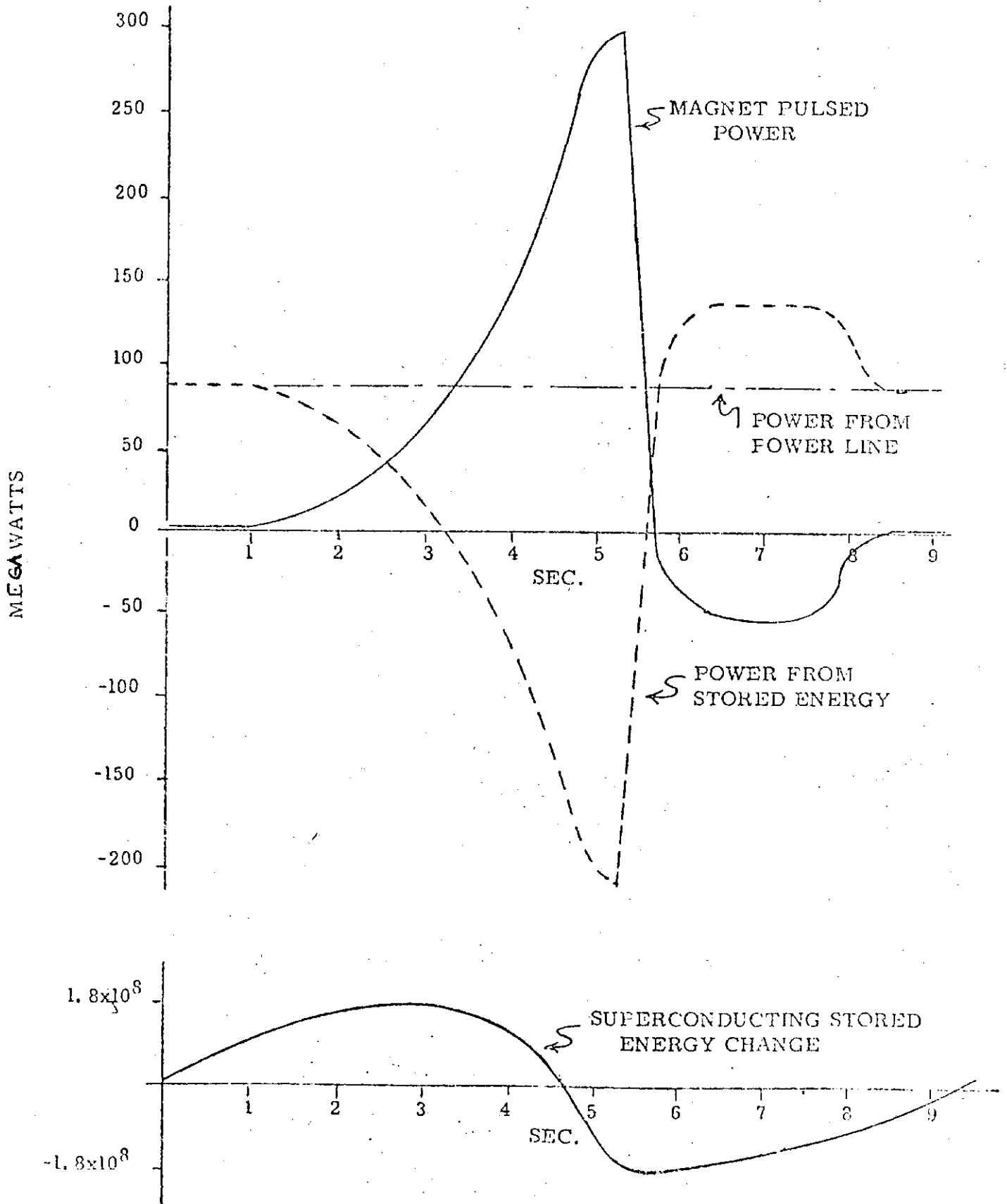


FIG. 1

## I. - INTRODUCTION

The NAL Main Accelerator was designed to operate at energies of at least 200 Gev, with the capability of modification to achieve higher energies of 400-500 Gev. Economics achieved during construction allowed the installation of a power supply with rectifier capability for 500 Gev operation. This supply is connected directly to the 345 kV utility line, without energy storage to smooth the load.

At the present time the accelerator operates routinely at 300 Gev, and has operated for extended test periods at 400 Gev. The continuous development of the power supply and the energy capability of the accelerator is being undertaken in close collaboration with the Utility Company. From the point of view of on site installations, the present limitation to the system is the voltage flicker caused by the large reactive power attendant during charge of the main ring. In order to overcome this, a series capacitor has been installed to compensate the leakage reactance of the system. Preliminary tests of this capacitor compensation have been made in which good reactive power compensation was achieved without serious problems from ferroresonance.

The effects of real power savings on the utility network have not yet been assessed. Encouraging as the results are with reactive power compensation, they do not yet provide a firm foundation upon which a 500 Gev program of accelerator operation can be based. Realizing that this might be the case, a study of on-site superconducting magnetic energy storage for complete compensation was undertaken. This report describes the preliminary results of that study.

Very early in the study it was realized that the program bore a close relationship to other activities planning to utilize superconducting magnets or planning to employ large pulsed power systems. These programs include studies

of energy storage for diurnal load smoothing in power systems and power systems for fusion reactors. As matters developed, the relationship between this activity and existing technology became clear. As a result of this, communication and collaboration with groups working in these areas were established. In particular, a close collaboration was established with the University of Wisconsin Engineering College, where there are experienced groups studying fusion system technology and superconducting magnetic energy storage systems.

Starting in September 1973 the collaborative effort was formed. The first problem was the eddy current and ac loss problem in superconducting magnets. If cryogenically stable magnets were to be used for load leveling during 5-10 sec pulses then these AC losses would be excessive during a  $\pm$  0.1 MWh pulse into the magnet system. The first alternative is to suffer the cryogenic loss in the magnet, the second alternative is to use unstable conductors without copper to reduce the AC losses and the third alternative was to devise a circuit method to circumvent the problem. The third alternative was chosen; a shield winding carries all the AC current and shields the DC superconducting magnet from AC magnetic fields. Losses are reduced and standard cryogenically stable DC superconducting magnets can be used.

The system was described briefly in a previous paper, "The NAL Energy Storage Inductor" by F. Mills and R. Cassel - March 5, 1974 at the CTR Power Supply Conference, AEC - Washington, as follows:

"In order to assure stable operation of such a system, one must solve the problem of AC losses at low temperature. What we have chosen to do is to use conventional, cryogenically stable superconductors to store the energy, and then, with a normal metal flux-forcing secondary winding, to protect the superconducting material and stabilizer from any appreciable internal

magnetic field change during operation. The secondary, or "shield" winding can be operated at higher temperature to reduce the refrigerator load."

Then the only essential difference between the superconducting magnet and a bubble chamber magnet, aside from its field shape, is that the coils must be insulated to accommodate the voltage which is necessary to transmit energy from that part of the magnetic field which is exterior to the shield winding.

A coil configuration which nearly optimizes stored energy with respect to superconductor volume at a given maximum magnetic field strength is a simple hoop of constant current density as shown in figure I-1. For our case, we are working with the following parameters:

$B_{\max}$	= 5T	Maximum Field
W	= 1 MWh	Stored Energy
J	= 1000 A/cm <sup>2</sup>	Average Current Density
N	= 188 turns	
I	= 80 kA	
V	= 2.5 kv	
R	= 8.8m	Major Radius of Coil
r	= .69m	Minor Radius of Coil

The 80 kA will be supplied by four parallel 20 kA conductors similar to that shown in figure VI-1.

The twisted filaments of superconductor are contained in a copper matrix soldered into a channel in the copper stabilizer. The composite conductor is insulated from the stainless steel support band, and supported on micarta spacers.

In this geometry, the axial stress problem is minimal, and structural banding material compacts the turns so that hoop and axial stress are shared. Then the details of construction of the coil differ only slightly from those employed in bubble chamber magnets.

The shield winding, indicated in figure I-1, is wound so as to produce zero field in its interior by proper distribution of its turns. The number of shield turns is equal to the number of turns in the superconducting coil. If the shield winding is connected in parallel to the main winding, then for times short compared to the L/R time of this combination, the only flux change which can occur is that which links both windings, that is, the flux exterior to the shield, and neither field nor current in the superconductor changes. Then the pulse or AC losses are in the shield, which can be of normal metal.

The temperature of the shield has not been optimized, but 20K is the location of the "knee" in the Al resistivity vs. temperature curve. The refrigerator (inverse) efficiencies are typically 50 W/W at this temperature instead of 300-500 W/W typical at 4.2K. By using a good grade of (not zone refined) Al, one can obtain an Al 20K resistivity less than  $5 \times 10^{-8} \Omega \text{ cm}$ , in which case the 20K loss is of order 10kW. Further, the 20K shield reduces the radiation losses to the 4.2K dewar, so that its losses are primarily due to current carrying leads and supports.

For pulse lengths comparable to the L/R time, (here  $\sim 50$  sec) the IR drop in the shield (which drives flux into the inner winding) can be compensated by a power supply in series with the shield, as indicated in figure I-2, so as to ensure no penetration of flux into the inner winding.

The principal problem with the rectifier-inverter, in light of the experience with the main ring power supply, is the control of reactive power in the system. In the main ring system, this is handled by placing all supplies in series with the magnet bus at separate locations in the ring. This is necessary in any case to have acceptable voltages to ground. Then each local power supply is operated in full rectify or full invert or is bypassed with a separate thyristor.

There is no continuous control of thyristor firing angle. The multiplicity of supplies assures sufficient smoothness of operation. A series capacitor is being installed to correct the power factor.

The alternative to bypass rectifiers is to control the flow of power by control of rectifier phase. This has the undesirable feature of requiring the full inductor current to flow into the line when no power is being exchanged, i.e., the maximum reactive power is as large as the maximum real power required.

The solution being pursued is as follows:

Since we need four series rectifiers to handle the peak inverse voltage (2500 volt operation), we will operate only those rectifiers needed to get the required voltage, the others being bypassed. Further, only one rectifier which is on will operate with variable phase, the others which operate, will be in full rectify (or full invert). As a result, the maximum reactive power is only slightly larger than that accompanying full rectify or full invert mode of operation of the whole system.

Since we need many parallel rectifiers to handle the total current, we can operate them in parallel banks at different phases, by the use of zig-zag Y connections or extended delta connections, so that we can achieve the ripple associated with twelve pulse bridge operation. Again, the reactive power can be balanced with a series capacitor as in the main ring system.

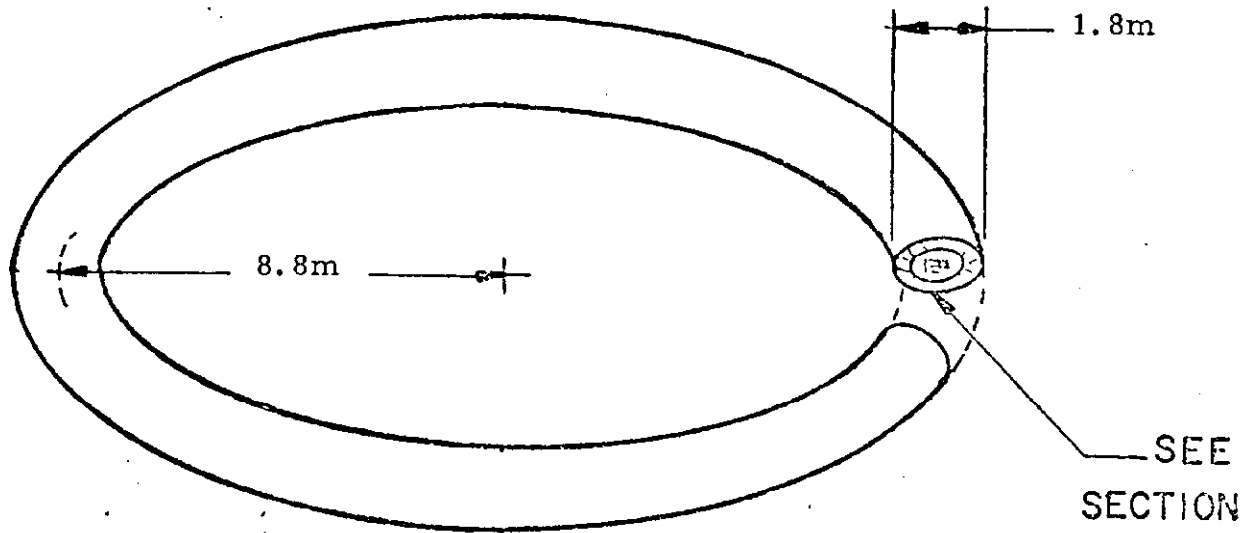
The system described here can be scaled up in total stored energy and pulsed power to meet some of the applications described in this meeting, and seems well suited to a variety of needs in the long range CTR program. The advantage of building it at NAL is manifold. First, there is a need for such a device to implement the research program of the Laboratory. Thus, the device would be operated over an

extended period of time as part of a major power system. Second, the NAL main ring is a flexible variable load which can be used to test the operation under a variety of operating conditions. Third, the Laboratory has made a commitment to develop superconductivity for a variety of applications. Fourth, the power supply technology necessary for the implementation of this device is already available at the Laboratory." (End of quote).

While more advanced design concepts have been undertaken since this March 1974 paper the general description above still applies. The remainder of this report will discuss in detail the present status of the 1 MWh storage unit for the accelerator.

SUPERCONDUCTING MAGNET  
STORED ENERGY SYSTEM

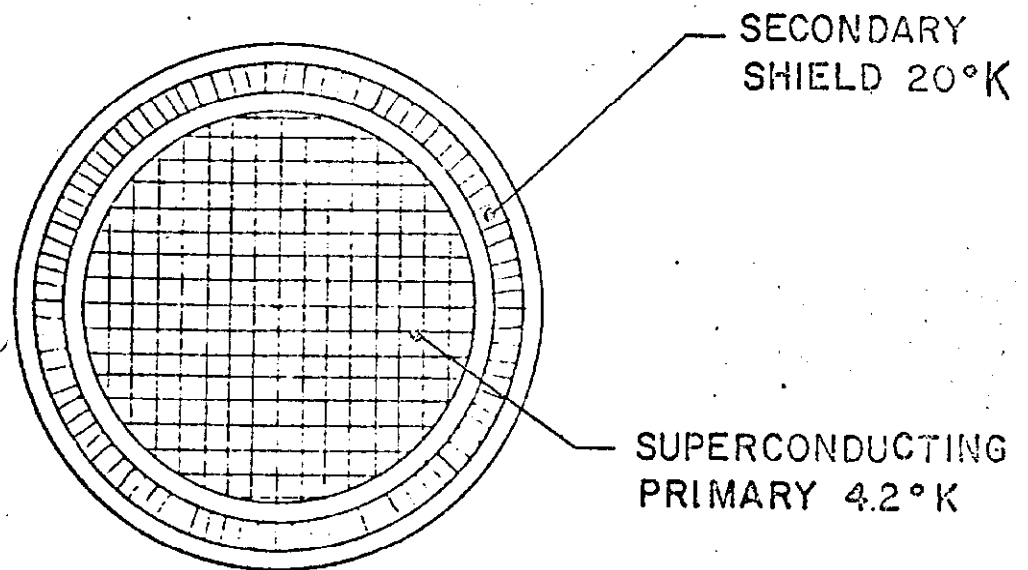
I-7



1 MWh

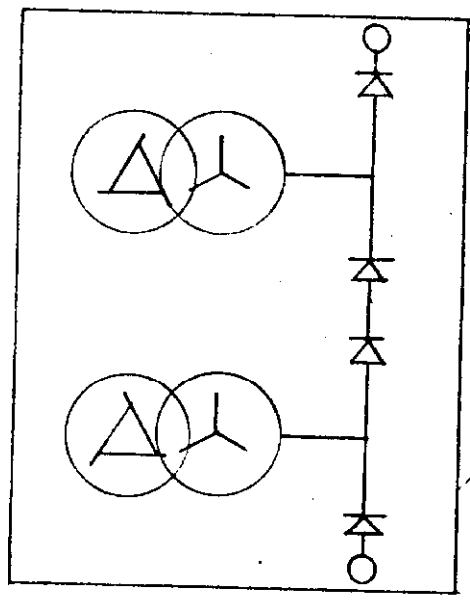
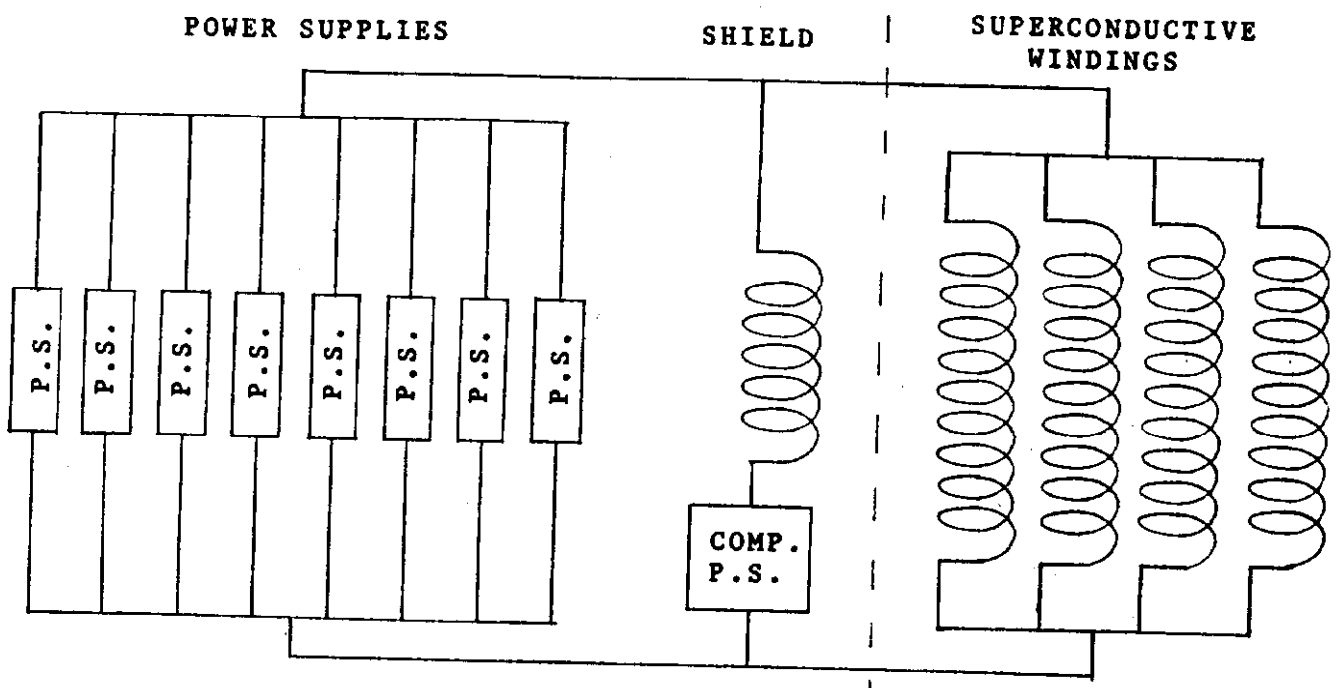
$1.50 \times 10^7$  A TURNS

188 TURNS

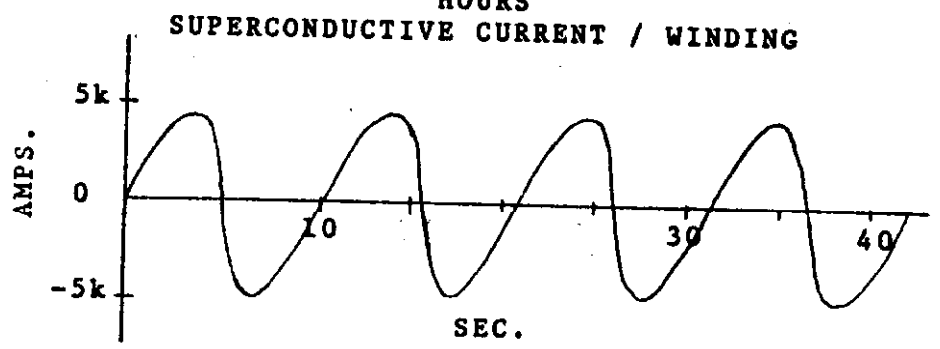
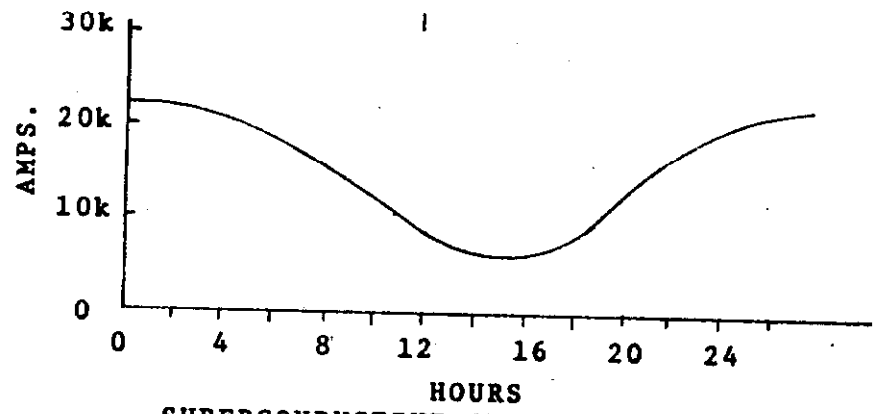


SECTION A

Figure I-1



**TYPICAL POWER SUPPLY**  
 12 PHASE FULL WAVE  
 MAX. VOLTAGE 2500 VOLTS  
 MAX. POWER 25 MEGAWATTS  
 RMS POWER 15 MEGAWATTS



**SHIELD WINDING CURRENT**  
 TOTAL CURRENT 80,000 AMPS.  
 PEAK POWER 200 MEGAWATTS

Figure I-2

## II. - D. C. MAGNET DESIGN

In this chapter the magnetic design for the hoop will be considered; the conditions and constraints imposed on the hoop by such design specifications as the choice of conductor will be discussed. It is important to mention here that this design has not been optimized. It is just a good example of several possible choices.

### A. CONSTRAINTS

Before the dimensions and properties of a superconducting hoop that will store 1 MWh can be determined three other decisions must be made:

- 1) ~~The~~ type of superconductor. This will determine the range of fields in the coils that will allow efficient use of the superconductor.
- 2) The degree of stabilization. In this case complete cryogenic stability has been chosen.
- 3) The current in each composite conductor; the composite conductor is the superconductor and stabilizing material. For this design four 20,000 A conductors will be wound in parallel to make an 80,000 A conductor.

Once these decisions have been made they in turn impose other conditions on the design. The design must not only meet the energy storage requirement but must also have an overall current density compatible with the number of turns required, with the volume of conductor, the stress levels must be compatible with the conductor, and the fields in the coils should not exceed a certain value.

### B. ANALYTIC MODEL

In order to get an estimate of the dimension of this magnet a relatively simple, but adequate, model of the hoop has been used. Since one of the basic quantities of interest is the magnetic field, and since the fields for finite size

hoops are hard to handle analytically, the hoop has been approximated by an infinitely long circular bundle of wires with a uniform current density  $J_0$  in a uniform background field. The basic equation for the field at the surface is given by

$$B = B_0 - B_1 \cos \theta \quad (2-1)$$

where  $B_0$ ,  $B_1$ , and  $\theta$  are illustrated in Figure II-1. The maximum field is at  $\theta = 180^\circ$ .

$$B_M = B_0 + B_1 \quad (2-2)$$

A useful expression can be derived by equating the radial force on the hoop due to  $B_1$  and the radial force derived from  $W$ ,

$$F_r = - \frac{\partial W}{\partial a} = - \frac{\partial}{\partial a} \left( \frac{1}{2} L_C I_C^2 \right) = \frac{1}{2} I_C^2 \frac{\partial L_C}{\partial a} \quad (2-3)$$

where the inductance as given by Smythe (1950) is

$$L_C \approx \mu_0 a \left( \ln \frac{8a}{r_C} - 1.75 \right) \quad (2-4)$$

On combining the preceding equations we get

$$\frac{B_M}{B_0} = 1 + \frac{1}{2} \beta_C \left( \ln \frac{8}{\beta_C} - 0.75 \right) \quad (2-5)$$

and

$$a = \left( \frac{W}{\frac{2\pi^2}{\mu_0} \left( \ln \left( \frac{8}{\beta_C} \right) - 1.75 \right) \beta_C^2 \left( \frac{B_0}{B_M} \right)^2 B_M^2} \right)^{1/3} \quad (2-6)$$

Here  $a$  and  $r_c$  are the major and minor radii respectively.  $W$  is the average stored energy and  $\beta = r_c/a$  is the aspect ratio.

Equation (2-6) may now be used to obtain several estimates for the hoop dimensions; some of which are presented in Table II-1. They were obtained by setting  $W = 1$  MWh,  $B_M = 5$  tesla, and varying the aspect ratio. Notice that as  $\beta$  increases,  $a$  decreases and  $I_c$  increases, but the average current density in the hoop decreases. This current density must be preserved in order to insure that the maximum field criteria has been met. Since  $J_c$  for each design is smaller than that proposed for the composite conductor,  $1150 \text{ A/cm}^2$ , each of these is suitable from the standpoint of providing space for stabilizing material. The larger  $\beta$  designs with smaller overall current densities require additional material to separate and support the conductor. It is simplest to choose a design with a  $\beta$  just large enough to accommodate the conductor, layer-to-layer spacers, electrical insulation and liquid helium and still have some space left over for miscellaneous uses. This is a major reason for choosing  $\beta = .078$ .

The mechanical stress in the hoop due to the magnetic fields can also be calculated. The hoop tension,  $T$ , produced by net radial expansion force, is

$$T = \frac{1}{4\pi} \frac{\partial L_c}{\partial a} I_c^2 \quad (2-7)$$

and the resulting hoop stress, is

$$\sigma = \frac{T}{\pi r_c^2} \quad (2-8)$$

A comparison of the hoop tension and stresses in Table II-I shows that as  $\beta$  increases the hoop tension increases but the hoop stress decreases. An average hoop stress of 8500 psi

for the  $\beta = .078$  design is well within the acceptable limits for the conductor. In addition to the hoop tension there is also a net compression on the hoop, tending to decrease  $r_c$ . For a long straight bundle of hoops the accumulated mechanical pressure on the axis is just twice the magnetic pressure at the outer surface. For this hoop design the accumulated pressure should be about 2260 psi; this stress is well within the safe limits of the conductor.

### C. NUMERIC MODEL AND COMPARISON

The approximations in Equations (2-1) and (2-4) were chosen so that the calculations could be made easily. This model is expected to be accurate for small  $\beta$  and decrease in accuracy as  $\beta$  increases. It is advisable to try another model and compare the results. The one proposed, the numeric model, consists of replacing each turn of the hoop with a thin hoop. In the  $\beta = .078$  design there are 188 turns of 80,000 A conductor, but each 80,000 A conductor is composed of 4 parallel 20,000 A conductors; therefore, there are 752 thin hoops each with 20,000 A. A program was written to perform this calculation. It computes the force on each conductor, the total energy, and the field produced at selected points.

Recall that the energy stored is an input parameter for the analytic model but is calculated on the basis of hoop position and hoop current in the numeric model. The energy determined by the numeric model is 1 MWh -- to within three decimal places. The hoop tension predicted by the two models also agrees to three places. In the analytic model the energy and hoop tension enter the problem through the self inductance relation of Smythe (1950), which is excellent for small aspect ratio. The maximum field in the analytic model is not as well founded but it agrees within 5% with the numeric model. These results show that the analytic model is quite adequate for preliminary hoop design.

As mentioned earlier, the numeric model provides us with the detailed magnetic forces on each conductor. Figure II-2 is a graph of the radial forces on each hoop in the first layer of the magnet; the first layer is the layer nearest the midplane. Notice that the radial force on the inside layer is in the positive radial direction and that about halfway across this layer the radial force goes to zero and reverses direction. The consequences of this will be discussed in Chapter VI.

#### D. EXTERNAL FIELDS

The external magnetic field produced by the hoop is a matter of concern. At the time of this writing there are no national standards for personnel safety in magnetic fields; however there are some general rules for various types of equipment. As a rule a field of one kilogauss is about the maximum external field for operation of an electric motor or refrigerator. With this design the one kilogauss region is reached at about 17 meters from the center line of the hoop (at 17 meters the total field in the midplane is 1.0 kG and at 18 meters it is .862 kG). It is clear that large fields are local to the hoop and that fields on the order of one gauss are reached within 155 meters. For this design at distances of 100 meters or more the external magnetic field may be estimated by

$$B_{\rho} = \frac{\mu_0 I a^2}{2\rho^3} \cos \theta$$

$$B_{\theta} = \frac{\mu_0 I a^2}{4\rho^3} \sin \theta$$

These relations only include the first term in the multipole expansion for the field of the hoop. The  $\rho^{-3}$  field

dependence may be reduced to a  $\rho^{-5}$  field dependence by building a second superconducting hoop concentric and coplanar with the energy storage hoop and by adjusting the current in the second hoop such that the dipole moments of the two magnets cancel. If the second hoop is carefully designed it will not decrease the total energy stored and in fact it will increase it since its self inductance will contribute more energy than the mutual inductance terms will cancel. Although this technique would work, it is felt at this time that it is not necessary.

#### E. VIRIAL THEOREM AND PRESENT DESIGN

The virial theorem (Longmire, 1963) provides two very effective means by which we can evaluate a magnet design for energy storage. First the particular design may be evaluated, i.e., average stress levels, material densities, and energy, by comparison with

$$M \geq \frac{\rho E}{\sigma} \quad (2-9)$$

where

- M mass of structural material
- $\sigma$  working stress
- E stored energy
- $\rho$  mass density of the structural material.

One must be careful when applying equation (2-9) since it assumes:

1. Uniform stress levels throughout the structural material.
2. All load carrying materials have the same mass density.

In addition to this, for the equality to hold in equation (2-9) all of the structural material must be in tension. Since

most of these assumptions and conditions are not met for practical magnet designs, it is best to use a slightly more sophisticated comparison.

This comparison appears naturally when one examines the virial theorem more closely. First of all the virial theorem requires that one assign a positive sign to the force times length of a structural member under tension and a negative sign to similar members in compression. Then the theorem requires that the sums of these quantities must equal the stored energy. This view also shows that the tension term must always be greater than the stored energy if there is any member in compression, and that designs may be judged on the basis of how closely the tension term approaches the stored energy. A comparison of several hoop designs with the same stored energy but with different aspect ratios can be found in Table II-1. Note that as the aspect ratio decreases, the circumference times the hoop tension tends to approach the stored energy of  $3.6 \times 10^9$  joules. When considering even smaller aspect ratios, keep in mind that the aspect ratio is coupled to the conductor design and space must be made available accordingly.

One important point to keep in mind is that the sum of the force times distance terms does not imply that the energy stored is all in mechanical strains, since the distances in the terms just mentioned are lengths of members and not strains.

#### F. CONCLUSIONS

In this chapter we have looked at the design requirements placed on the energy storage hoop and their consequences. A simple analytic model was shown to be adequate for the first order design of systems of this kind with small  $\beta$ . The design has been shown to be compatible with the mechanical

constraints such as the proposed conductor. The external fields produced by the hoop have been discussed and they appear to fall very fast in the near vicinity of the hoop, and since we have no clear standard at this time for external fields additional field shielding is not recommended.

G. REFERENCES

Longmire, C. L., Elementary Plasma Physics, Interscience Publishers, 1963.

Smythe, W. R., Static and Dynamic Electricity, 2nd edition, McGraw-Hall, 1950.

Table II-1.

Aspect Ratio $\beta_c$	Radius $a$ (m)	Total Current $I_c$ (A)	Average Current Density $j_c$ (A/cm <sup>2</sup> )	Average Hoop Tension $T$ (N)	Average Hoop Stress $\sigma$ (lb/in <sup>2</sup> )	Tension Term Virial Theorem (N -m)
.078	8.85	$1.50 \times 10^7$	1000	$8.72 \times 10^7$	8285	$4.85 \times 10^9$
.1	7.86	$1.66 \times 10^7$	856	$1.00 \times 10^8$	7328	$4.44 \times 10^9$
.15	6.56	$1.98 \times 10^7$	651	$1.26 \times 10^8$	5892	$5.19 \times 10^9$
.20	5.83	$2.25 \times 10^7$	527	$1.49 \times 10^8$	4962	$5.46 \times 10^9$

Table II-1. Comparison of several 1 MWh storage hoops. Maximum field is 5T. These models are based on the analytic model. Note that as the aspect ratio decreases the tension term of the virial theorem approaches the stored energy  $3.6 \times 10^9$  joules.

# ANALYTIC MODEL

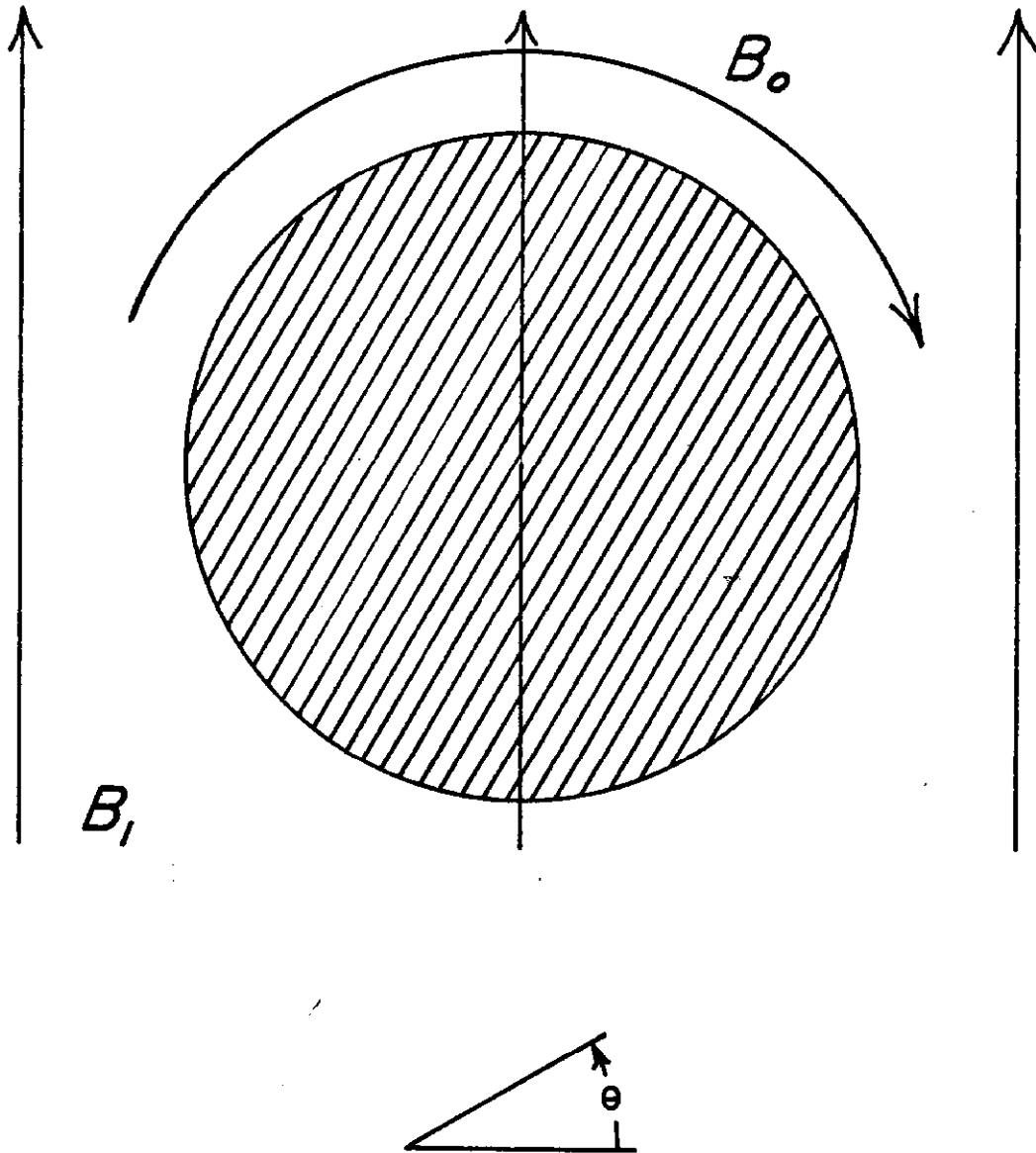


Figure II-1. Analytic model.  $B_0$  is self field.  $B_1$  is impressed background field. The angle  $\theta$  is measured counter clockwise from the horizontal.

RADIAL FORCE IN MIDPLANE  
 UW/NAL HOOP

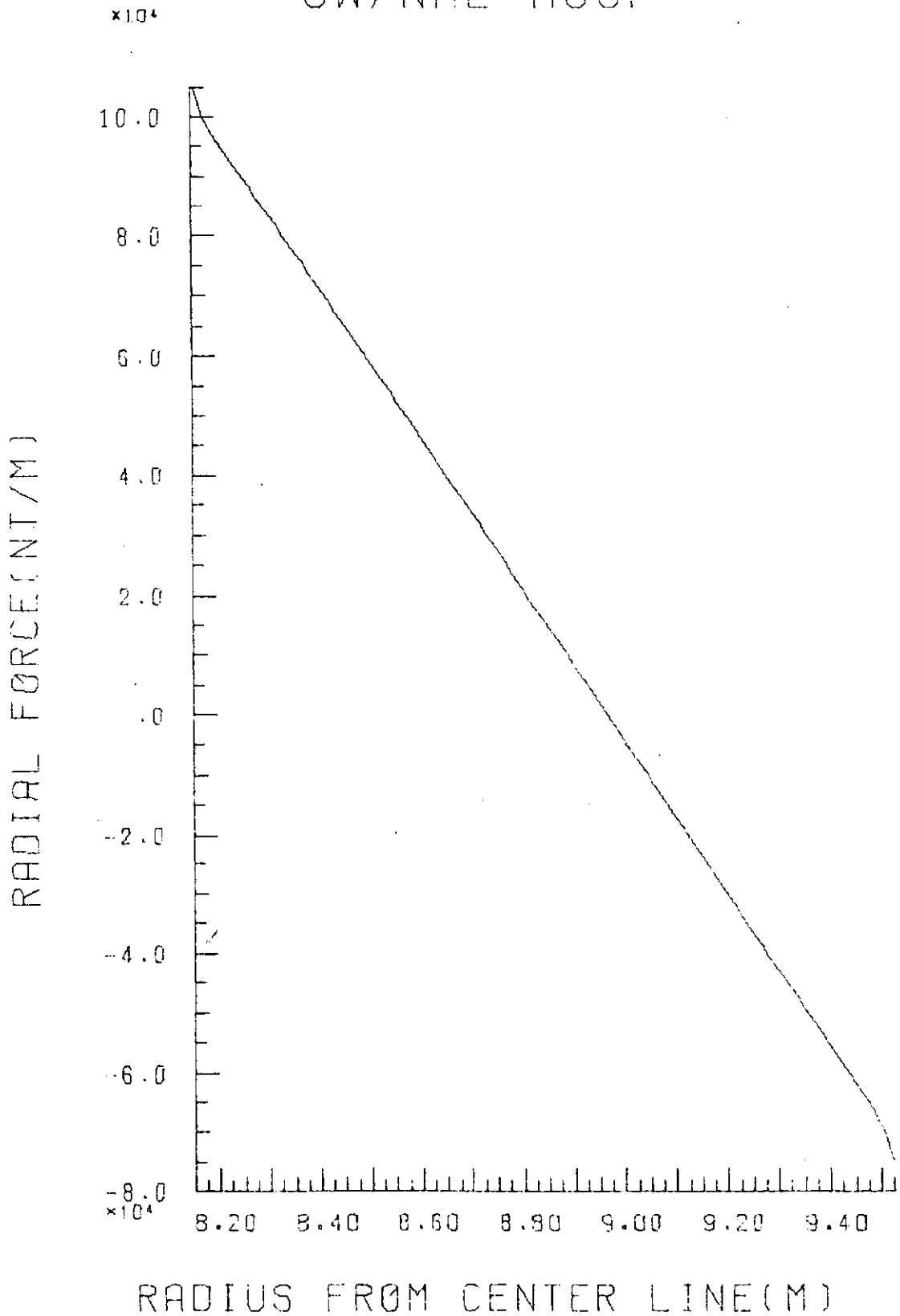


Figure II-2 Distribution of radial force in the layer of conductor nearest the midplane of the hoop. Note the change in sign of the force across the hoop.

### III. SUPERCONDUCTOR SHIELDING

The short duty cycle of this energy storage device introduces significant new problems for the design of large superconductive magnets. If 10% of the mean energy,  $W$ , were cycled in 10 seconds and  $B_M$  were 5T, there would be at least a 500 gauss/second field change inside an unshielded magnet. If the peak power demand were 200 MW, the maximum rate of field change would be 1400 gauss/second. The eddy currents induced in the copper stabilizer would generate a prohibitive amount of heat to be carried out of the liquid helium bath.

We have proposed that the superconductor and stabilizer be surrounded by a shielding coil of high conductivity aluminum. The superconductor and shield are electrically connected to the converter as shown in Figure III-1. For brevity, the superconductive coil will subsequently be referred to as the "hoop," while it and the shield will be designated by subscripts  $c$  and  $s$  respectively in the notation.

The shield is intended to keep the field at the hoop effectively constant. Two things required for this are

1. The pulse current,  $I_s$ , caused by power transfer to and from the system must be diverted through the shield so that the hoop current,  $I_c$ , is fixed and its self field is constant.
2. The pulse current in the shield should produce no field back at the superconductor.

#### A. SHIELD CURRENT DISTRIBUTION

To fulfill the second requirement the shield is wound to form a toroid with the current flowing about the vertical axis as shown in Figures III-2 and III-3. If the current were properly distributed in a continuous sheet over the toroidal surface, there would be no magnetic field anywhere inside the shield. For the proposed 1 MWh machine the shield is designed to have 188 turns of conductor. The turn to turn separation of the conductor is inversely proportional to the current density in the uniform sheet mentioned above. Although this does not make a continuous current distribution it still produces a negligible field in the region of the superconductor. See Appendix III-A for a more detailed discussion of shielding.

It should be noted that here the direction of current flow is orthogonal to that encountered in the toroidal magnets frequently used in plasma experiments. There the field is contained within the toroid and is zero everywhere else, but here the opposite is the case to shield the interior of the toroid.

B. SHIELD-HOOP COUPLING

The coupling between the shield and the hoop must be carefully considered to fulfill the condition that  $I_c$  effectively remain constant. The circuit equations associated with Figure III-1 are most easily understood in terms of Fourier analysis; therefore, we write the three most important variables as

$$V(t) = \sum_{n=1}^{\infty} V_n \cos (n\omega t + \Theta_{vn}) \tag{3-1}$$

$$I_c(t) = \sum_{n=0}^{\infty} I_{cn} \cos (n\omega t + \Theta_{cn}) \tag{5-2}$$

and

$$I_s(t) = \sum_{n=1}^{\infty} I_{sn} \cos (n\omega t + \Theta_{sn}) \tag{3-3}$$

The fundamental harmonic is the duty cycle of the NAL accelerator. Here it is taken to be 10 seconds and we have

$$\omega = 2\pi/10 \text{ sec.} \tag{3-4}$$

On solving the circuit equations for Figure III-1 it is found that the peak ac currents in the shield and hoop are

$$I_{sn} = \frac{V_n}{n\omega L_s} \left[ \frac{(L_c - M)^2}{(L_c - M^2/L_s)^2 + R_s^2 L_c^2 / \omega^2 L_s^2} \right]^{1/2} \tag{3-5}$$

and

$$I_{cn} = \frac{V_n}{n\omega L_s} \left[ \frac{1 + n^2 \omega^2 (L_c - M)^2 / R_s^2}{L_c^2 / L_s^2 + n^2 \omega^2 (L_c - M^2 / L_s)^2 / R_s^2} \right]^{1/2} \tag{3-6}$$

Meanwhile the resistance of the shield forces the steady state current to flow in the superconductor. This is related to the mean energy as follows

$$W_o \approx \frac{1}{2} L_c I_{co}^2 \quad (3-7)$$

To make  $I_{cn}$  as small as possible over a wide range of frequencies we first set  $L_s \approx M$ . This is accomplished directly by making the number of turns in the shield equal to that in the hoop. Now  $I_{sn}$  and  $I_{cn}$  take the forms

$$I_{sn} \approx V_n / n\omega L_s, \quad (3-8)$$

$$I_{cn} \approx I_{sn} / [n^2 \omega^2 \tau_n^2 + L_c^2 / L_s^2]^{1/2} \quad (3-9)$$

where

$$\tau_n = (L_c - L_s) / R_{sn} \text{ and } \omega \tau_n \gg 1.$$

Clearly there would be no ac current in the hoop if the shield resistance were zero. This would be the ideal situation because there would be no power lost in either the shield or the hoop. Such cannot be the case since even if the shield were superconducting it would have a significant resistance when operated in the ac mode. If we make the shield of high purity aluminum and run it at 40 K (Chapter IV) most of the pulse current is diverted through the shield, greatly reducing the losses in the superconductor and stabilizer.

## C. RESISTIVE HEATING IN THE SHIELD AND HOOP

## 1. Theory

The ac resistances of the shield and hoop have been estimated for the 1 MW hr machine to be ( See Appendicies III-B, IV-A and IV-B.)

$$\begin{aligned}
 R_{sn} &\approx s \rho_s / (h \delta_{sn}) \\
 &= \frac{S}{h} \sqrt{0.5 n \rho_s \mu_o \omega} \\
 &= 9.6 \times 10^{-3} \sqrt{n} \Omega
 \end{aligned} \tag{3-10}$$

and

$$\begin{aligned}
 R_{cn} &\approx \frac{N^2 a \rho_c}{r_c \delta_{cn}} \sum_{k=1}^m \left[ \left( \frac{m-k+1}{m} \right)^3 + \left( \frac{m-k}{m} \right)^3 \right] \\
 &= \frac{\omega^2 N^2 a d^2 \rho_c^2 \mu_o^2}{2\pi^2 r_c^2 \rho_i} \sum_{k=1}^m n_k \left[ \frac{\cos^2 \theta_k}{3} + \left( \frac{B_1}{B_o} \right)^2 \right] \\
 &= 8.8 \times 10^{-3} \sqrt{n} + 1.03 \times 10^{-2} \Omega
 \end{aligned}$$

where

- a = major radius = 8.85 m
- r<sub>c</sub> = minor radius of hoop = 0.69 m
- ω = cycling frequency = 2π/10 sec
- n = Fourier harmonic number
- S = Shield conductor length 1.029 × 10<sup>4</sup> m
- h = shield conductor height .015 m
- ρ = resistivity (ρ<sub>s</sub> = 5 × 10<sup>-10</sup> Ω m, ρ<sub>c</sub> = ρ<sub>1</sub> = 10<sup>-10</sup> Ω m)
- δ<sub>n</sub> =  $\sqrt{2\rho/\mu_o n\omega}$  = skin depth

$N$	=	number of turns in shield and hoop = 188
$m$	=	layers of conductor in hoop = 6
$d$	=	width of twisted conductor = 0.005 m
$l$	=	twist pitch = 0.1 m
$\Theta_k$	=	angular position of end conductor in $k$ th layer
$n_k$	=	number of conductors in $k$ th layer
$B_1/B_0$	=	0.1513

Although the hoop is superconducting, it exhibits resistive effects in the ac mode. These are caused by eddy currents in the stabilizer and twist losses and ac resistance in the superconductors.

The average power produced as heat in the shield and hoop at each frequency  $\omega$  can be written as follows:

$$\dot{Q}_{sn} = \frac{1}{2} I_{sn}^2 R_{sn} \quad (3-11)$$

$$\dot{Q}_{cn} = \frac{1}{2} I_{cn}^2 R_{cn} \quad (3-12)$$

These expressions can now be used in a Fourier analysis of the power demand wave for the NAL accelerator.

## 2. Examples

Two examples of heat dissipation in the shield and hoop are considered. First let us take an idealized case where 0.1 MWh of energy is transferred to and from the inductor system every ten seconds. The power as applied to the inductor is

$$P = I_c V = 113.1 \text{ MW} \cos \omega t. \quad (3-13)$$

It is specified in advance that  $I_{co}$  is 80 kA, and this corresponds to a stored energy of 1 MWh. Therefore, it can be stated that

$$I_{cn} \ll I_{co} \quad (3-14)$$

and

$$P \approx I_{co} V_1 \sin \omega t, \quad (3-15)$$

Employing Equations (3-8), (3-9) and (3-15) and noting that  $L_c = 1.131H$ ,  $L_s = 0.930 H$  and  $\tau_1 = 21 \text{ sec}$ , one finds

$$\begin{aligned} I_{s1} &= P_1 / \omega I_{co} L_s & (3-16) \\ &= 2420A \end{aligned}$$

and

$$\begin{aligned} I_{c1} &= I_{s1} / 13.25 & (3-17) \\ &= 183 A \end{aligned}$$

The resistive heat dissipation in the shield and hoop is given by entering these into Equation (3-11) and (3-12)

$$Q_s = 28.1 \text{ kW} \quad (3-18)$$

$$\begin{aligned} Q_c &= 146 \text{ W (eddy currents)} & (3-19) \\ &+ 172 \text{ W (twist losses)} \\ &= 318 \text{ W} \end{aligned}$$

This gives a convenient standard independent of the complex power wave forms that may be applied to the inductor.

An example of such a wave form is given by the power input to an inductor which completely compensates for fluctuations in the power demand of the NAL accelerator operating at 400 GeV. The first ten Fourier coefficients are shown in Table III-1 along with the corresponding currents and resistances (see Chapter V).

n	P <sub>n</sub> MW	I <sub>sn</sub> A	A	R <sub>sn</sub>	R <sub>cn</sub>
1	93.3	2000	151	9.59 x 10 <sup>-3</sup>	1.91 x 10 <sup>-2</sup>
2	23.3	505	38.1	1.36 x 10 <sup>-2</sup>	2.27 "
3	6.70	143	3.63	1.66 "	2.55 "
4	4.93	106	2.00	1.92 "	2.78 "
5	3.30	70.6	1.07	2.14 "	2.99 "
6	1.66	35.7	0.450	2.35 "	3.19 "
7	0.741	15.9	0.171	2.54 "	3.35 "
8	0.693	12.6	0.120	2.71 "	3.51 "
9	0.798	17.1	0.143	2.88 "	3.66 "
10	0.681	14.6	0.110	3.03 "	3.80 "

Table III-1. Fourier coefficients for complete load leveling of the NAL accelerator demand at 400 Gev.

The heat dissipation now becomes

$$\dot{Q}_s = 21.3 \text{ kW} \quad (3-20)$$

$$\dot{Q}_c = 234 \text{ W} \quad (3-21)$$

Although the energy transferred is the same in the two preceding examples, the heat dissipation is about 25% lower in the second case. This happens because  $\dot{Q}_s$  and  $\dot{Q}_c$  depend on the power transfer wave form. A convenient rule of thumb is that the longer the inductor energy is near its extreme, the larger  $\dot{Q}_s$  and  $\dot{Q}_c$  will be.

#### D. COMPENSATION OF THE SHIELD RESISTANCE

The shield has greatly reduced the refrigeration required for eddy current losses, but these refrigerators are still a major part of the machine's total cost. We estimate that

eddy current heating alone will add \$1,250,000 and \$125,000 to the costs of cooling the shield and hoop, respectively. These may be significantly lowered when a small power supply is added to prevent the pulse current from leaking into the superconductive hoop.

#### 1. Reduction of Hoop Losses

A low impedance voltage source is added to the circuit as shown in Figure III-4. No pulse current will be seen in the hoop if  $V_r$  is controlled so that

$$V_r = I_s R_s. \quad (3-22)$$

This gives the shield circuit the appearance of having no resistance and  $I_{cn}$  is zero by Equation (3-9).

If  $R_s$  is known precisely,  $V_r$  can be obtained by metering  $I_s$  and multiplying it by  $R_s$ . Although  $I_s$  is on the order of 2500 A and can be read quite easily,  $R_s$  is a function of current frequency and shield temperature so it may not be known with sufficient accuracy. In addition to allowing some pulse current to reach the hoop, errors in  $V_r$  could cause serious instabilities in the circuit. When  $V_r$  is greater than  $I_s R_s$ , the shield appears to have a negative resistance and an exponentially increasing current will be developed by  $V_r$ .

Although more complex, it may be better to take the control signal from  $I_c$ . Here the average current is 80,000 A, but small current changes can be detected by a transducer or other device. Then  $V_r$  would be driven to minimize the change in  $I_c$ , consequently minimizing  $\dot{Q}_c$ . The net effect is still to make  $V_r$  equal to  $I_s R_s$ .

In the examples in the preceding section, the maximum shield current is 2420 A and we have  $R_s = 10^{-2} \Omega$ . Hence, the resistance compensating power supply should be rated at

least  $\pm 2500$  A at  $\pm 25$  V. Depending on the control circuitry, this would cost several thousand dollars, much less than the \$125,000 needed to refrigerate for the  $\dot{Q}_c = 234$  W in the un-compensated system.

## 2. Room Temperature Shields

Until now, it has been assumed that the shield is operated at 40 K for two reasons. First, a substantial fraction of the pulse current leaks into the hoop if there is no compensating power supply and the shield is at room temperature. Second, when the shield is operated at cryogenic temperatures, the minimum refrigeration power occurs at about 40 K (see Chapter IV).

The resistance compensating power supply should greatly reduce the pulse current leakage to the hoop; hence the shield can now be operated outside the cryogenic temperature range. We believe that it may be cheaper to build and operate a water-cooled shield at 300 K than a refrigerated one at 40 K.

As an example, let us consider a copper shield of dimensions identical to the 40 K case considered throughout this paper. Copper is taken in preference to aluminum because their resistivities are  $1.55 \times 10^{-8} \Omega\text{m}$ , and  $2.5 \times 10^{-8} \Omega\text{m}$ , respectively, at 300 K. Here, the shield is a 10,290 m long strip of 1.5 cm x 6 cm copper with a 1 cm diameter hole inside. The resistance is  $R_s = 0.20 \Omega$ . On combining Equation 3-11 and Table III-1 we find

$$\dot{Q}_s = 430 \text{ kW.} \quad (3-23)$$

This is less than the 554 kW needed to drive the refrigerator for the 40 K shield (not counting safety margin cooling capacity in either case). Basically, we have replaced a 40 K refrigerator with a circulating water system and a relatively small resistance compensating power supply.

The trimming supply does become considerably more complex for a 300 K shield. The peak current is still  $\pm 2420A$ , and now  $R_s = 0.2 \Omega$ ; hence, Equation (4.22) gives

$$V_{r \max} = 484V. \quad (3-24)$$

Consequently, the peak power rating of the trimming supply should be about 1.2 MW. Assuming a cost of approximately \$40/kW, this would require about \$50,000 plus the cost of the feedback controls.

There are two major disadvantages to the room temperature shield. First, with a 300 K shield much more care is required to insulate the hoop, since there is no longer a 40K thermal shield. Some loss in shield-hoop coupling will occur if the shield is moved farther from the hoop to make room for additional insulation, and it may also be necessary to replace the stainless steel hoop supports with better insulating epoxy fiberglass.

The second problem is that the high resistance of the 300 K shield makes it virtually impossible to operate the system without the trimming power supply. Further the high gain stable feedback loop must be developed with care.

In the remainder of the paper, we pursue both the 40K and 300K shield designs. A more complete study of both systems is required before a clear choice can be made.

#### E. REFERENCES

- Longmire, C. L., Elementary Plasma Physics, Interscience Publishers, 1963.
- Smythe, W. R., Static and Dynamic Electricity, 2nd edition, McGraw-Hill, 1950.

## CONVERTER - INDUCTOR SYSTEM

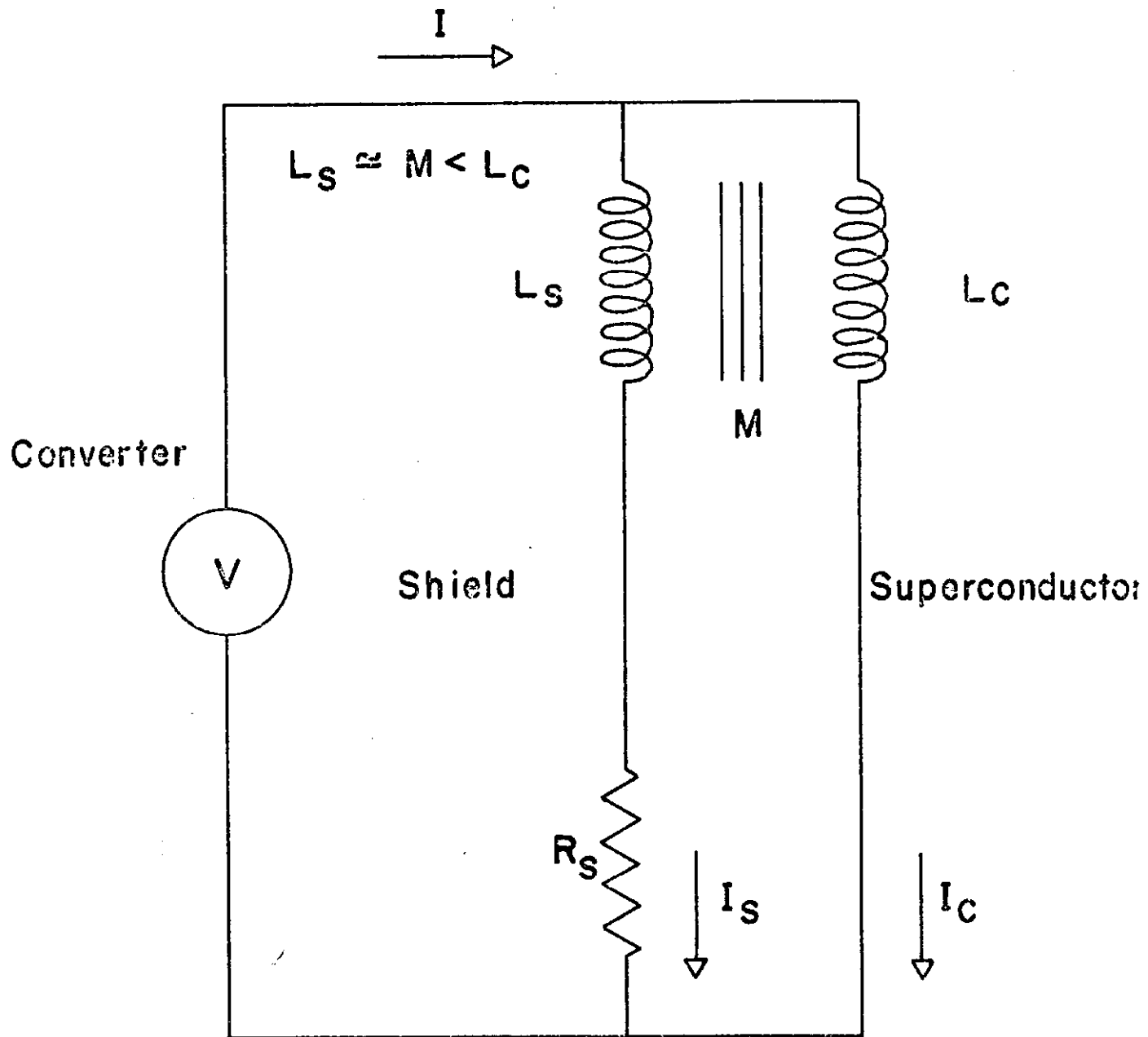


Figure III-1

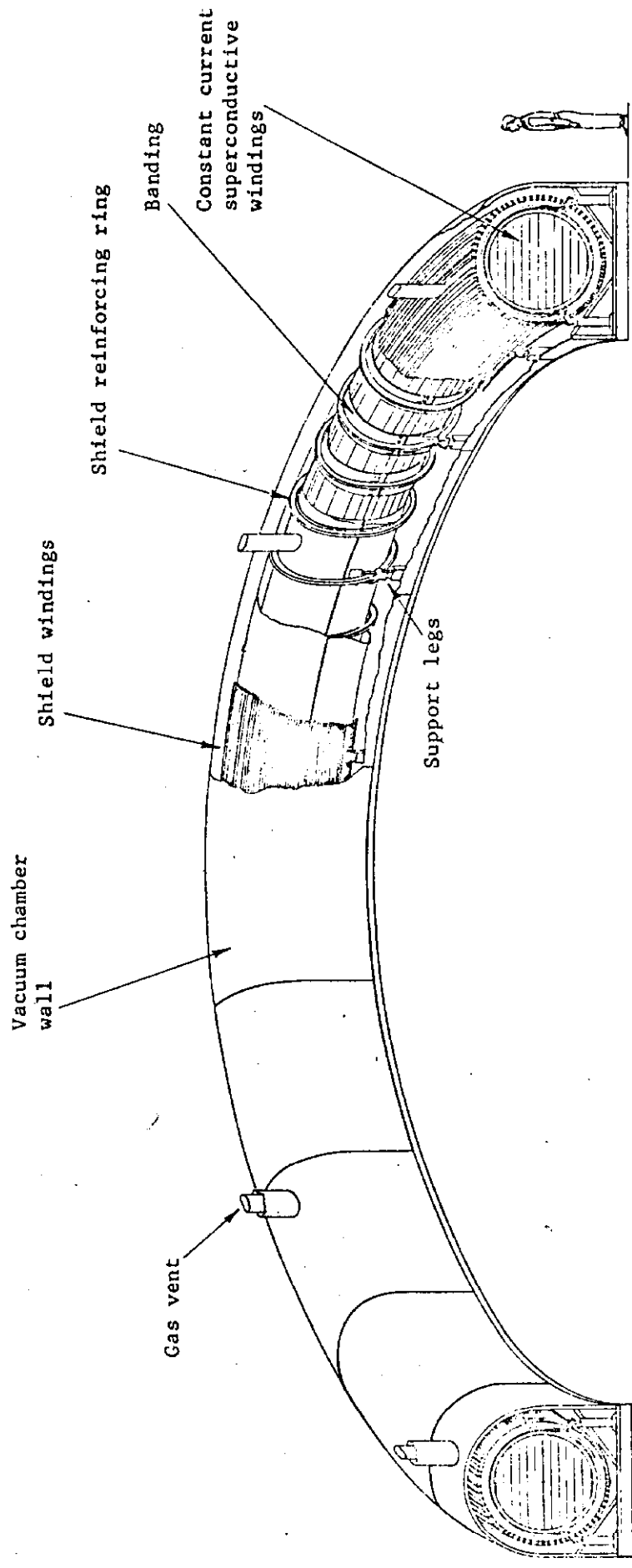


FIG. III-2. ISOMETRIC VIEW OF N.A.L.- U.W. PULSED ENERGY STORAGE

Scale  
1 m.

# INDUCTOR CROSS SECTION

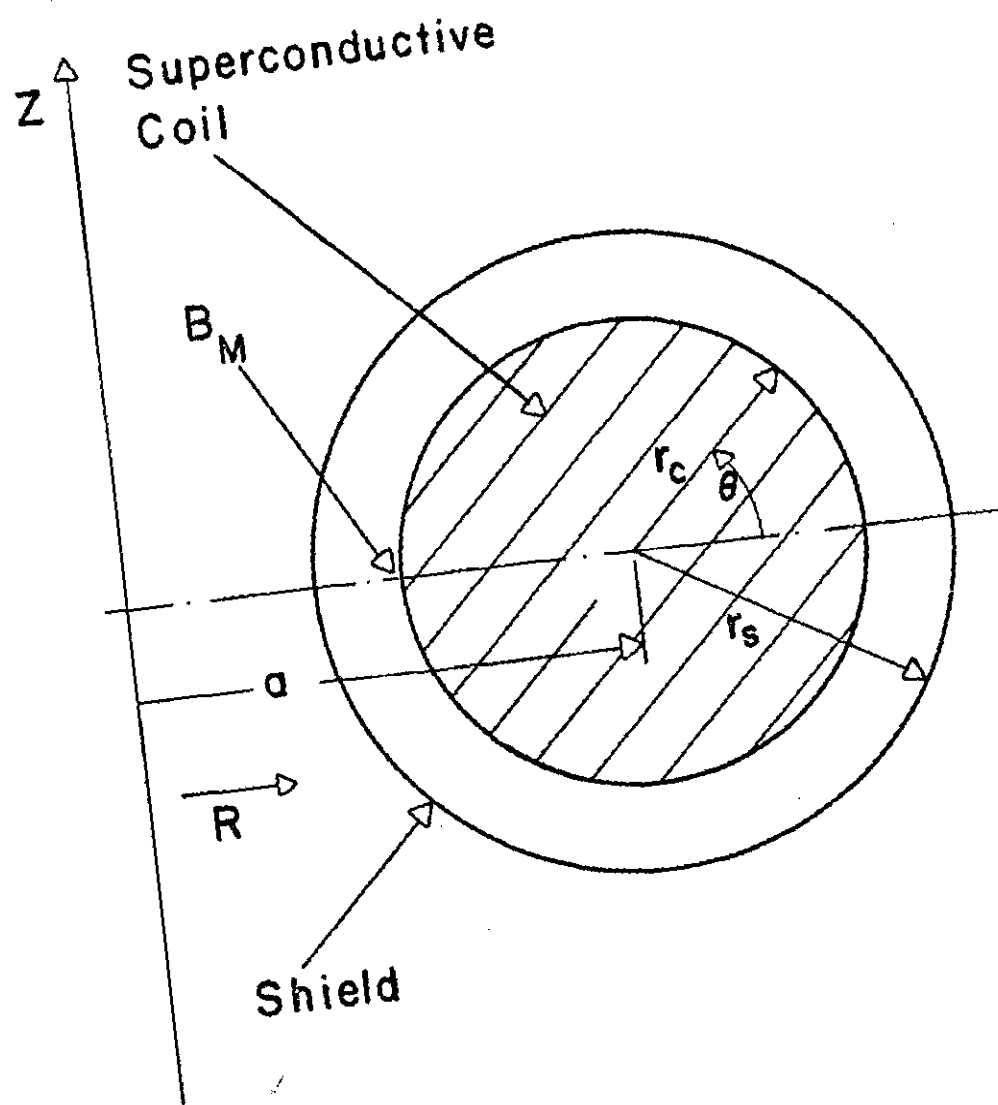


Figure III-3

# CONVERTER - INDUCTOR SYSTEM WITH RESISTANCE COMPENSATION

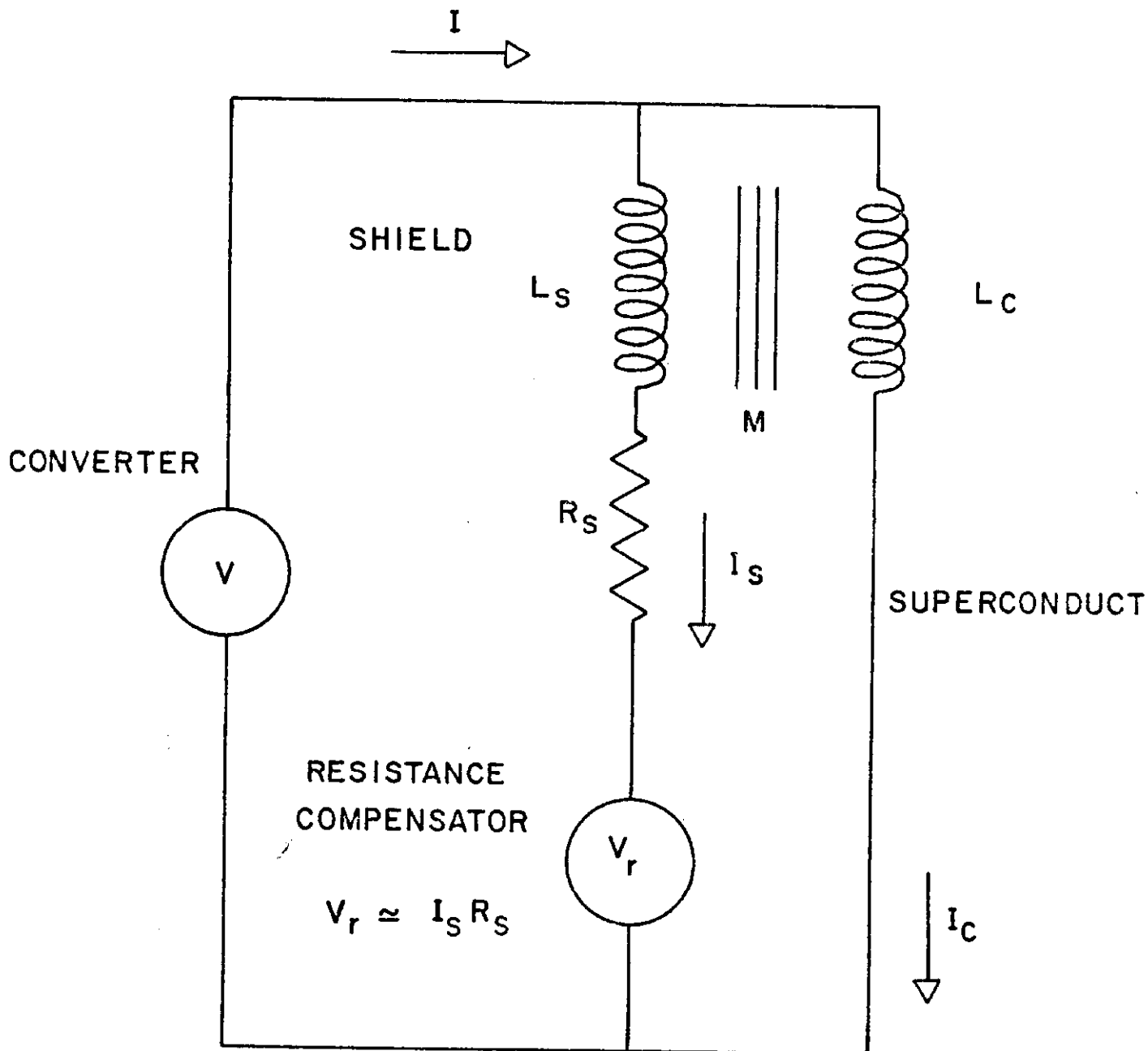


Figure III-4

## APPENDIX III-A

### CONDUCTOR LOCATION IN THE SHIELD

The shield is designed to surround the superconductive coil as shown in Figures III-2 and III-3. The time varying pulse current is diverted through the shield, and it must produce no appreciable magnetic field at the superconductor. The purpose of this section is to describe how we locate conductor in the shield to achieve this internal field reduction.

Complete exclusion of the pulse field would be possible if the shield formed a continuous surface enclosing the superconductor, but we must use a finite number of turns,  $N$ , located at angles  $\theta_i$  around the surface. This discrete nature of the windings leads to a slight but insignificant penetration of field into the core.

To begin with we place  $N'$  poloidal turns around the surface of the shield with angular positions

$$\theta_i = (i - \frac{1}{2})/2\pi N', \quad i = 1, 2, \dots, N' \quad (3-A-1)$$

as shown in Figure III-A-1. Each carries a current  $I_i$  which is a function of  $\theta_i$ . This is convenient for computational purposes, but later we will allow the turn-to-turn spacing to vary and set the current to the same value in all conductors.

It can be shown that the field inside the shield is zero if all paths within it are linked by the same amount of magnetic flux. Here it is assumed that each of the paths traverses the toroid only once. Let us consider  $M$  test hoops concentric to the shield windings and located on a circle of radius  $r_t < r_s$  as shown in Figure III-A-1. The flux passing inside of each hoop is defined as  $\phi_j$ . The flux linking hoop  $j$  as caused by a current in the concentric hoop  $i$  is relatively simple to calculate (Smythe, 1950). We represent this by a matrix  $f_{ji}$  and the current  $I_i$ ; hence, the flux  $\phi_j$  becomes

$$\phi_j = \sum_{i=1}^{N'} f_{ji} I_i \quad (3-A-2)$$

Rather than have a great many variables in  $I_i$ , we make a Fourier expansion of the current distribution

$$I_i = \sum_{n=0}^K I_n \cos n\theta_i . \quad (3-A-3)$$

Equations (3-A-2) and (3-A-3) can be combined as follows

$$\begin{aligned} \phi_j &= \sum_{i,n} f_{ji} I_n \cos n\theta_i \\ &\equiv \sum_{n=0}^K F_{jn} I_n . \end{aligned} \quad (3-A-4)$$

If the average flux is  $\bar{\phi} \equiv \frac{1}{M} \sum_{i=1}^M \phi_i$ , then the mean square flux deviation through the test hoop is

$$D = \frac{1}{M} \sum_{j=1}^M (\phi_j - \bar{\phi})^2 \quad (3-A-5)$$

The average current in the  $N'$  hoops is normalized by setting  $I_0 = 1$  amp/ $N'$ .  $I_1, I_2, \dots$  and  $I_K$  are explicitly determined by using the method of least squares to minimize  $D$  in equation (3-A-5).

The technique described above gives an extremely accurate means of determining the current distribution for guiding the field around the outside of the shield. For example, we used  $N' = 48$ ,  $M = 34$ ,  $r_s = 98.5$  cm,  $r_t = 75$  cm,  $K = 6$  and  $a = 7.9$  m to get a flux variation of less than  $10^{-3}\%$  inside  $r_t$ . A contour plot of lines of constant flux is shown in Figure III-A-2 to illustrate the field exclusion from inside the shield.

As mentioned earlier, we now turn to the case where all of the conductors carry the same current,  $I$ , and the field exclusion is achieved by adjusting the conductor locations,  $\theta_i$ .

Equation (3-A-3) gives a good approximation of the uniform current density which gives complete shielding

$$I(\theta) \approx \sum_{n=0}^K I_n \cos n\theta \quad . \quad (3-A-6)$$

By definition we have  $\int_0^{2\pi} I(\theta) d\theta = 1A$ , and we want to divide the shield into  $N$  new segments such that

$$I(\theta_{i+1}) - I(\theta_i) = 1A/N \quad \text{for all } i = 1, 2, \dots, N-1. \quad (3-A-7)$$

This is done with the use of the recursion relation

$$\theta_{i+1} = \theta_i + \frac{1}{N} \left( \frac{dI}{d\theta} \right)_{\theta=\theta_i}^{-1} \quad (3-A-8)$$

where

$$\theta_1 \equiv \frac{1}{2N} \left( \frac{dI}{d\theta} \right)_{\theta=0}^{-1} .$$

The accuracy of this method is enhanced by solving for  $\theta_i$  from  $\theta=0$  to  $\theta=\pi$  then reversing the process and going from  $\theta=\pi$  to  $\theta=0$ . Afterward a weighted average of the two solutions is taken.

After the angles  $\theta_i$  are calculated as above their accuracy is checked by explicitly computing lines of constant flux as shown in Figure III-A-2. These were found to be in excellent agreement with those calculated for the uniformly distributed hoops discussed earlier.

In conclusion the shield is now designed to have individual conductors located on the circle  $r_s$  at angles  $\theta_i$  as depicted in Figure III-A-3. It will be necessary to depart from this distribution to insert supports and helium vents as shown in Figure VI-2, but the basic angular distribution will be maintained. Field errors caused by this alteration will be calculated at a later date.

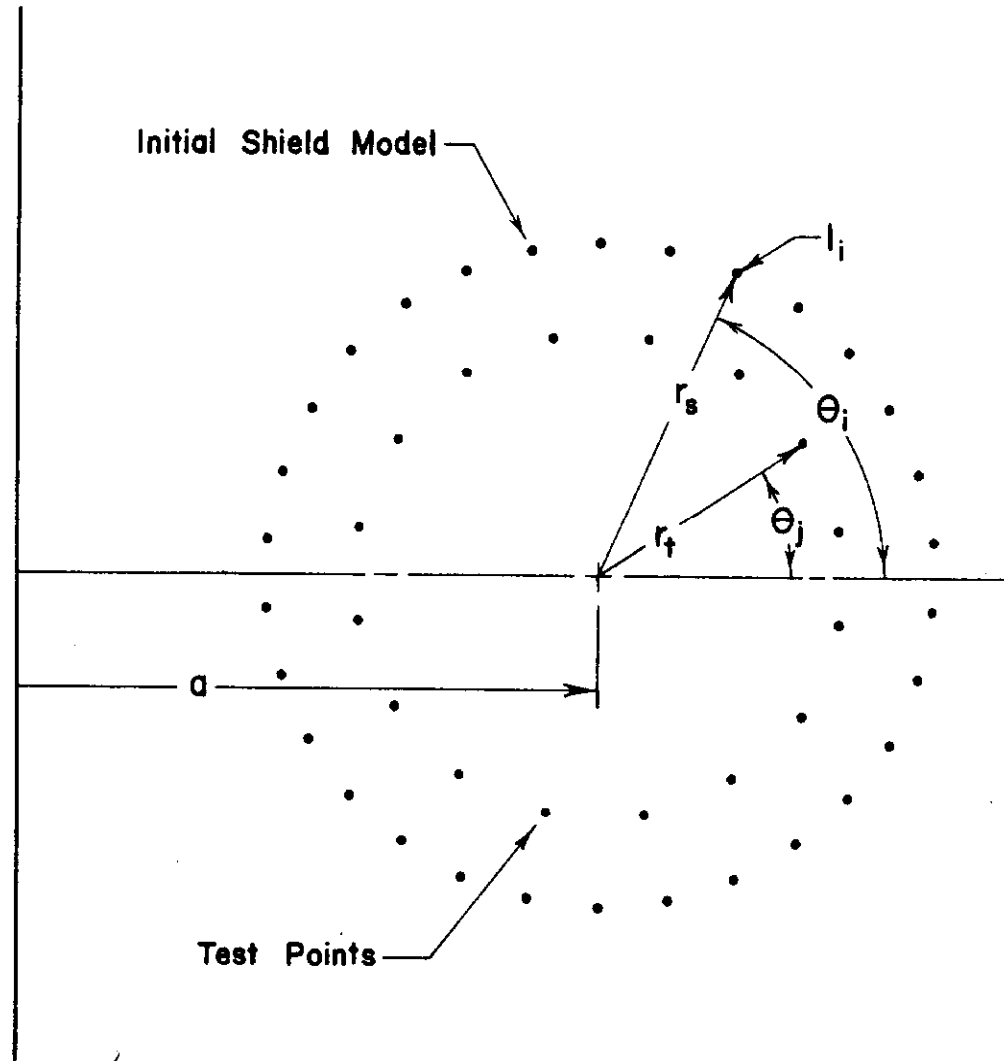


Figure III-A-1. Initial shield model with uniformly separated conductors having variable currents.

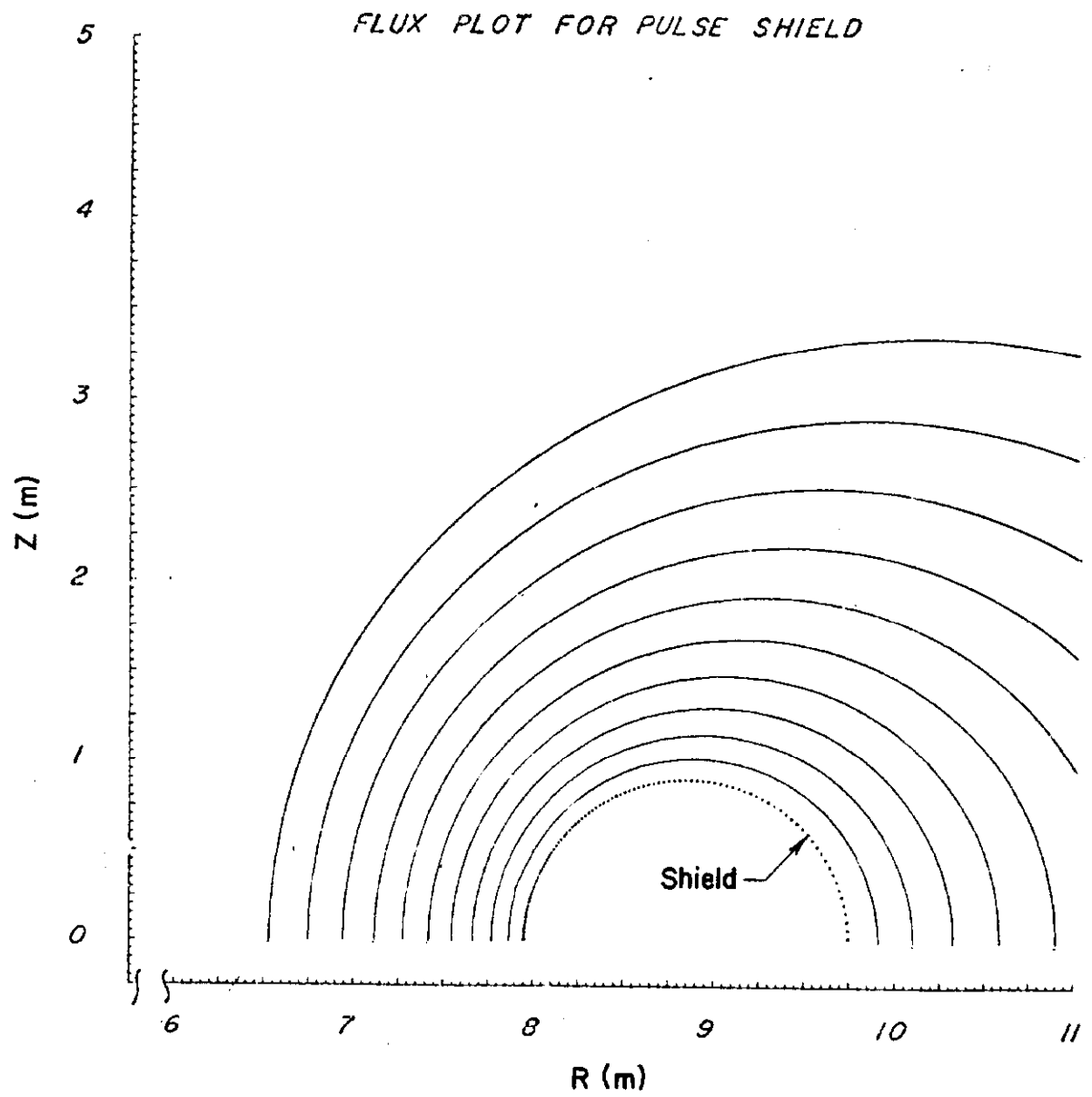


Figure III-A-2. Lines of constant magnetic flux produced by a current in the shield.

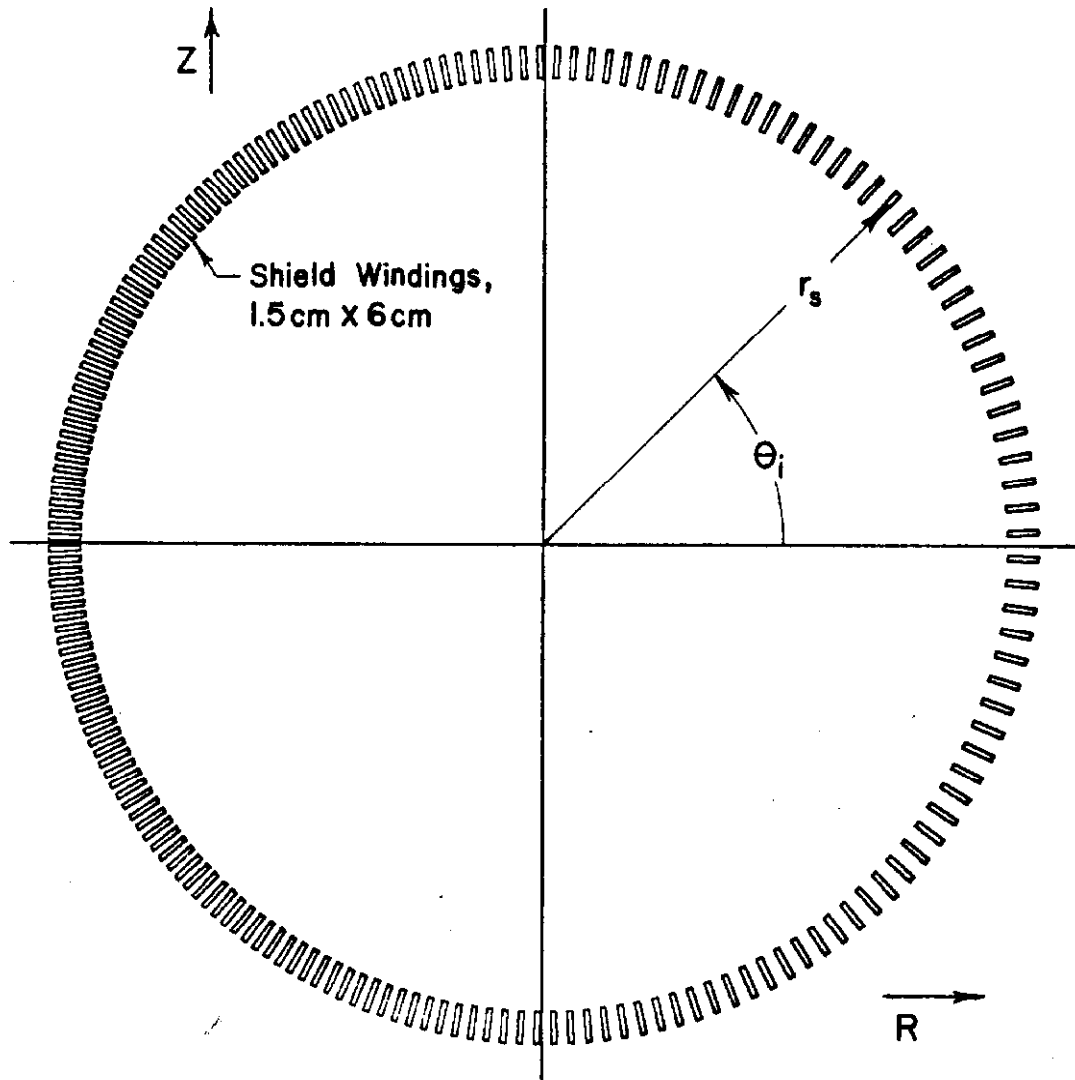


Figure III-A-3. Shield conductors with equal currents and variable separations.

## APPENDIX III-B

### SHIELD RESISTANCE

Let us assume that the shield is made of a conductor of width  $w = 0.06$  m, and height  $h = 0.015$  m with a 0.01 m diameter hole inside to carry coolant. The total conductor length is  $S = 1.029 \times 10^4$  m.

If the shield current were constant the resistance would be

$$\begin{aligned} R_s &= S\rho_s / (hw - \pi \times 10^{-4} / 4) \\ &= 6.26 \times 10^{-3} \Omega \end{aligned} \tag{3-B-1}$$

where  $\rho_s$  is taken as  $5 \times 10^{-10}$   $\Omega$  m for aluminum at 40K.

In reality the current is oscillating with a fundamental frequency of one cycle per ten seconds, and the current does not uniformly penetrate the conductor. If all of the shield conductors were closely packed together, the shield would be very similar in appearance to a continuous slab of aluminum carrying a current and excluding all field from one side. Assuming an infinite thickness and neglecting the circular effects and inner coolant channel, the resistance becomes

$$R_s \approx S\rho_s / h\delta \tag{3-B-2}$$

where  $\delta$  is the skin depth  $\delta = \sqrt{2\rho_s / \mu_0 \omega}$ . On considering higher Fourier harmonics,  $n\omega$ , the corresponding resistances are

$$R_{sn} = \sqrt{n} R_s \approx 9.6 \times 10^{-3} \sqrt{n} \Omega \tag{3-B-3}$$

The approximation above has many shortcomings. First, no consideration is given to the conductor separation which is large on the outside of the machine (see the right-hand side of Figure III-A-3). Some field penetration between the turns should slightly lower the shield resistance. A second error arises from the use of Equation (3-B-2) which assumes a slab of infinite thickness. The actual resistance is alternately above and below this value when  $\omega$  is in the range of  $2\delta$  to infinity. It is reasonably

accurate for  $w \approx \delta$  but useless for  $w < \delta$ . When the shield is made of aluminum at 40K we have  $w \approx 2\delta$  and Equation (3-B-2) is used. In the case of a room temperature shield,  $\delta$  is much larger than  $w$  and Equation (3-B-1) is taken for the shield resistance.

It is clear that much analysis of coupled ac conductors is still required. Perhaps this can be developed from the work of D. Hartmann and H. A. Peterson currently underway at the University of Wisconsin.

## APPENDIX III-C

### SCALING LAWS

A fundamental parameter for a pulsed storage unit is the energy  $\Delta E$  to be stored and retrieved during a cycle. The energy  $\Delta E$  can be obtained from a wide variety of storage magnets whose internal parameters are characterized by  $B_M$  and  $E$ .  $B_M$  and  $E$  can be selected largely on the basis of the construction and operating costs for a machine or particular research goals inherent in the project. Up to now we have emphasized the design of one particular machine, a 1 MWh, 5 T unit. It would be useful to have some basic scaling laws that could be applied to this and other models in order to estimate machine parameters for devices with different values of  $E$  and  $B_M$ .

In the following discussion we assume that a basic machine configuration is held fixed while  $E$ ,  $\Delta E$  and  $B_M$  are variable. For example the aspect ratio of a dipole is held constant while the energy or field is changed. Only proportionalities are given here, but more detailed relationships are presented in Chapter V of the Wisconsin Superconductive Energy Storage Project report.

#### Scaling Laws for Constant Configurations

1. Major Radius =  $a \propto E^{1/3}/B_M^{2/3}$
2. Machine Volume =  $V \propto E/B_M^2$
3. Hoop Tension =  $T \propto E^{2/3} B_M^{2/3}$
4. Minimum Structural Mass =  $M \propto E$
5. Average Current Density =  $j_c \propto B_M^{5/3}/E^{1/3}$
6. Ampere - meters of superconductor and stabilizer =  $I_c S_c \propto E^{2/3}/B_M^{1/3}$
7. Ampere meters of shield conductor =  $I_s S_s \propto \Delta E/E^{1/3} B_M^{1/3}$  (This approximation only applies for  $\Delta E \ll E$ .)

8. Surface area =  $A_s$  and mass of conductor =  $M_s \propto E^{2/3} / B_M^{4/3}$  for shield. (This assumes that the shield covers the machine with the same thickness and density of conductor regardless of the size of the storage unit.)

9. Resistive Power Loss in the shield =  $P_s \propto I_s^2 S_s^2 / A_s$   
 $\propto B_M^{2/3} \Delta E^2 / E^{4/3}$

No attempt will be made to derive or use the above proportionalities here, rather they are being made available for future application.

## IV. - CRYOGENICS

The cryogenic design is divided into two sections. These are the design of the shield and of the superconducting magnet.

### A. SHIELD CRYOGENIC DESIGN

For the shield the following problems and parameters are to be considered:

1. Choice of the shield operating temperature.
2. Refrigeration power required.
3. Heat transfer calculations and cooling scheme.
4. Pressure drop calculations.

#### 1. Choice of the Operating Temperature.

It is not possible to operate the shield at 4.2K, where superconducting materials can be used, because eddy currents would produce too much heat in the low temperature region. If aluminum is used, a higher operating temperature is advantageous. Below 20K, a reasonable purity aluminum has a constant resistivity; hence, the operating temperatures should be 20K or higher. Table IV-1 shows the effect of higher temperature, on the coefficient of performance and on the theoretical (Carnot) refrigeration power required. The shield will be cooled by forced helium flow through tubes inside it. The coefficient of performance in Table IV-1 is calculated assuming the temperature rise of helium is the same at the different temperatures ( $T = 4K$ ). It should also be mentioned that the power loss in Table IV-1 is normalized to one KW at 20K.

The operating temperature of the shield is chosen to be 40K for the following reasons:

- a. The knee of the resistivity curve of aluminum is near 20K. It will be difficult to operate the shield at 20K because any change in the purity will appreciably change the resistivity and the power loss will change accordingly. The change in the purity will have less effect at 40K.

Table IV-1

T, K	$\times 10^{-8}$ cm	$\delta$ , cm	$P_1$ , KW	C.O.P.	$P_R$ , KW
20	1.8	2.12	1.00	14.05	14.05
30	3.0	2.77	1.30	9.01	11.71
40	5.0	3.58	1.69	6.51	11.00
50	8.0	4.52	2.14	5.00	10.70
60	12.5	5.67	2.67	4.00	10.68
70	20.0	7.16	3.38	3.28	11.09
80	30.0	8.76	4.14	2.75	11.39
90	45.0	10.73	5.07	2.33	11.81
100	57.3	12.13	5.73	2.00	11.46
300	250.0	25.00	11.80		

$\delta$  = Skin depth, cm

$P_1$  = Power loss, KW

$P_R$  = Refrigeration power, KW

b. The refrigeration power required at 40K is 20% lower than the power required at 20K.

The disadvantages of operating at 40K instead of 20K is the increase in the skin depth and the increase of the losses in the superconducting magnet (because the shield becomes more resistive). [If the thickness of the shield is  $2\delta$ , the increase of the aluminum thickness may be allowed.] The increase in the losses in the superconducting magnet will be smaller than the decrease of the refrigeration power required for the shield.

## 2. Refrigeration Power Required.

We calculate first the theoretical refrigeration power required. We assume that helium enters the shield at temperature  $T_i$  and leaves at  $T_f$ . Figure VI-1 shows the temperature as a function of the entropy along the tube. Assuming the operation with the Carnot cycle we have

$$W = \text{Power required} = \int \dot{m} C_p (T_o - T) \frac{dT}{T}$$

If we further assume constant specific heat we obtain

$$\text{C.O.P.} = \dot{W}/\dot{Q} = \left[ \frac{T_o}{T_f - T_i} \ln(T_f/T_i) - 1 \right] \quad (4-1)$$

Where

C.O.P. is the coefficient of performance

$\dot{Q}$  the power loss

$T_o$  room temperature

Table IV-2 shows the dependence of the coefficient of performance on the inlet temperature.  $T_o$  is usually taken equal to 300K and  $T_f$  is taken equal to 42K.

Table IV-2

$T_i$	C.O.P.	$T_i$	C.O.P.
4.2	17.27	28	7.69
8	14.54	32	7.16
12	11.53	36	6.71
16	10.14	38	6.51
20	9.12	40	6.31
24	8.33	42	6.14

The inlet temperature is taken to be 38K, the outlet temperature 42K and the average temperature will be 40K. The theoretical C.O.P. of performance in this case is 6.51 (Table IV-2) compared to a minimum of 6.14. Smaller temperature rises ( $T_o - T_i$ ) increase the mass flow rate appreciably since  $\dot{m}$  is inversely proportional to  $(T_f - T_i)$ . Also smaller temperature rises lead to higher pressure drops especially in the heat exchangers. Needless to say, greater temperature rises are also not desirable on account of the higher coefficient of performance. Figure IV-2 shows the coefficient of performance including pressure drop losses, and demonstrates that the optimum temperature rise is 4K.

The actual coefficient of performance is taken equal to four times the theoretical C.O.P. The average power loss in the shield is 21.3KW. The refrigerator will be designed for a load of 30KW (38% excess). The refrigeration power required accordingly will be .782MW.

### 3. Heat Transfer Calculations and Cooling Scheme

The first parameter of interest in this heat transfer calculation is the temperature difference between aluminum and the bulk of helium. It was mentioned before that the average temperature of helium is taken to be 40K. To find the aluminum temperature we use McAdams correlation

$$N_{Nu} = 0.2 N_{Re}^{.8} N_{Pr}^{.6}$$

where

$N_{Nu}$  is the Nusselt number ( $hD/k$ )

$N_{Re}$  is the Reynolds number ( $\rho DV/\mu$ )

$N_{Pr}$  is the Prandtl number ( $C_p\mu/k$ )

The Prandtl number for helium at  $P = 10$  atm and  $T = 40K$  is about .8 and  $(N_{Pr})^{.6}$  is taken equal to one. The heat transfer correlation reduces to

$$h = .024 (k/D) (\dot{m}/\mu D)^{.8} \quad (4-2)$$

In the above equation

$h$  is the heat transfer coefficient

$k$  is the thermal conductivity of helium

$\dot{m}$  is the mass flow rate in a tube

$D$  is the diameter of each tube

If we have  $N$  tubes of diameter  $D$ , the heat balance equation, assuming no conduction along the tube, is

$$N\pi DL = \dot{Q}/h\Delta T \quad (4-3)$$

also

$$NmC_p(T_f - T_i) = \dot{Q} \quad (4-4)$$

Combining Equations (4-2), (4-3), and (4-4) we get the following expression for  $\Delta T$ , the temperature difference between the aluminum surface and helium,

$$\Delta T = \frac{13.26}{L} \left( \frac{\dot{Q}}{NK} \right)^{.2} \left[ D(T_f - T_i) \right]^{.8} \quad (4-5)$$

The recommended scheme of cooling is shown in Figure VI-10.

The helium travels for one complete turn of the shield before it returns to the refrigerator. The flow tubes in the shield have a diameter of one centimeter, and the number of tubes is 188. If  $\dot{Q}$  is taken equal to 30KW,  $T$  calculated from Equation (4-5) will be about .1K which is negligible (in this calculation  $k$ , the thermal conductivity, was taken equal to .27 mW/cmK). The temperature of a certain channel of the shield is expected to have the profile shown in Figure IV-3. Heat conduction along the tube has not been considered here. Such conduction will make the aluminum temperature higher than 38.1K at the inlet. The temperature difference across the aluminum is given by

$$(\Delta T)_{al} = 2.5 \frac{\dot{Q}}{N L} (\delta/k) \quad (\text{If the aluminum thickness} = 3\delta)$$

and

$$(\Delta T)_{al} = 1.5 \frac{\dot{Q}}{N w L} (\delta/k) \quad (\text{If the aluminum thickness} = 2\delta)$$

In the above equation,  $w$  is the width of each conductor in the shield,  $L$  is the length and  $\delta$  is the skin depth. The temperature difference across the aluminum will be .017K if the  $w = 3\delta$  or .0096K if  $w = 2\delta$  which is insignificant ( $k$  is taken equal to 3 watt/cmK).

The power dissipation used in the above calculations is the average power. If the time of flight of a helium atom is larger or equal to the cycling time, the above approximate calculations are valid. This flight time should not be allowed to be shorter than the cycling time because of the bad effect on the refrigerator of an oscillating outlet helium temperature. The flight time,  $\tau$ , is given by

$$\tau = (NL\pi D^2/4)/\dot{V} = (\pi N L \rho D^2 C_p (T_f - T_i))/4\dot{Q}$$

Where  $\dot{V}$  is the volumetric flow rate, We will take the operating pressure to be 10 atm.  $T_f$  and  $T_i$  are taken as before, 42 and 38K respectively. Entering the various parameters we get  $\tau$  equal to 15.6 seconds. This is greater than the necessary 10 seconds.

#### 4. Pressure Drop Calculations.

To calculate the pressure drop in the shield we use the following equation for the friction factor,  $f$ .

$$f = .046 N_R^{-.2} = .044 \left(\frac{m}{\mu D}\right)^{-0.2}$$

The pressure drop will be given by

$$\begin{aligned} \Delta P &= 4f (L/D) \frac{\delta v^2}{2g_c} = \frac{.29L}{\delta D^{4.8}} \left[ \frac{\dot{Q}}{N(T_f - T_i)} \right]^{1.8} \frac{1}{2g_c} \frac{(k)^{0.2}}{C_p^2} \\ &= .17/D^{4.8} \text{ atm (D in cm)} \end{aligned}$$

If D is taken as one cm, the pressure drop will be .17 atm. The power loss due to this pressure drop is given by

$$W_p = \dot{V} \Delta P = \dot{Q} \Delta P / e C_p \Delta T = 1.94 \text{ kW}$$

The mass flow rate of helium will be 1.4 kg/sec and the volumetric flow rate will be 117 litre/sec which is equivalent to 11.7 litre/sec of liquid helium.

B. SUPERCONDUCTIVE MAGNET, CRYOGENIC DESIGN.

The cryogenic design of the magnet includes:

1. Composite Conductor Design
2. Heat load calculation
3. Helium requirement and flow.

1. Composite Conductor Design

Early in the system design the decision was made to use a conductor similar to the one used by Purcell in the 15 ft. NAL bubble chamber magnet. This conductor is a composite of Nb-Ti and C designed to operate at 5,000 amps in a He bath at 4.2K, and worst case conditions of superconductor temperature of 5.7K. Our present magnet design calls for four 20,000 A conductors to be wound in parallel to make an 80,000 A conductor. In order to determine the conductor dimensions necessary to carry 20,000 A, a simple extrapolation of the bubble chamber conductor was used. The conductor outline can be found in Figure IV-4. It will be made of two parts, the copper stabilizer section and the Nb-Ti copper composite section. The conductor will be wound with a .5 cm strip of stainless steel backing it up for additional strength. The stabilizer section will have a height to width ratio of 10:1. For cooling half of the front face, half of the edges, and none of the back face (because of the stainless steel strip) will be used. The cooling available to the conductor will be at least 1.56 W/cm (using Purcell's values) while the total heat load can only be 1.40 W/cm when the copper stabilizer is carrying all of the current; therefore the conductor is stable.

The extrapolation from the 5,000 A bubble chamber conductor size to the 20,000 A size can be done in two ways:

1. Hold the ratio of the volumetric power dissipation to surface area constant.

2. Derive a stability relation taking into account the heat transfer for each surface for this type of conductor and simply solve for the necessary conductor.

Both of these techniques lead to the same conductor, and both will be discussed here. In the first case, one equates the power/surface ratios for the two cases and solves for one dimension of the conductor. The power/surface ratio is

$$\frac{P}{S} = \frac{I^2 \rho}{2Hw(H + w)} \quad (4-6)$$

and with the substitution

$$w = kH \quad (4-7)$$

Equation (4-6) becomes

$$\frac{P}{S} = \frac{I^2 \rho}{2kH^3(1 + k)} \quad (4-8)$$

where in Equations (4-6), (4-7), and (4-8) P is the power dissipated per unit length by joule heating,  $\rho$  is the resistivity of the copper stabilizer at 4.2K, I is the current in the conductor, H is the height of the conductor, and w is the conductor width. Now writing Equation (4-8) for the 5,000 A and the 20,000 A conductors with the same ratios between height and width and with the same stabilizing material we find that

$$H(20,000 \text{ A}) = 2.52 H(5000). \quad (4-9)$$

Since  $H(5,000 \text{ A}) = 3.8 \text{ cm}$ ,  $H(20,000 \text{ A}) = 9.57 \text{ cm}$ . This is taken to be 10 cm for convenience of manufacture and safety. Then for the 20,000 A conductor:  $h = 10 \text{ cm}$  and  $w = 1 \text{ cm}$ .

The second method requires that the heat conduction for each surface be taken into account. In addition to the different heat transfer coefficients for each surface, the

fraction of each surface available for cooling must also be taken into account. For this design the back side of the conductor is not used for cooling because of the stainless steel reinforcing strip. Only half of the conductor edges may be used because of the micarta spacers between conductor layers, and only half of the front surface of the copper stabilizing strip can be used. In general, then the stability criteria is

$$H (2k^2 \eta h \cdot \Delta + kh_2 \Delta t \xi) + H^2 h_2 \Delta t sk(1 - \xi) \geq I^2 \rho \quad (4-10)$$

where

- k width to height ration  $w = kH$
- $\eta$  fraction of edge available for cooling
- $\xi$  fraction of front surface available for cooling
- s height of superconducting insert
- $h_1$  heat transfer coefficient for the front surface
- $h_2$  heat transfer coefficient for the edges
- $\Delta t$  temperature difference
- I conductor current
- $\rho$  resistivity of copper

Using

$$\begin{aligned} k &= .1 & h_1 &= .4 \text{ 2/cm}^2\text{K} \\ \eta &= .5 & h_2 &= .15 \text{ w/cm}^2\text{K} \\ \xi &= .5 \\ s &= 2.54 \text{ cm} \\ t &= 1\text{K} \end{aligned}$$

We can obtain the curve in Figure IV-5. This curve is a graph of the left hand side of Equation (4-10) as a function of H. If we now take Purcell's value of resistivity ( $3 \times 10^{-8} \Omega \text{-cm}$ ) for the copper stabilizer and the design value of 20,000 A, the  $I^2$  term is  $12 \text{ A}^2 \text{ cm}$  which corresponds to a height for

for the conductor of 9.7 cm which we increase to 10 cm for safety.

The two conductor design procedures outlined above have lead to the same conductor design as we expected.

The number and size of the superconducting filaments is chosen on the basis of several criteria; temperature rise in the superconductor at the worst case during current sharing, the amount of superconductor necessary to carry the required current at its maximum temperature, and the diameter of superconductor available. For a superconductor temperature rise of 1K above the copper temperature, we find that a minimum of 24 filaments is necessary; however if 15 mil. diameter Nb-Ti is used at a current density of  $70,000 \text{ A/cm}^2$  a minimum of 251 conductors is necessary to carry the current. Purcell used 15 mil. wire and 60 filaments at 5,000 A. Since this conductor will carry 20,000 A under the same conditions, we expect that there should be four times as many or 260 filaments which agrees very well with the other value of 251 filaments. In order to make a conservative design this conductor will have 260 filaments.

Although the conductor design has been fixed for this report, we feel that it is important to point out that other conductor designs should be considered before the final magnet design is fixed. These considerations may possibly lead to the following benefits:

1. Less stabilizer needed due to increased cooling efficiency.
2. D. C. magnet designs that approach the virial theorem limit due to increased conductor packing densities, and better use of the stabilizer or structural material.

Two possibilites along this line are:

1. Optimizing the present conductor design with respect to the size of the superconductor composite insert and face grooves.
2. Adding additional grooves along the conductor edges to increase the surface area.

In both cases the heat transfer characteristics must be compatible with the mechanical stresses, and of course, must be cryogenically stable.

## 2. Heat Load Calculations.

The heat losses to the superconducting magnet are:

- a. A. C. losses
- b. Conduction losses along the magnet supports
- c. Radiation losses
- d. Current leads losses.

The a.c. losses are mainly caused by a.c. current leaking to the superconducting magnet due to the finite resistance of the shield. These losses are divided into:

- i Eddy current losses in the normal conductors trying to shield their interiors.
- ii Eddy current losses in the normal conductors due to eddy current loops between the twisted filaments (twist losses).
- iii Hysteresis losses in the superconducting filaments.

Models for calculating each one of these a.c. losses are discussed in Appendix IV-A. The first one of these a. c. losses is given by

$$P \approx .5P_{\max} = \frac{2\pi^2 a A \rho}{\delta \mu_0^2} B_{\max}^2 \left[ \sum_{k=1}^m \left\{ \left( \frac{mk + 1}{m} \right)^3 + \left( \frac{m-k}{m} \right)^3 \right\} \right]$$

where  $a$  is the minor radius  
 $A$  is the major radius  
 $\delta$  is the skin depth  
 $\mu$  is the number of layers

$\delta$  is taken 1.5 cm.,  $B_{\max} = 99.1$  gauss, and  $n$  is equal to 6. Substituting these different values we get  $P = 147.2$  watts.

To calculate the twist losses, we first calculate the critical twist pitch,  $l_c$ .  $l_c$  is given by

$$l_c = \sqrt{\frac{\pi^3 \rho d}{16 B}}$$

where  $d$  is the diameter of the filament and is taken .038 cm. The max  $\dot{B}_a$  is about 36 gauss/sec. Taking  $\ell = 10^{-10}$  m,  $l_c$  will be 14 cm. In the present calculation the twist pitch is taken as 10 cm. The formula obtained for calculating the twist losses using the model discussed in Appendix IV-B is

$$P = \frac{2w^2 \rho^2}{e_i} A B_m^2 \sum_k \left\{ n_k \left[ \frac{\cos^2 \theta_k}{3} \right] \left( \frac{B_0}{B_m} \right)^2 + \left( \frac{B_1}{B_m} \right)^2 \right.$$

where

$w$  is the thickness of the conductor and,  $\rho_i$  some effective resistivity taken in the present case to be about  $10^{-10}$  m, and  $A$  is the major radius. The twist losses calculated from the above equation are 172 watts. These twist losses however, may have been overestimated for the following reasons:

1. No decay of the vertical component of the field has been considered. This may have a significant effect on the calculations.
2. The time constant of the twist eddy currents is approximately given by Morgan .

$$\tau = (2\ell/\pi)^2 \frac{\mu_0}{\pi\rho} \ln(2w/d)$$

where  $d$  is the diameter of the filament,  $w$  is the thickness of the conductor and  $\ell$  is the twist pitch. The time constant calculated from the above equation is 53 seconds and is larger than the cycle time. The power loss accordingly is expected to be smaller.

The hysteresis losses in the superconductor is found to be negligible (Appendix IV-C). The total a.c. losses, will be about 320 watts.

The conduction losses along the magnet support is calculated by taking the cross sectional area of supports about  $400 \text{ cm}^2$ , necessary for supporting the magnet at a stress level of 20,000 psi. The heat leak from 40K (the temperature of the shield) to the magnet assuming a supports lengths of 12 cm is 33 watts.

The radiation losses are calculated taking an average thermal conductivity between 40K and 4.2K of  $.15 \text{ w/cm K}$  and superinsulation thickness of about one cm. The radiation losses are estimated to be 15 watts.

For the current leads the losses are taken as 240 watts, four pairs of leads (1.5 mw/amp is assumed).

All the above losses add to 608 watts. Adding 82 watts allowance for a normal region, the total losses are taken to be 690 watts.

### 3. Helium Requirement and Flow.

The liquid helium required to fill the superconducting magnet cryostat, is estimated to be 20,000 litre. There will be a storage dewar to supply liquid helium to the magnet. The amount of liquid helium in the storage dewar is required to be 50,000 litre. This amount of liquid helium is enough to cool the magnet for 72 hours while the refrigerator is shut off for maintenance.

The number of helium vapour outlets is taken to be eight. The level of liquid helium at these outlets must be controlled so that it is 2 cm below the top of the magnet cryostat. In normal operation the helium velocity will be .02 m/sec and the level of liquid helium changes very little (.0025 cm lower at a point midway between two outlets). (See Appendix IV-D).

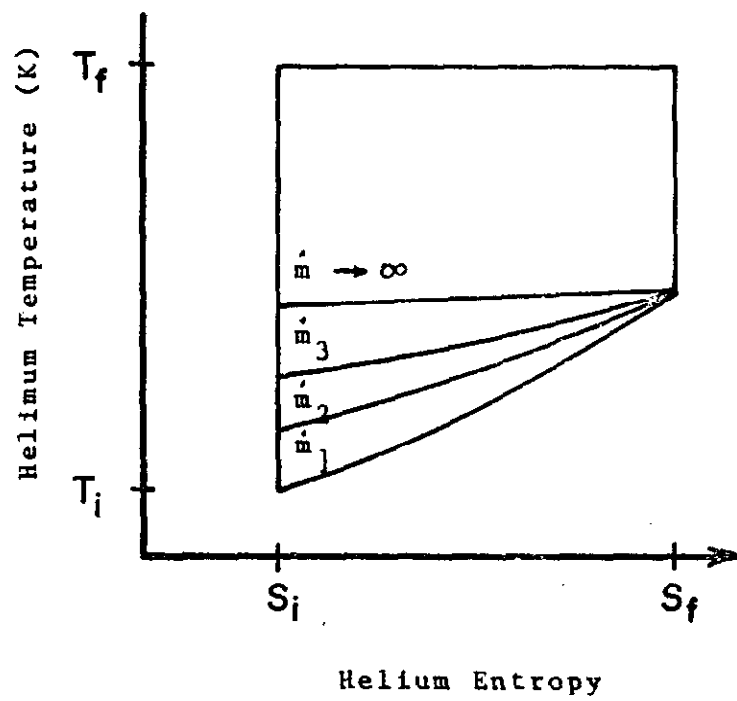


Fig. IV-1. Carnot cycle for helium in shield.

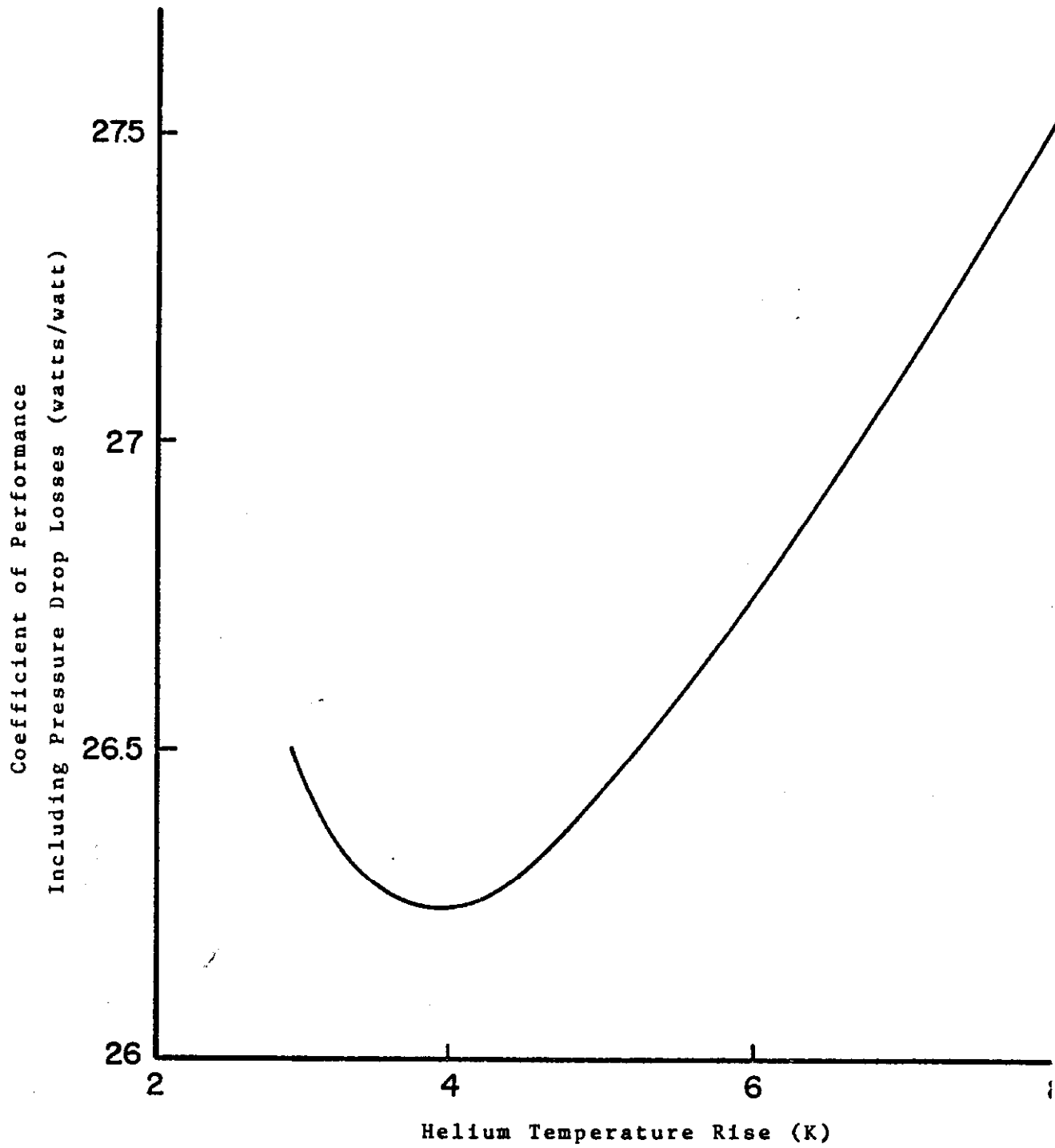


Fig. IV-2. Coefficient of performance including pressure drop losses.

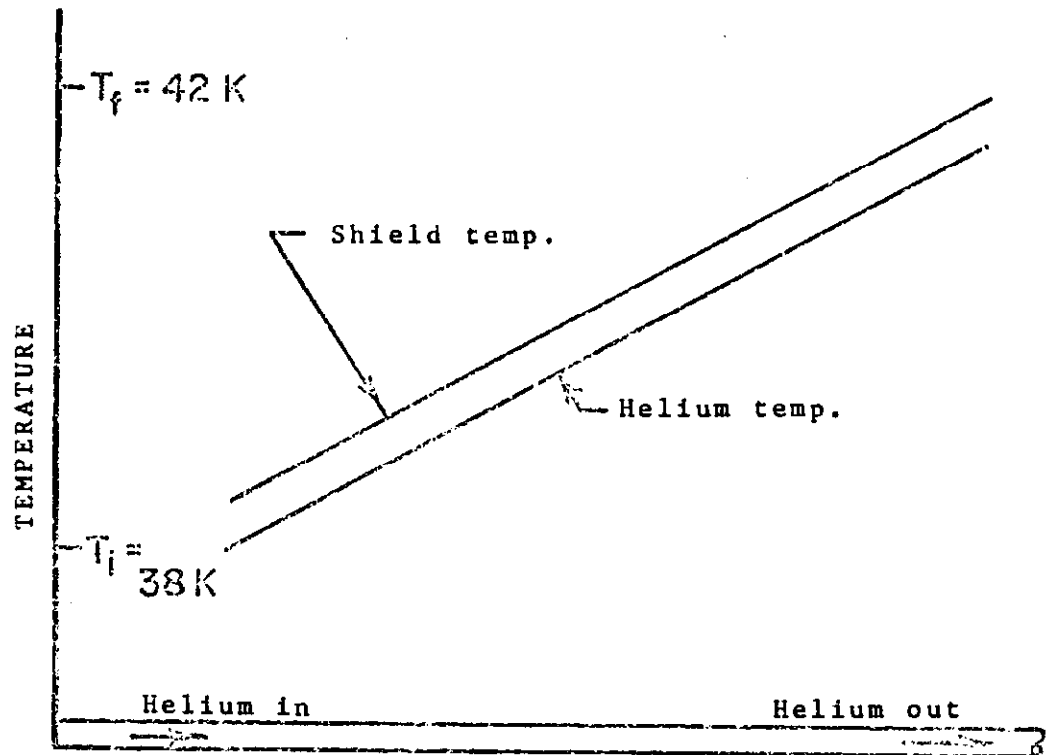


Fig.IV-3, Helium and conductor temperature in shield.

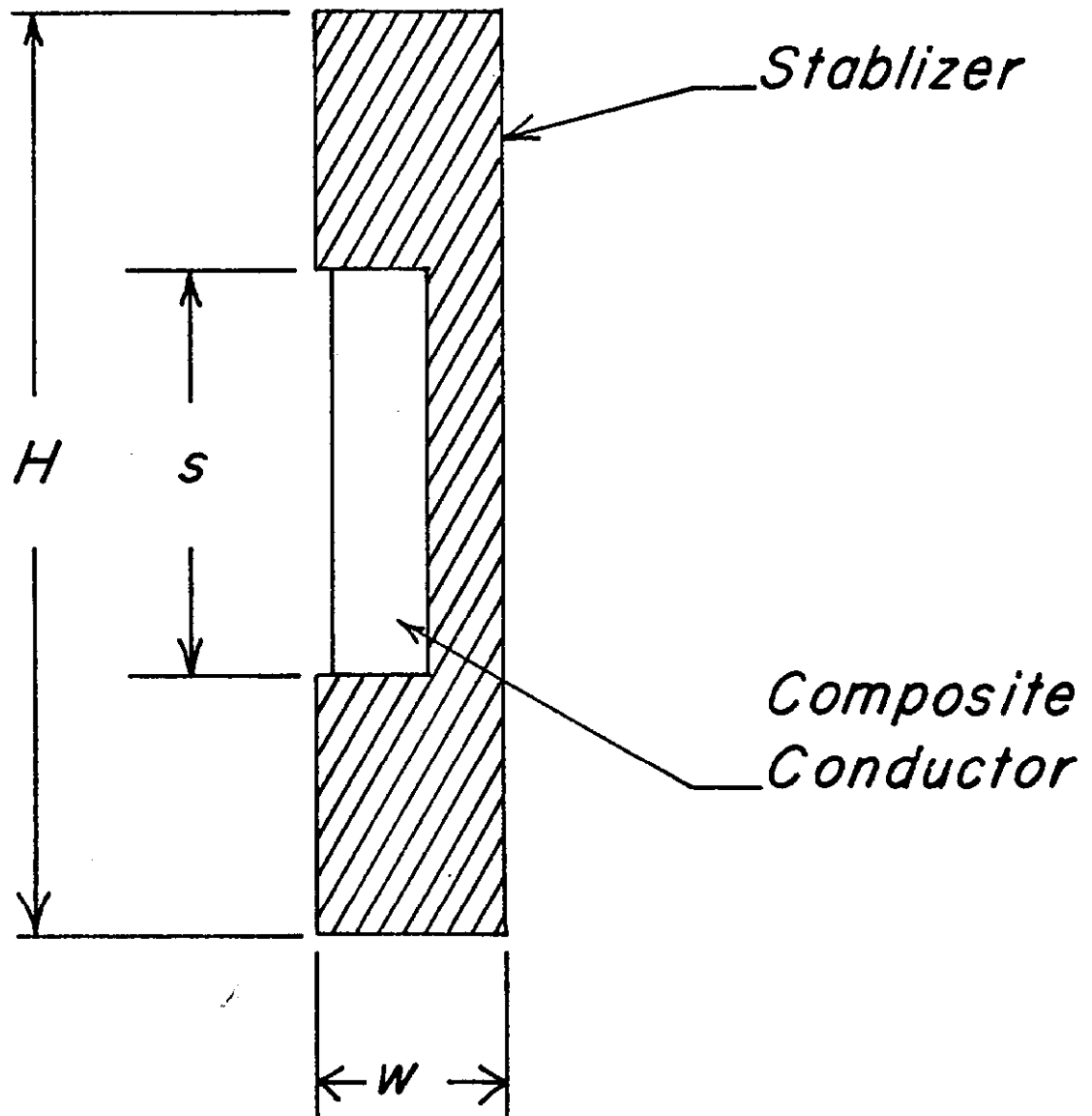


Figure IV-4. Composite Conductor Cross Section.

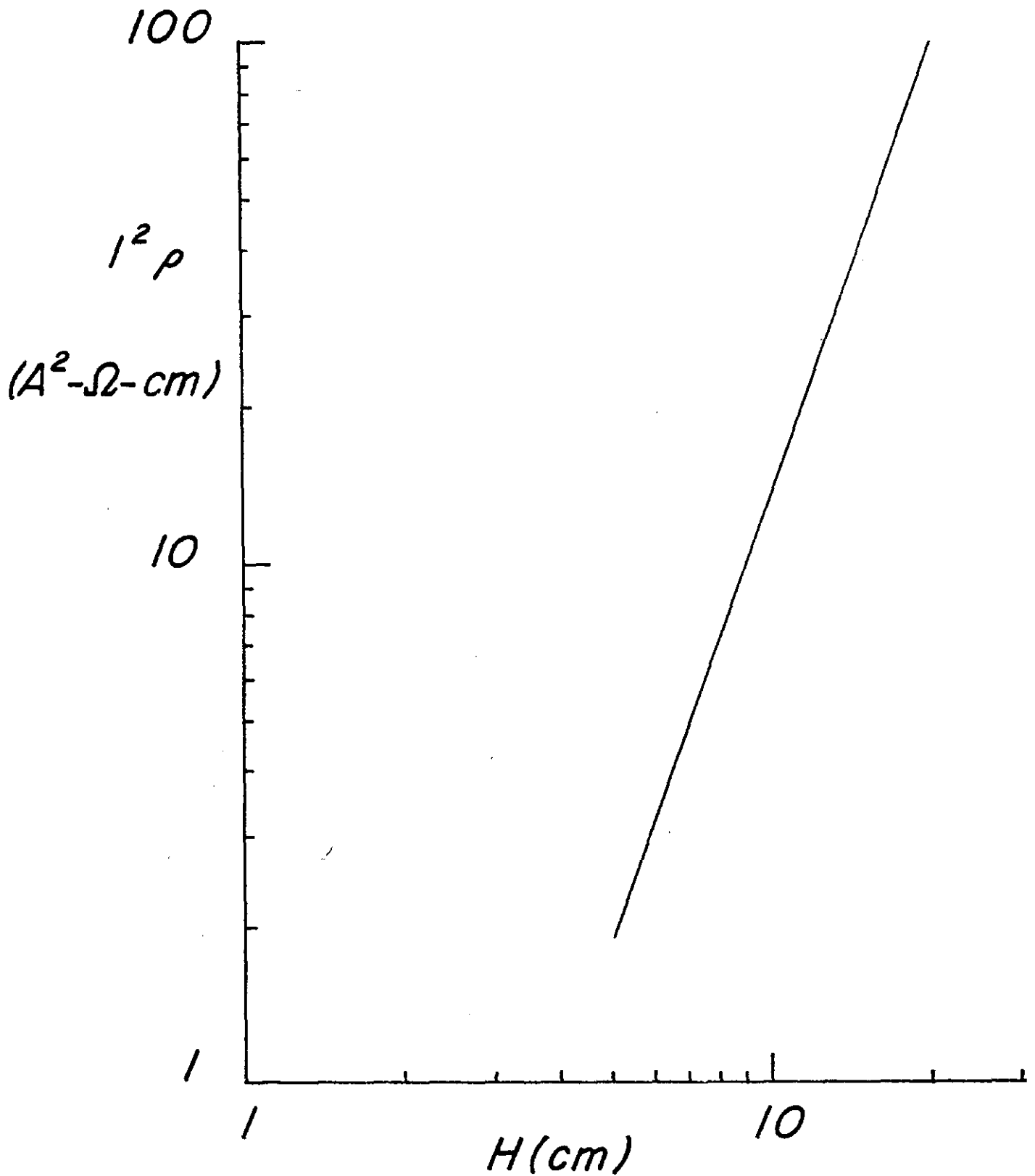


Figure IV-5. Stability curve for Purcell type conduction with a 10:1 height to width ratio, and copper stabilizer at 4.2 K. The height of the conductor is H.

APPENDIX IV-A  
AC LOSSES IN THE NORMAL METAL

To calculate the ac losses in the normal metal, the following assumptions are made:

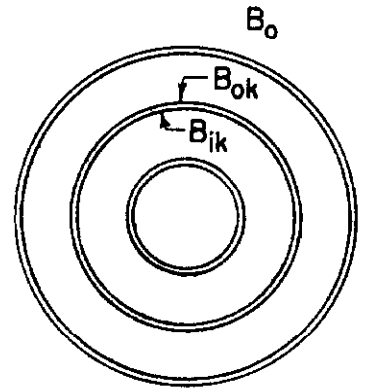
1. The conductors are arranged in circular layers as shown.
2. The r- component of the magnetic field has been neglected.
3. Each layer is considered thick enough so that the solutions on the two faces are independent.

Let us assume that the number of layers is  $m$ . For the layer  $k$ , the fields on the outer and inner surface are given by:

$$B_{ok} = B_o \frac{(m-k+1)}{m}$$

$$B_{ik} = B_o \frac{m-k}{m}$$

where



$B_{ok}$  is the field on the outside surface of the  $k^{\text{th}}$  layer.

$B_{ik}$  is the field on the inner surface of the  $k^{\text{th}}$  layer.

$B_o$  is the field outside the windings.

Subscript  $k$  is the number of the layer and equals  $m$  for the inside layer.

The total currents on the outer and inner surfaces of the  $k^{\text{th}}$  layer are given approximately by:

$$I_{ok} = \frac{2\pi a B_o}{\mu_o} \left[ \frac{m-k+1}{m} \right]^2$$

and

$$I_{ik} = \frac{2\pi a B_o}{\mu_o} \left[ \frac{m-k}{m} \right]^2$$

and the resistances of the inner and outer sides of the  $k^{\text{th}}$  layer are given by:

$$R_{ok} = \frac{\rho A}{a\delta} \frac{m}{m-k+1}$$

and

$$R_{ik} = \frac{\rho A}{a\delta} \frac{m}{m-k}$$

where  $a$  and  $A$  are the minor and major radii respectively and  $\delta$  is the skin depth.

The maximum instantaneous power corresponding to  $B_0$  is:

$$\begin{aligned} P_{\max} &= k (I_{ok}^2 + I_{ik}^2 R_{ik}) \\ &= \frac{4\pi^2 A a B_0^2}{\delta \mu_0^2} \left[ \sum_{k=1}^m \left\{ \left(\frac{m-k+1}{m}\right)^3 + \left(\frac{m-k}{m}\right)^3 \right\} \right] \end{aligned}$$

If the magnet is considered to be one layer, then the maximum power loss is:

$$P_{\text{one layer}} = \frac{4\pi^2 A a \rho a B_0^2}{\delta \mu_0^2}$$

Using the  $P_{\text{one layer}}$  form we get:

$$P_{\max} = P_{\text{one layer}} \left[ \sum_{k=1}^m \left\{ \left(\frac{m-k+1}{m}\right)^3 + \left(\frac{m-k}{m}\right)^3 \right\} \right]$$

The table below gives the summation of the above two series for different values of  $m$ .

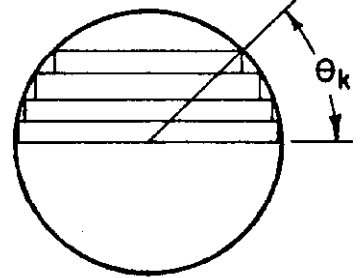
$m$	$(\frac{m-k+1}{m})^3$	$(\frac{m-k}{m})^3$	Total
2	1.125	.125	1.250
3	1.333	.333	1.667
4	1.563	.563	2.125
6	2.042	1.042	3.083
8	2.531	1.531	4.063
10	3.025	2.025	5.050
15	4.267	3.267	7.533
20	5.512	4.512	10.025

On noting that  $B_o = \mu_o \cdot NI/2\pi a$ , we can write the effective resistance due to ac losses as follows:

$$R_{ac} = \frac{N^2 A \rho}{a \delta} \sum_{k=1}^m \left[ \left( \frac{m-k+1}{m} \right)^3 + \left( \frac{m-k}{m} \right)^3 \right].$$

APPENDIX IV-B  
AC TWIST LOSSES

The magnet consists of many layers constructed as shown. On the surface of each layer there are two components of the field,  $B_x$  parallel to the surface and  $B_y$  perpendicular to the surface. The superconductor filaments inside a layer are about  $2\delta$  away from the surface and are assumed to be shielded from  $B_x$ .  $B_y$  is considered in calculating the twist losses.



Morgan's [1970] expression for a multifilament circular core is:

$$P' = \frac{D^2 \ell^2 \dot{B}_a^2}{\pi \rho_i}$$

where

- $P'$  is the average power loss/unit length
- $\ell$  is the twist pitch
- $D$  is the diameter of the cable of superconductive filaments
- $\rho_i$  is an effective resistance

To use the above expression  $w$ , the thickness of the conductor, is taken as  $D$ . Furthermore, an average  $\dot{B}_a^2$  is used.  $\langle \dot{B}_a^2 \rangle$  is given by:

$$\langle \dot{B}_a^2 \rangle = \frac{1}{n_k} \sum_k \langle \dot{B}_y^2 \rangle_k$$

where  $n_k$  is the number of conductors in the  $k^{\text{th}}$  layer.

and

$\langle \dot{B}_y^2 \rangle_k$  is the average of  $\dot{B}_y^2$  on the surface of the  $k^{\text{th}}$  layer

$(\dot{B}_y)_k$  at a particular  $x$  is given by:

$$(\dot{B}_y)_k = \dot{B}_0 \frac{x}{a} - \dot{B}_1$$

then

$$\begin{aligned} \langle \dot{B}_y^2 \rangle_k &= \frac{1}{2a \cos \theta_k} \int_{-a \cos \theta_k}^{a \cos \theta_k} \left\{ \dot{B}_0^2 \frac{x^2}{a^2} + \dot{B}_1^2 - 2 \dot{B}_0 \dot{B}_1 \frac{x}{a} \right\} dx \\ &= \frac{\dot{B}_0^2 \cos^2 \theta_k}{3} - \dot{B}_1^2 \end{aligned}$$

where  $a$  is the minor radius

and

$$(P')_k = \frac{w^2 \ell^2}{\pi \rho_i} \dot{B}_{\max}^2 n_k \left[ \frac{\cos^2 \theta_k}{3} \left( \frac{\dot{B}_0}{\dot{B}_{\max}} \right)^2 + \left( \frac{\dot{B}_1}{\dot{B}_{\max}} \right)^2 \right]$$

where

$$B_{\max} = B_0 + B_1$$

$n_k$  is the number of conductors in the layer  $k$

$\theta_k$  is the angle shown in Figure

The total power loss is given by:

$$P = \frac{w^2 \ell^2 A}{\mu \rho_i} \dot{B}_{\max}^2 \sum (n_k \left[ \frac{\cos^2 \theta_k}{3} \left( \frac{B_0}{\dot{B}_{\max}} \right)^2 + \left( \frac{B_1}{\dot{B}_{\max}} \right)^2 \right])$$

where  $A$  is the major radius

The effective resistance due to twist losses is

$$R_t = \frac{\omega^2 N^2 A w^2 \ell^2 \mu^2}{2 \pi^2 a^2 \rho_i} \sum_{k=1}^m n_k \left[ \frac{\cos^2 \theta_k}{3} + \left( \frac{B_1}{B_0} \right)^2 \right]$$

Morgan, G.H., "Theoretical Behavior of Twisted Multicore Superconducting Wire in a Time-Varying Uniform Magnetic Field", J. of Applied Physics, No. 9, 3673-3679, August 1970.

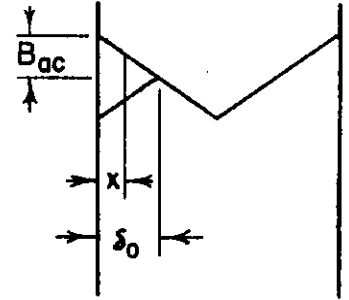
APPENDIX IV-C  
HYSTERESIS LOSSES

In order to estimate the hysteresis losses in the superconductor we simplify the problem as follows:

1. No normal metal is surrounding the superconducting filaments.
2. The superconducting filaments are arranged in circular rings.

We consider first the problem of a slab in an ac field. The energy loss (per cycle per unit area)  $\Delta E$  on one side of the slab is given by:

$$\begin{aligned} \Delta E &= 2 \int_0^{\delta_0} B_{ac} (1-x/\delta_0) (\delta_0-x) J_c dx \\ &= 2/3 J_c B_{ac} \delta_0^2 \end{aligned} \quad (1)$$



and the power loss is given by:

$$P/\text{unit area} = 1/3 J_c B_{ac} \delta_0^2 f \quad (2)$$

where

- $B_{ac}$  is the amplitude of the ac component of the field
- $\delta_0$  is the penetration depth
- $J_c$  is the critical current density
- $f$  is the frequency

We assume that the superconducting filaments are layers. Following the procedure used in calculating the losses in layers of normal metal, the total power loss for the  $k^{\text{th}}$  ring may be written as:

$$P_k = \frac{2}{3} 2\pi J_c f A \left[ (B\delta_0^2)_{ok} 2\pi a_{ok} + (B\delta_0^2)_{ik} 2\pi a_{ik} \right] \quad (3)$$

where

A is the major radius, a is the radius of the layer, and the subscripts  $_{ok}$  and  $_{ik}$  refer to the outside of the inside of the  $k^{\text{th}}$  layer.

We have

$$B_{ok} = B_{ac} \frac{(m-k+1)}{m} \qquad a_{ok} = a \frac{m-k+1}{m}$$

$$B_{ik} = B_{ac} \frac{(m-k)}{n} \qquad a_{ik} = a \frac{m-k}{m}$$

substituting we get

$$P_k = \frac{8\pi^2}{3} J_c f A a B_{ac} \left[ (\delta_o^2)_{ok} \left( \frac{m-k+1}{m} \right)^2 + (\delta_o^2)_{ik} \left( \frac{m-k}{m} \right)^2 \right] \quad (4)$$

and

$$\delta_{ok} = \frac{B_{ok}}{\mu_o J_c} \quad \text{and similarly} \quad \delta_{ik} = \frac{B_{ik}}{\mu_o J_c} .$$

To correct for having filaments instead of slabs, we take the current flowing on the surface of the slab to be the same as that flowing in the wires. This is done by changing the value of  $\delta_o$  to

$$\delta = \frac{\delta_o}{r}$$

where  $r$  is  $\frac{nd}{w}$ ,  $n$  is the number of filaments per conductor,  $d$  is the diameter of the filaments and  $w$  is the width of the conductor. Substituting  $\delta$  in terms of  $B_{ok}$  (or  $B_{ik}$ ) and  $J_c$  in equation 4 we get:

$$P_k = \frac{8\pi^2}{3} \frac{Aaf}{r} \frac{B_{ac}^3}{\mu_o^2 J_c} \left[ \left( \frac{n-k+1}{n} \right)^4 + \left( \frac{n-k}{n} \right)^4 \right] \text{ watts/layer}$$

and

$$P = \sum P_k \quad \text{total power for all layers.}$$

APPENDIX IV-D  
HELIUM VAPOR FLOW IN THE SUPERCONDUCTING MAGNET

Helium off-gas flows inside the magnet dewar are as shown in figure IV-D-1. The liquid helium level at all points should always be above the windings. The liquid helium level depends on:

1. Evaporation rate (losses)
2. Liquid helium level at inlet (this can be controlled, e.g., by controlling the level in the storage dewar).
3. The length of the helium vapor flow paths between outlets.

To determine the level approximately, we use the pressure drop equation in the following differential form

$$dP = 4f \frac{dx}{D_h} \frac{\rho_g v^2}{2}$$

where

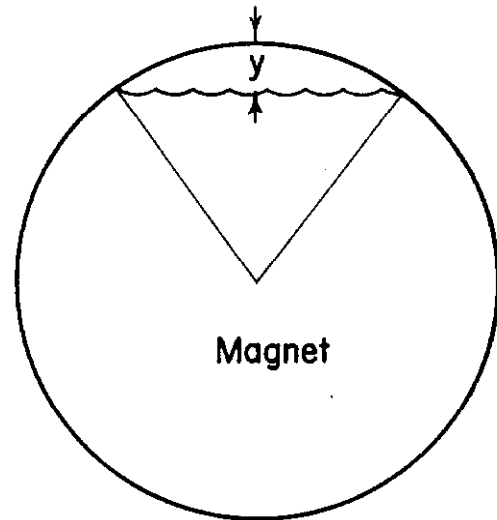
- $f$  is the friction factor  
 $D_h$  is the hydraulic diameter  
 $\rho_g$  is the vapor density.

From the cross section in the figure the velocity is:

$$v = \frac{\dot{m}(x_f - x)}{\rho_g \left[ a^2 \cos^{-1} \left( \frac{a-y}{y} \right) (a-y)(2ay-y^2)^{\frac{1}{2}} \right]} \quad (2)$$

where

- $x_f$  is the half distance between two outlets  
 $x$  is the distance from the inlet to any point  
 $a$  is the minor radius.



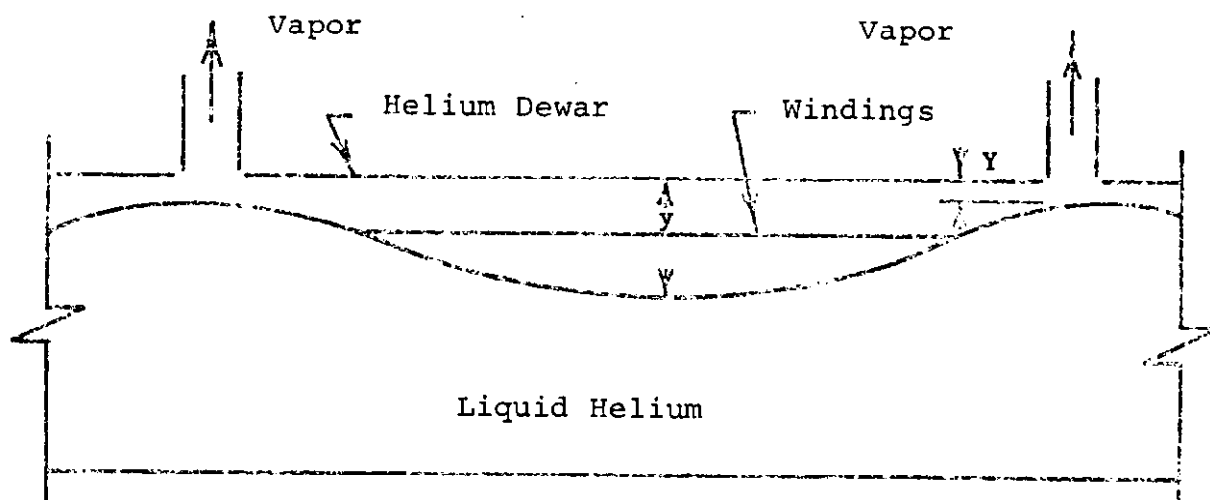
The hydraulic diameter is given by:

$$D_h = 2 \frac{a \cos^{-1}\left(\frac{a-y}{y}\right) - (a-y)(2ay-y^2)}{a \cos^{-1}\left(\frac{a-y}{y}\right) + \sqrt{2ay-y^2}} \quad (3)$$

and

$$d_p = -\rho_f g dy \quad (4)$$

where  $\rho_f$  is the fluid density. Combining equations 1, 2, 3 and 4 we get a differential equation for  $y$  at any point. Table IV-D-1 shows the depth of liquid helium between two inlets,  $y$ , for different number of inlets and outlets and for different exit depth.



$P = 2000 \text{ Watts}$

$f(\text{friction factor}) = .008$

No. of outlets	$Y = 1 \text{ cm}$		$Y = 2 \text{ cm}$	
	$Y, \text{cm}$	$v \text{ m/sec}$	$y, \text{cm}$	$v, \text{m/sec}$
1	5.04	1.845	5.05	0.654
2	3.19	0.923	3.26	0.327
4	2.03	0.461	2.34	0.164
10	1.23	0.185	2.03	0.065

Figure IV-D-1. Helium vapor flow in the superconducting magnet.

## V. - REAL AND REACTIVE POWER COMPENSATION

The equivalent representation of the proposed superconductive inductor and the NAL pulsed load connected to the power source is shown in Figure V-1. For the total 200 MW converter rated at 2500 volts and 80,000 amps, four 50 MW 625 V converters in series are envisioned to handle the peak inverse voltage as shown in Figure V-2.\* In the following analysis, the inductor current is assumed to be constant at 80,000 amperes at all times. The results are later modified in order to accommodate the 5% reduction in the inductor current for the 1 MWh unit during the ten second period.

Once compensation for the pulsed real power, which will eliminate the system frequency changes, is chosen to be the primary objective, one of the following two operating philosophies may be chosen in connection with the reactive power compensation:

1. To keep the total reactive power  $Q_T$  which is the sum of the reactive powers drawn by the NAL pulsed load and the superconductive inductor converters, to its minimum at all times. This will reduce the need for capacitive compensation for power factor correction. This is achieved by operating only those series converters needed to get the required voltage, others being bypassed. Further, only one converter which is on will operate with the variable control angle  $\alpha$ , the others which operate will be in full rectify (or invert).

2. To make the total reactive power  $Q_T$  a constant thereby eliminating the voltage flicker on the system. This objective is achieved by proper control of the firing pulses of the series converters, including the ones in the bypass mode. The fact that a bridge with the bypass thyristors on can be used for controlling the reactive power is illustrated

---

\*The basic theory of converters in power systems has been well developed in the books by Adamson and Hingorani (1960) and Kimbark (1971).

in Appendix V-A.

The resultant changes in total real and reactive power for each of these philosophies during 400 and 500 Bev operation are summarized in the Table below, as obtained from computer solutions. Graphical confirmation and the details are discussed in Appendix V-A. The effect of the 5% reduction in the inductor current during a ten second period can be compensated for by increasing the converter rating by 5%.

Table V-1

Comparison of the converter operation under the two operating philosophies for reactive power control.

NAL Operation in Bev		400 Bev	500 Bev
$\bar{P}_P$		56.5 MW	54.8 MW
$\Delta P_T \text{ max}$		0	49
Minimum $Q_T$	$Q_T \text{ min}$	29 MVA	29 MVA
	$Q_T \text{ max}$	145	184
	$\Delta Q_T$	116	155
Constant $Q_T$	$Q_T \text{ min}$	145	164
	$Q_T \text{ max}$	145	184
	$\Delta Q_T$	0	20

$\bar{P}_P$  = average of the pulsed real power for NAL load.

$\Delta P_T \text{ max}$  = maximum deviation of the total real power from  $\bar{P}_P$ .

$\Delta Q_T = Q_T \text{ max} - Q_T \text{ min}$ .

Note: As shown in the table above, the  $\Delta P_T \text{ max}$  remains the same regardless of how  $Q_T$  is controlled. This is due to the fact that compensation for the pulsed real power is chosen to be the primary objective.

Keeping  $Q_T$  to its minimum will result in reduced rms ratings for the converter transformers, a better average power factor for the AC system and reduced losses. On the other hand, if the voltage flicker caused by the change in  $Q_T$  is beyond the acceptable limits, it may become necessary to maintain  $Q_T$  as nearly constant as possible. Since the  $Q_T$  will now be higher than the average of  $Q_T$  in the previous case, the power factor correction can be made by shunt capacitors which will also act as filters for the harmonics generated by the converters.

#### REFERENCES

- Adamson, C., and Hingorani, N.G., "High Voltage Direct-Current Power Transmission," London, Garraway, Ltd., 1960.
- Kimbark, E.W., "Direct Current Transmission," New York, John Wiley & Sons, Inc., 1971.

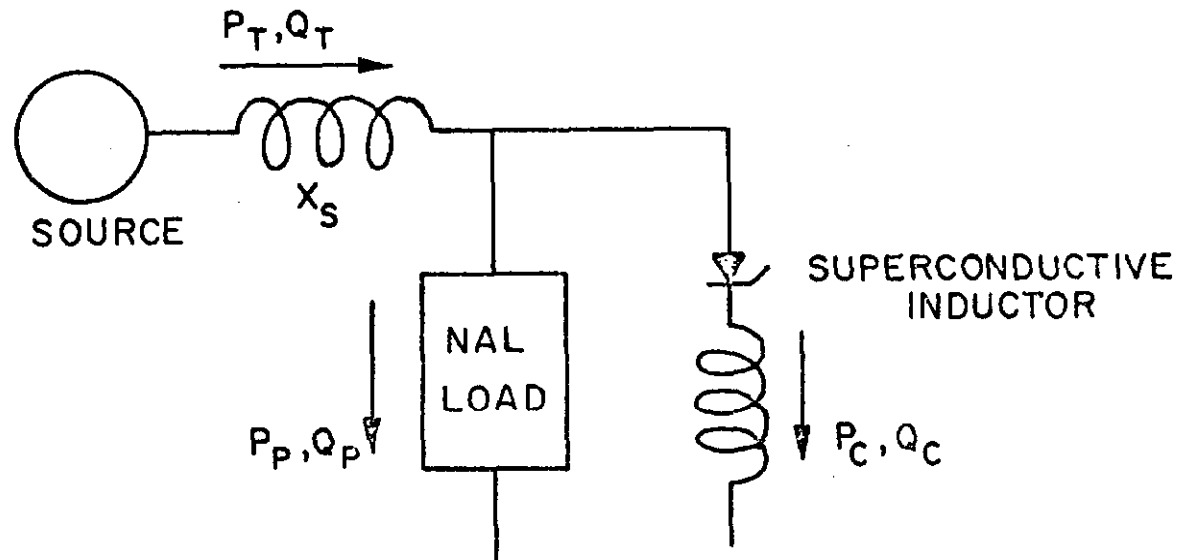


Figure V-1. Equivalent representation of the superconductive inductor and the NAL pulsed load connected to the source.  $X_S$  is the source reactance.

$P_P, Q_P$  = pulsed real and reactive power of the NAL load.

$P_C, Q_C$  = real and reactive power drawn by the inductor.

$P_T, Q_T$  = total real and reactive power drawn from the source.

$$P_T = P_P + P_C \text{ and } Q_T = Q_P + Q_C$$

Note: A positive value of  $P_C$  as shown signifies that the inductor is being charged whereas a negative value means that it discharges energy to the system.

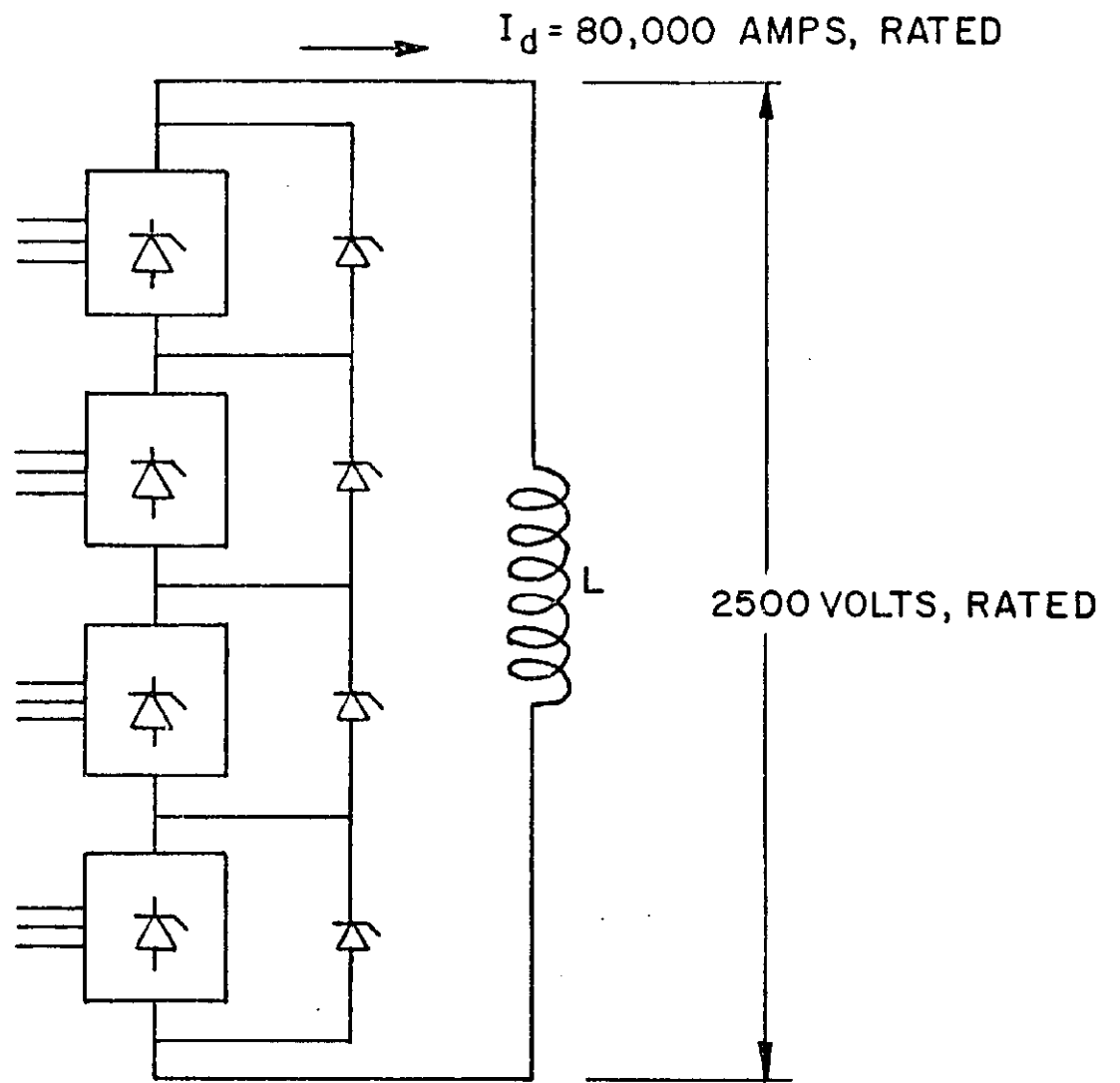


Figure V-2. NAL Proposed Four Converter Series Arrangement With Bypass Thyristors.

## Appendix V-A

### Reactive Power Control

The four series connected converters with the bypass thyristors are shown in Figure V-A-1. Each converter representation can be an equivalent of a number of bridges in parallel. The voltage and current rating of each converter is 625 volts and 80,000 amps.

Assuming a 0.2 pu commutating reactance for each converter on its own base, the maximum no load direct voltage across each converter will be 687.5 volts. In order to avoid commutation failure, the minimum angle of extinction during inverter operation is chosen to be  $10^\circ$ . This yields an operating range of -49 MW in full invert to 50 MW in full rectify for each converter, provided the inductor current remains constant at 80,000 amperes.

Before proceeding to the case of four converters in series, it should be pointed out that a single converter with its bypass thyristor on can be used for controlling the reactive power as shown in Figure V-A-2. The real power transfer across the converter is nearly zero. By properly controlling the firing pulses, a purely reactive current  $i_Q$  can be made to flow as shown in Figure V-A-2. The magnitude of  $i_Q$ , which directly relates to the reactive power drawn by the converter, can be varied in the range all the way from 0 to slightly less than  $I_d$  without turning the bypass thyristor off. In a practical situation, a very small inductance will always be present in the path of  $i_Q$  on the DC side and it can be shown that the control on the reactive power is achieved in the range all the way from 0 to the power rating of the converter, without producing excessively high harmonic magnitudes.

Figure V-A-3 shows the P-Q operating characteristics of the four series connected converters. For a single converter P-Q characteristic will be along the path M'M'M and when the converter is in the bypass mode, it will be along OM'.

The  $Q_C$  which is the sum of the reactive powers drawn by individual converters, is maximum along the arc EFG. This is achieved when all the converters are operated at equal delay angle  $\alpha$  thereby equally share the real power  $P_C$  and  $Q_C$  drawn by the total converter unit. The  $Q_C$  will be minimum along the solid lines GG'kk'LL'MM' etc. as shown in Figure V-A-3. This is achieved by operating only those series converters needed to get the required voltage, others being bypassed with zero reactive power. Further, only one converter will operate with the variable control angle  $\alpha$ , the others which operate will be in full rectify (or invert). It is possible to obtain any value of reactive power within the bounds of maximum and minimum values of  $Q_C$  by properly selecting the delay angle  $\alpha$  of each converter and also by using the bypassed converters to control reactive power.

Knowing the P-Q characteristic of the inductor-converter, the next step is to determine the total real and reactive power drawn from the source.

The pulsed NAL load with series capacitors can be represented on the P-Q plane by a load line OA as shown in Figure V-A-3. For a constant total real power drawn from the source,

$$P_C = P_{av} - P_p \text{ where}$$

$P_{av}$  = average of the pulsed real power ( $P_p$ ) since the average of  $P_C$  is zero (as the losses in the inductor-converter are assumed to be negligible).

According to the above relation, the load line OA is displaced by  $P_{av}$  to O'A'. This is valid for 400 Bev as well as 500 Bev operation since  $P_{av}$  in both cases is almost identical.

The maximum value of  $P_C$  required (in inverter mode) is given by  $(P_{Pmax} - P_{av})$ . So long as this required maximum is less than 200 MW (actually 196 MW since in inverter mode),  $\Delta P_T \text{ max}$ , the maximum deviation of the total real power from  $P_{av}$ , is zero. In Figure V-A-3, OB and OD are the maximum

values of  $P_C$  for 400 and 500 Bev operations respectively with the corresponding values of  $\Delta P_T \text{ max}$  equal to 0 and 46 MW.

Similarly, it can be shown that for 400 Bev operation, a constant  $Q_T$  (shown by  $Q_4$  in Figure V-A-3) equal to 148 MVA reactive, with  $\Delta Q_T$  equal to zero, can be drawn from the source. For the 500 Bev operation, the  $\Delta Q_T$  is 22 MVA reactive as shown in Figure V-A-3.

The computer calculations and the graphical results obtained from Figure V-A-3 for  $\Delta P_T$  and  $\Delta Q_T$  show a very close agreement.

The real and reactive powers drawn from the source are shown in Figures V-A-4 and V-A-5 respectively for 400 Bev operation. Figures V-A-6 to V-A-9 show the real and reactive powers drawn by the individual converters operating under the philosophy of keeping  $Q_T$  constant during 400-BeV operation.

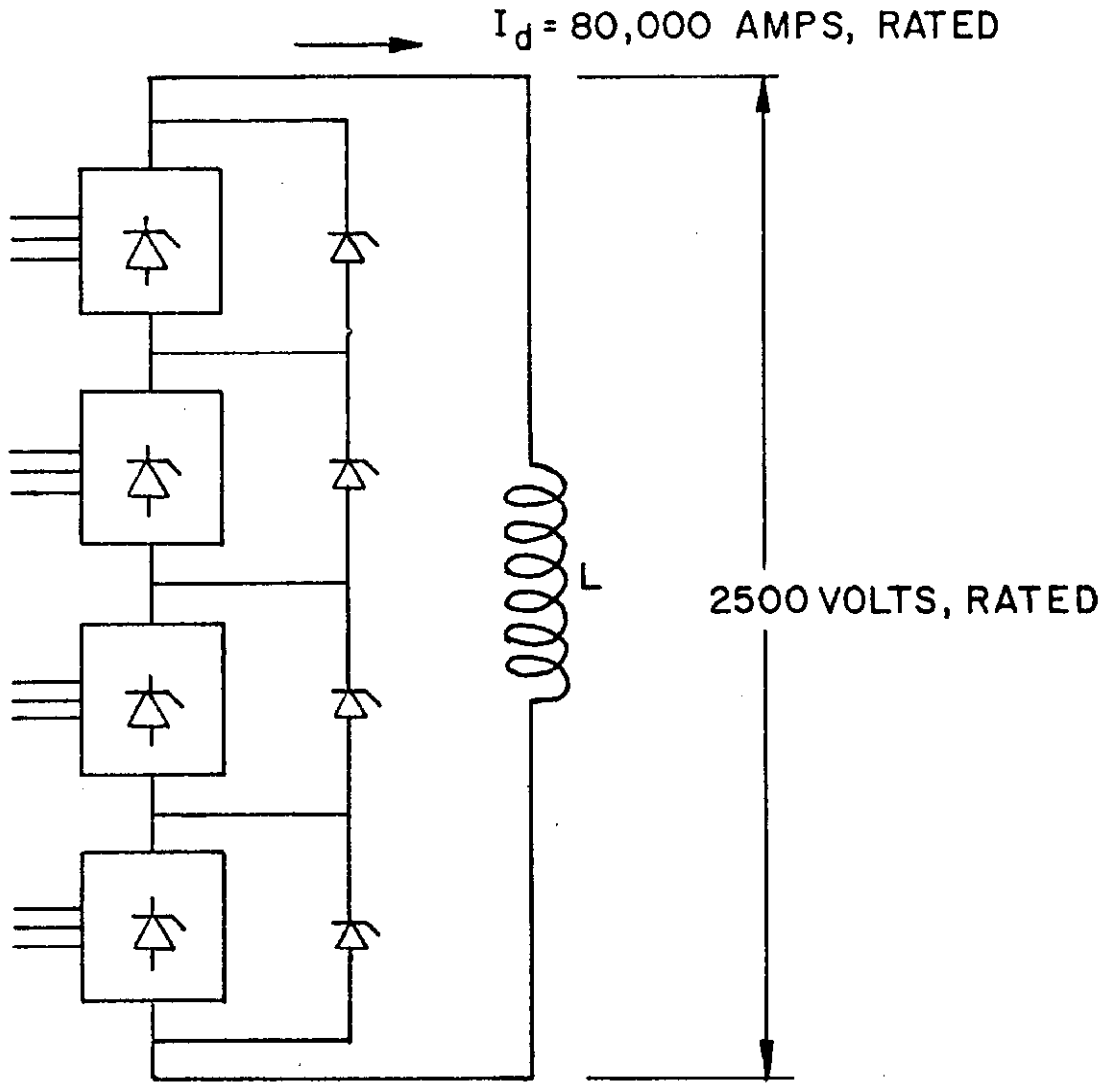


Figure V-A-1. NAL Proposed Four Converter Series Arrangement With Bypass Thyristors

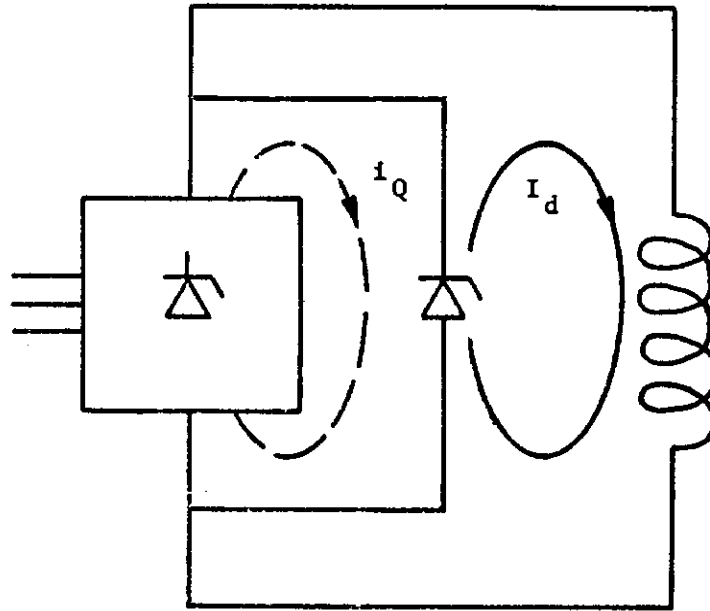


Figure V-A-2. Reactive power control by the converter bridge with the bypass thyristor on.



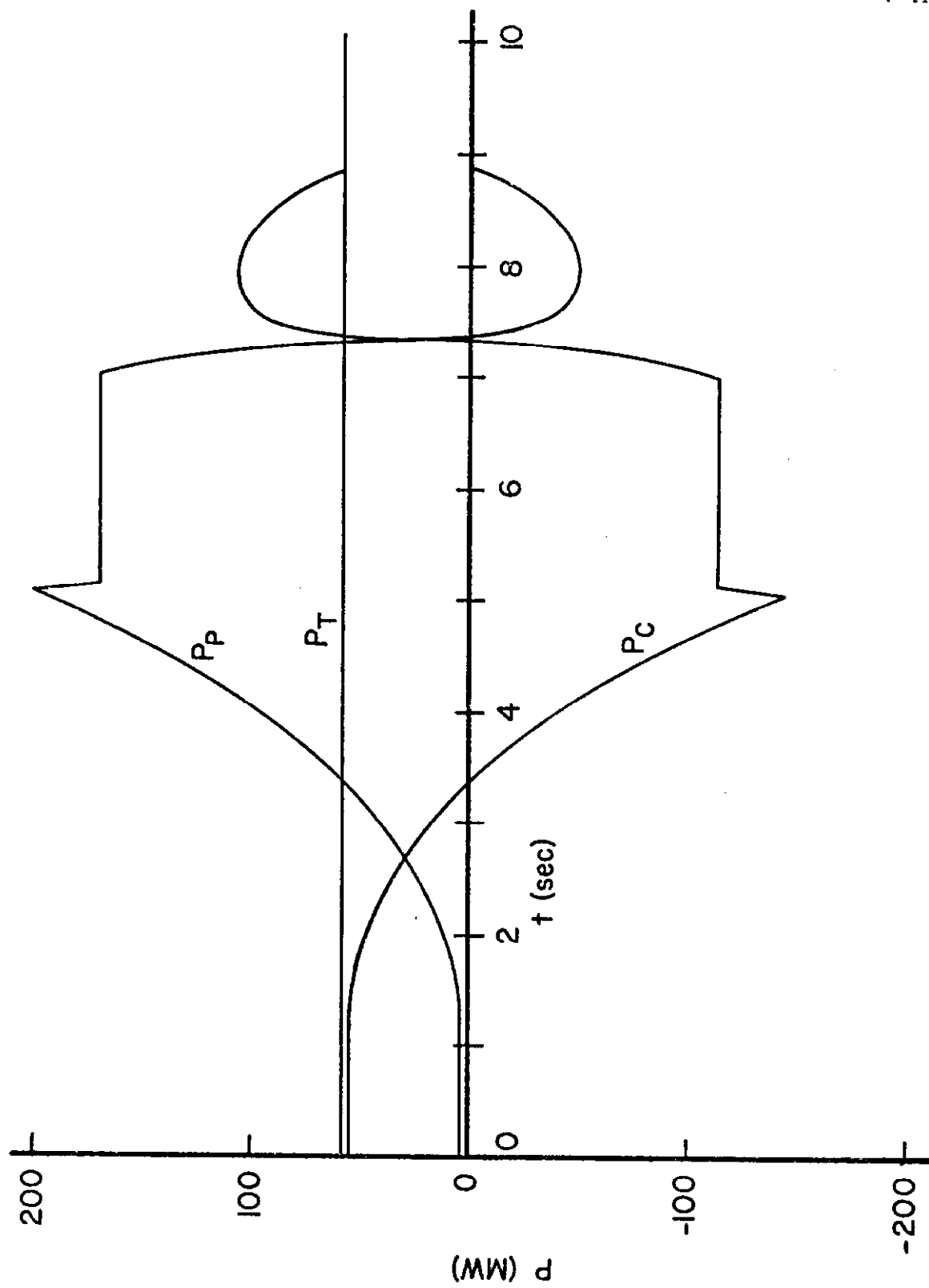


Figure V-A-4. NAL pulsed real power and the converter-inductor power requirement at 400 GeV. Total real power drawn from the source is constant.

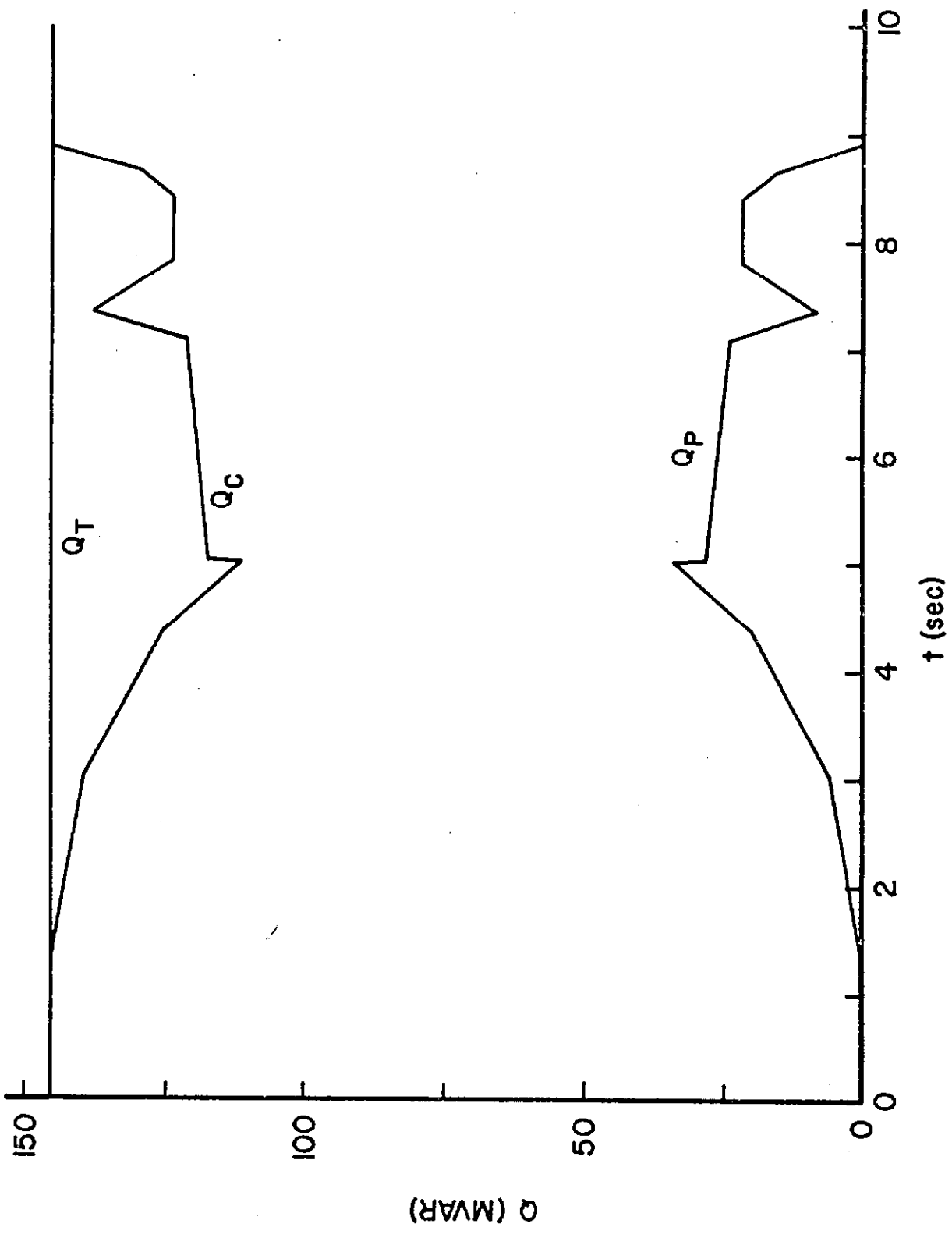


Figure V-A-5. Reactive power drawn by NAL pulsed load and converter-inductor. Total reactive power drawn from the source is constant.

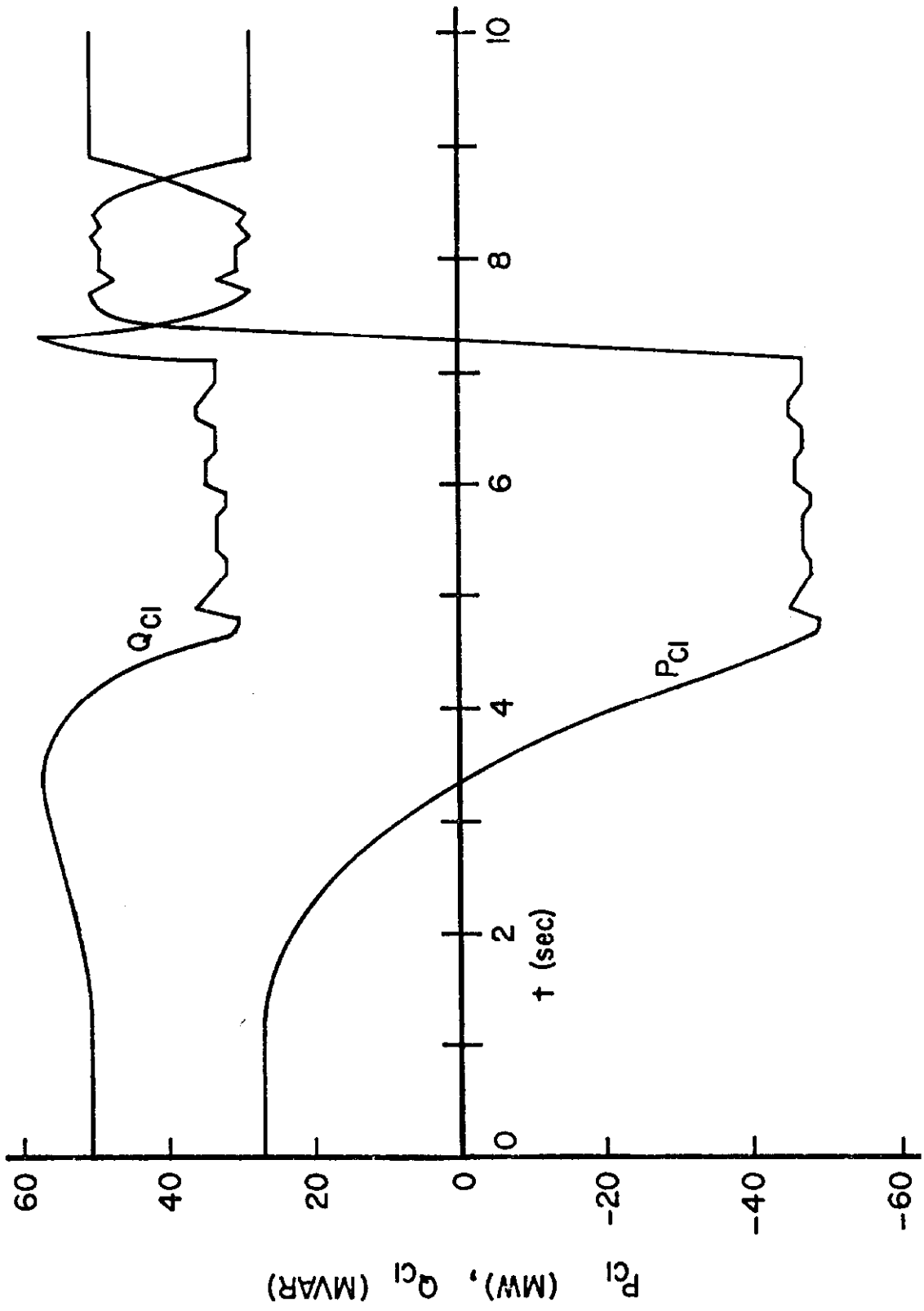


Figure V-A-6. Real and reactive power requirements on converter 1 at 400 GeV.

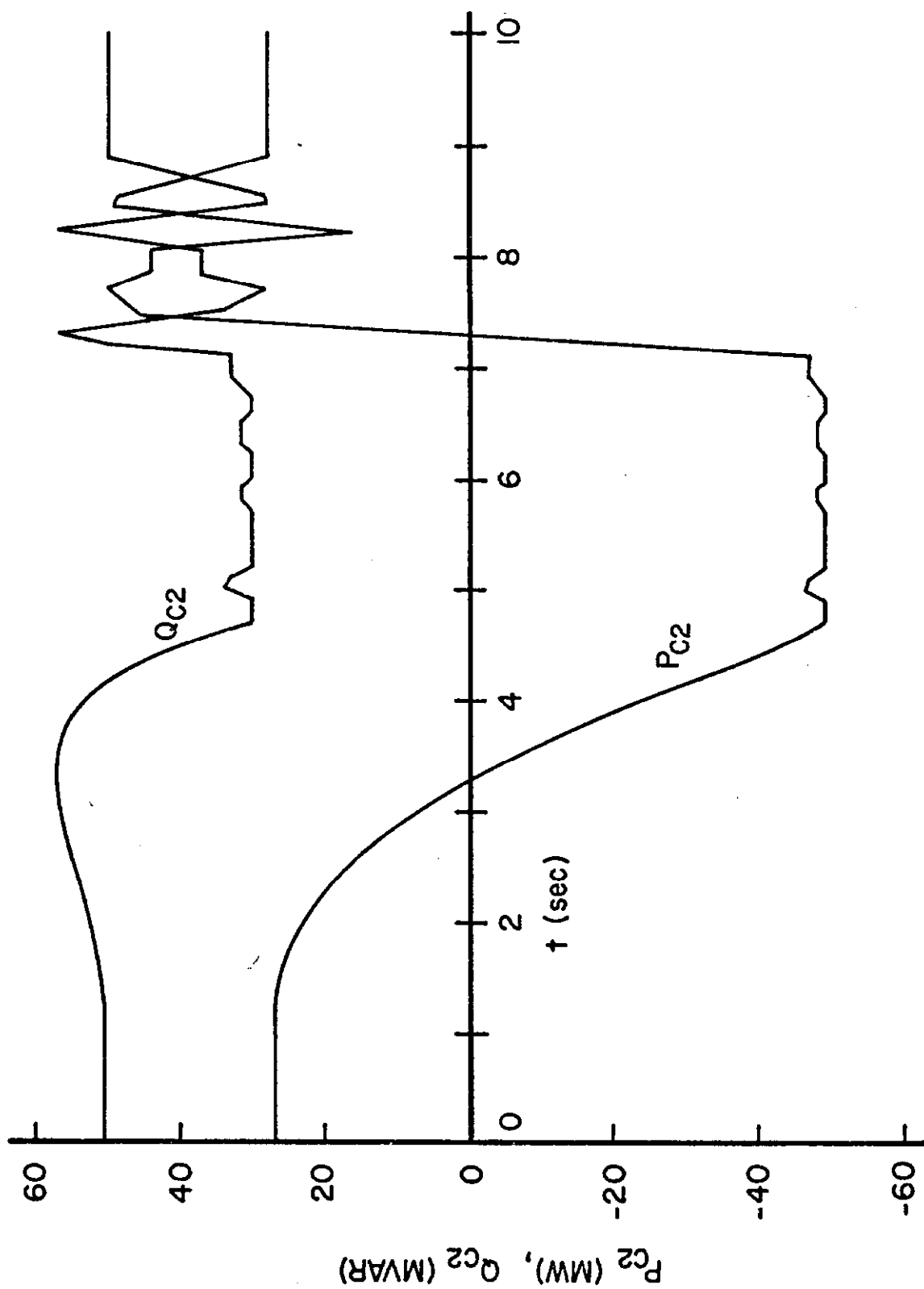


Figure V-A-7. Real and reactive power requirements on converter 2 at 400 GeV.

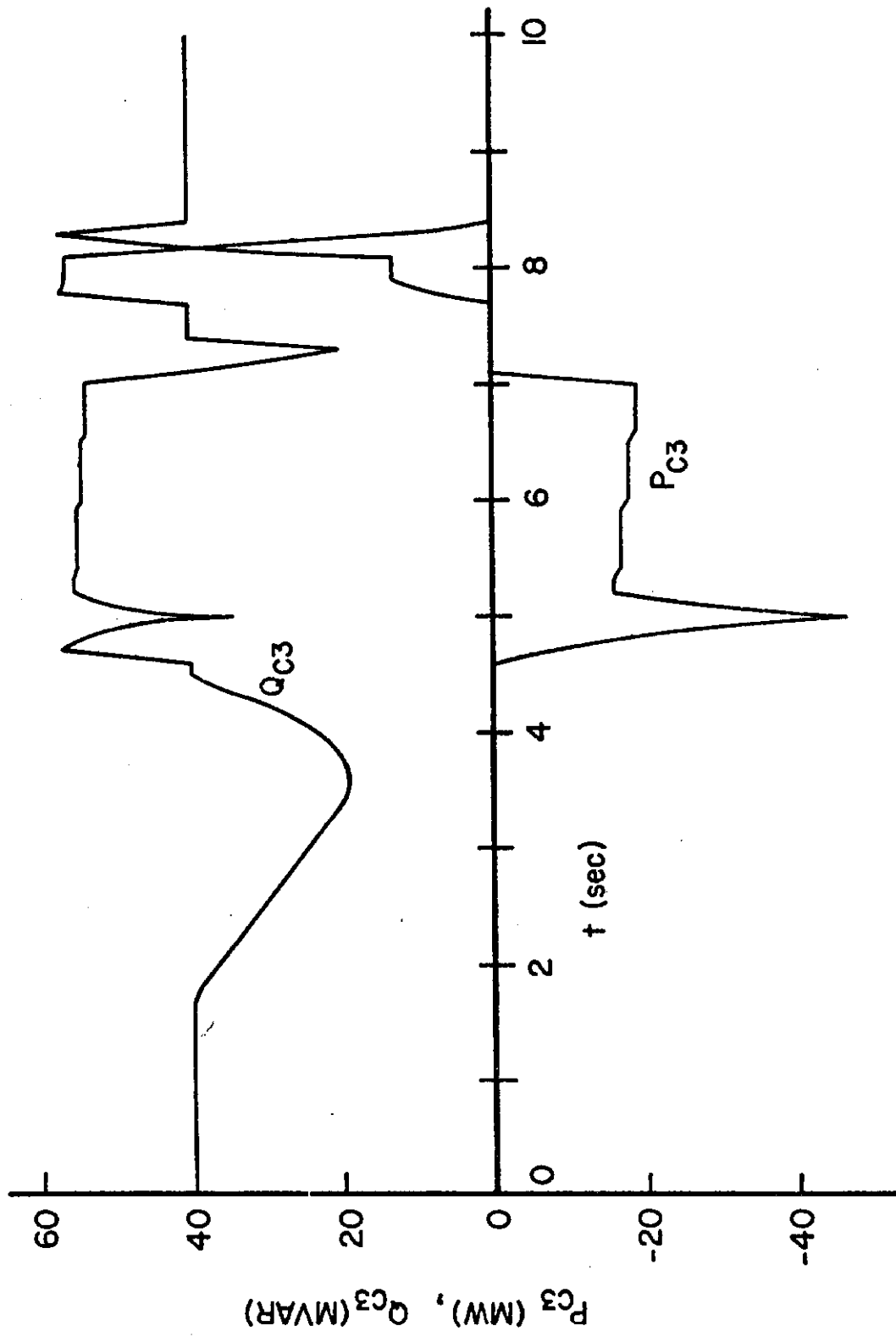


Figure V-A-8. Real and reactive power requirements on converter 3 at 400 GeV.

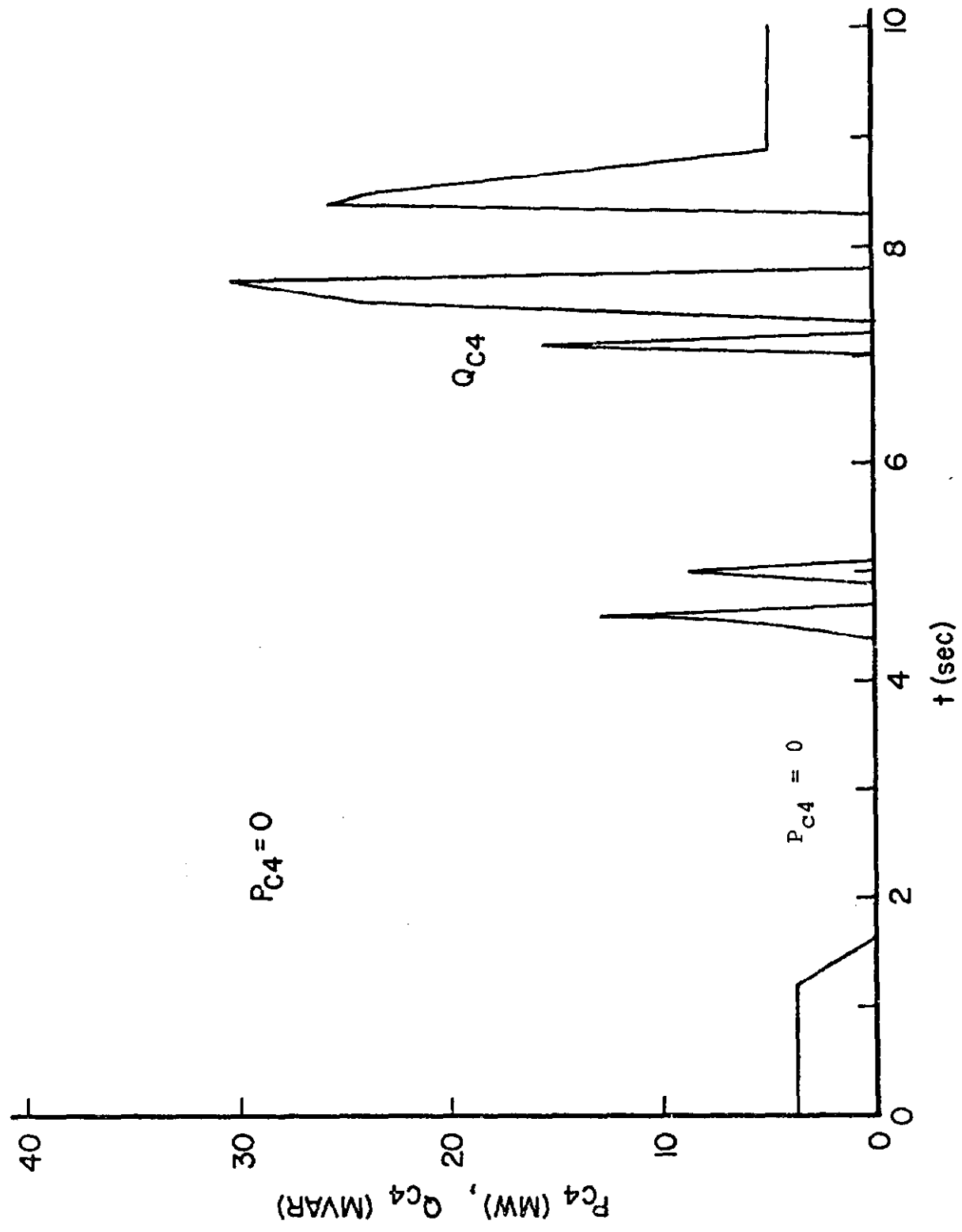


Figure V-A-9, Real and reactive power requirements on converter 4 at 400 GeV.

## VI - SYSTEM DESIGN

### A. D. C. MAGNET DESIGN

The following is a general discussion of the mechanical design of the DC magnet and the shield. The ideas and schemes presented here are preliminary and should only be considered as a starting point for a more detailed design.

The conductor which was chosen for the DC magnet is similar to that used by J. Purcell in the NAL 15-foot bubble chamber. Since this conductor will carry 20,000 A, four times greater than the NAL bubble chamber conductor, it was scaled up to insure that adequate copper was provided both from the standpoint of complete cryogenic stabilization as well as heat transfer area.

The final shape of the conductor is shown in Figure VI-1. It is 3.94 in. (10 cm) high and 0.44 in. (1.12 cm) thick. The superconductive bundle which is 1.0 in. (2.54 cm) high and 0.20 in. (.51 cm) thick is recessed in the copper such that its heat transfer surface is 0.1 in. (.25 cm) from the surface of the copper. It contains 240 15 mil NbTi filaments in a copper matrix which is soldered within the stabilizing copper conductor. The surface of the copper conductor has vertical cooling grooves 0.25 in. (1 cm) wide, spaced 0.25 in. (1 cm) apart and about 0.1 in. (.25 cm) deep. These grooves are on the same side as the superconductor and besides providing additional heat transfer area they also allow easy access of liquid helium to the superconductor as well as vertical venting of the boil-off gas.

Economic consideration dictated that the NAL bubble chamber conductor be fabricated from a soldered composite of several rectangular copper sections. However, from the quantities required for the pulsed energy storage system, it would appear that the copper could be rolled from a single section and there is no reason why the vertical cooling grooves could not be rolled in at the same time. A subsequent annealing operation would have to be performed to render the copper soft again.

In order to contain the hoop stress developed in the torus, it would be necessary to use 304 stainless strip wound in parallel with the conductor. This strip will have the same height as the conductor (10 cm) and will be .19 in. (0.5 cm) thick. Mylar insulation 20 mils (0.5 cm) thick will be placed on each face of the conductor making it possible to use continuous shortcircuit testing during winding.

It is contemplated that four conductors will be energized in parallel in order to provide a current bundle of 80,000 A. A total of 188 such bundles will be needed in the D. C. magnet. The rectangular shapes in Figure VI-2 represent 80,000 A bundles. The top layer shows the individual conductors in the innermost and outermost turns.

The forces on the conductor are always directed radially inward. It will be noticed in Figure VI-2 that the location of the superconductive bundle relative to the copper stabilizer changes as it proceeds from the inner to the outer radius of the layer. The superconductive bundle always faces outwards from the center of the magnet section so that the magnetic force will not dislodge it from the copper. Since there will be several splices of conductor within a single layer, a change in the orientation of the superconductive bundle will be made at the point where the magnetic field changes sign in that particular layer.

The major radius of the magnet is 29 ft. (8.85 m), and the minor radius is 27.2 in. (0.69 m). Taking into account the height of the conductor and using micarta (linen reinforced phenolic) spacers 5/8 in. (1.6 cm) thick between layers, it soon becomes obvious that 12 layers of conductors can best be accommodated within the specified minor radius dimension. Limited by the fact that 188 turns are needed and by the dimensional constraints of the conductors, the most suitable turn distribution which can be fitted within the 0.69 m radius circle is as shown in Figure VI-2. If we number the layers 1-12, starting with the bottom layer, then

the turn distribution is 8, 13, 16, 18, 19 and 20 in the 1st, 2nd, 3rd, 4th, 5th and 6th layers, respectively. The upper half of the layers is a mirror image of the lower half.

Winding the DC magnet is a formidable task. Generally speaking, there are two schools of thought regarding the winding procedure. The first one is to have a stationary winding form and revolving winding stations carrying the reels and all the other necessary hardware. The second is to have a revolving winding form and fixed winding stations. Both methods have merits and demerits, but on balance it would seem that the second method comes out ahead. This is particularly true when one contemplates winding the shield, a discussion of which is covered in section B of this chapter.

For the present, it will be assumed that the second method will be used. Since the complete magnet in its final form will weigh on the order of 640 t (580 mt), it will almost certainly be wound on the spot where it will be ultimately used. For this a foundation will have to be cast, and the floor of the vacuum chamber assembled and attached to it. The rails on which the winding form will ride can now be installed on top of the vacuum chamber floor and a carriage built to ride the rails. A guide post will have to be located in the center of the torus with spokes connecting it to the carriage. Synchronized motors located appropriately around the torus will be capable of driving the carriage in either direction by means of a rack and pinion system.

The winding form can now be assembled on the carriage. It will be made in sections for easy removal. As each layer is wound, more form sections are added on to prepare the base for the next layer, and so on.

In order to wind four parallel sets of conductors, it will be necessary to have four winding stations located appropriately around the torus. Figure VI-3 shows how this might be accomplished. Each station will supply a copper

conductor with the superconductor already in place, mylar tape, stainless steel strip and another mylar tape. As the form is rotated, each winding station lays down a single turn of conductor, reinforcing and insulation such that each revolution of the winding form will wind one complete 80,000 A turn.

Obviously, many splices will have to be made to complete a single layer. While a splice is being made either in the copper or the steel, tension will have to be applied to the form to prevent the windings from loosening. It is believed that an overlapping splice in the superconductor copper composite can be made without changing the shape of the cross section. This means that there should not be any bumps in the vicinity of a splice. Similarly, the steel can be butt welded and filed to insure a smooth transition.

After a complete layer is wound, the last coil has to be restrained to prevent unwinding. This can be accomplished by laying a thin steel tab across two major turns and tack welding it to the steel strips. After all the layers are wound and the magnet is banded, the tabs can be removed.

As the lower layers are being wound, additional form sections which will be flush with the coils will have to be added on the outer periphery. These are needed to provide a base for subsequent layers which overhang the preceding ones.

As each layer is completed, micarta spacers are laid radially across its face covering 50% of the surface. These spacers are  $5/8$  in. (1.6 cm) thick and 2 in. (5.1 cm) wide. They will have to be fixed so as not to be dislodged when the next layer is wound.

The second layer will have to be wound with the form rotating in the opposite direction from the first. Each subsequent layer will also alternate directions. This, of course, has to be done to keep the current going in the same direction as it goes from layer to layer. Figure VI-4 shows a scheme for making electrical connections between layers.

This scheme achieves decoupling of the 4 conductors.

A two-dimensional program was used to calculate the hoop stresses in the windings due to the magnetic loading. It should be pointed out that stresses due to cool down and due to vertical loading are not included in this analysis. Figure VI-5 shows the hoop stresses in the steel, copper and mylar in the 6th and 7th layers (considered as the median plane) as functions of the radial distance from the inner to the outer radius. Maximum stresses occur on the median plane at the inner radius and are  $\sim 10,500$  psi ( $7240$  N/cm<sup>2</sup>) in the steel,  $5650$  psi ( $3894$  N/cm<sup>2</sup>) in the copper, and  $580$  psi ( $400$  N/cm<sup>2</sup>) in the mylar. The same graph also shows the magnetic field strength along the median plane. Note that the field reverses sign slightly past midway through the layer. This would be the point at which the superconductor location relative to the copper conductor will be reversed as mentioned previously.

After the twelve layers of superconducting coils are wound on the winding form, they will have to be banded together into a rigid homogenous unit. Specially shaped mica spacers will be placed at the inner and outer radii of each layer. These spacers will be used only at the banding locations and will provide a circular surface for the bands. A thin layer of Teflon sheet will then be wound around the spacers and the bands placed over it. This will reduce the friction between the band and the spacers, making it possible to produce a tight bundle.

The bands will be spaced about a meter apart along the average major radius of the torus, making a total of 57 bands. They will be made of stainless steel, 1/2 in. (1.27 cm) thick and 6 in. (15.2 cm) wide. As conceived, the bands will be assembled from two halves, and will present a

circular surface on their outer side. The four 1/2 in. Allen head bolts which are used to tighten the bands together will have recessed heads. This design will facilitate the construction of the liquid Helium containment dewar around the superconducting magnet. Every third band will have a ledge cast into it with provision for mounting legs in it which will ultimately support the DC superconducting magnet. These details can be seen in Figure VI-7.

In order to be able to assemble the bands around the coil bundle, it will be necessary to remove portions of the winding form. This will have to be done progressively until all the bands are in place and tightened down.

The final step in the construction of the DC magnet is the liquid Helium containment dewar. It will be made of 1/16 in. (1.6 mm) 304 SS and will come in the form of horizontally split torroidal sections (as shown in Figure VI-7). The length of the sections will depend on fabrication capability but for the present we will assume that each section will cover three meters such that there will be a circumferential seam on top of every third band. Horizontal welds along the inner and outer radii will join the two halves together and circumferential welds will join adjacent sections.

Figure VI-8 shows the rectangular holes cut out of both sides of the lower half section where the support ledges on every third band will protrude as is shown in Figure VI-7c. Welding around the edges of the rectangular opening to the band provides the seal for the dewar.

There will have to be an insulated gap at some point on the dewar to prevent eddy currents from materializing. Several methods can be used to accomplish this and we will not elaborate on that point. Figure VI-6 also shows the vent tubes which are oval shaped and located at the top of the dewar. They are shaped this way to minimize the spread of the shield conductors. All the necessary connections to the DC magnet

will be made through such openings at the top.

Again it is obvious that in order to assemble the dewar sections it will be necessary to remove large portions of the winding form. It might be prudent at this time to think about how the magnet will be supported while the shield shell structure is assembled and the shield coils wound. Placing the magnet on mechanically synchronized jacks located under the bands will make winding the shield coils much easier. Let us say that 19 40-ton (36.2 m tons) jacks will be used, each one located under every third band starting with one not equipped for supporting the DC magnet. The total weight of the DC magnet and its shield is  $\sim 640$  tons (580 m tons), so that when completely assembled, each jack will carry 34 tons (30.8 m tons). The weight of the DC magnet itself is  $\sim 580$  tons (525.5 m tons).

The jacks will need special heads for spreading the load through the dewar and onto the band. The heads will also have provisions for supporting the shield toroidal shell reinforcing rings. Once the magnet is lowered onto its permanent legs, the heads of the jacks should be capable of being retracted and the jacks removed altogether.

#### B. SHIELD DESIGN

To minimize the radiant heat transfer between the 40 K shield and the 4.2 K DC magnet dewar, it will be necessary to superinsulate on the outside of the dewar. This can be accomplished fairly easily by simply wrapping aluminized mylar bandage-wise all the way around the magnet.

Since energy will be taken from and returned to the shield, the coils will experience a pulsing force which when distributed over the whole toroidal shell will amount to a pressure of  $\pm 75$  psi ( $51.7 \text{ N/cm}^2$ ). It has been decided that this pulsing load should not be transmitted to the DC magnet and this then dictates that the shield should be completely self-supporting.

If one were to design a toroidal shell capable of sustaining a pulsing compressive pressure of 75 psi, he would need a wall thickness of  $\sim 0.7$  in. (1.8 cm) assuming he used a material of modulus  $30 \times 10^6$  psi ( $20.7 \times 10^6$  N/cm<sup>2</sup>). This would end up weighing  $\sim 47$  tons (42.6 m tons).

In this case it was decided to use reinforcing rings, again, spaced every meter. On further thought, it became apparent that these rings could also be used as the means of transferring the weight of the DC magnet through the shield windings to permanent legs as is shown in both Figures VI-2 and VI-6.

The reinforcing rings will be 1 in. (2.5 cm) thick, 2 in. (5.8 cm) wide 316 SS. Every third ring, which will be located under the special bands equipped for carrying the DC magnet, will also have ledges on both sides of it to receive the other end of the DC magnet support rod. At the same location, a foot will extend out radially through the shield windings, terminating in a specially designed socket for transferring the load to the permanent leg (see Figure VI-9). From Figure VI-6 it can be seen that each load bearing ring will have two DC magnet support rods on each side of it. With 19 load bearing rings around the machine, there will be a total of 76 support rods. These rods will be solid 1 in. (2.5 cm) diameter 316 SS, approximately 5 in. long.

The shield reinforcing rings will also be made in two halves. They will be assembled around the DC magnet and welded together in place.

The toroidal shell which ties all the reinforcing rings together can now be installed and welded to the rings. This shell will be 1/4 in. (0.64 cm) thick 304 SS. It will not be vacuum tight, as a matter of fact, it will have to have holes in it so that the region inside it can be pumped out.

Sections of this shell can be made in much the same way as the Helium dewar shown in Figure VI-8. The ends will overlap the load bearing rings and be welded to them. In order to attach the shell to the intermediate rings, it would be possible to drill holes through it at the location of the ring and weld through the holes. It may also be possible to bolt them together, however the bolt hole would weaken the reinforcing ring. The combined moment of inertia of the shell and the ring can withstand the bending moment from the DC magnet supports.

It has been mentioned earlier that the jacks which will support the DC magnet will have provisions for supporting the shield structure as well. As the shield shell is assembled, the DC magnet support rods can be inserted progressively until they are all in place. The shield structure is now attached to the DC magnet through the rods but the jacks are still holding up the whole magnet. The weight of the shield shell and the reinforcing rings is  $\sim 20t$ , (13,8 m tons) which is less than half of what a solid shell would have weighed.

The shield coils can now be applied to the shell. Although the locations of the windings has been precisely determined on the computer, it is difficult to imagine how to machine slots on the shell for them to fit into. As presently visualized, studs will be welded to the shell at appropriate locations and these will be used to hold the windings in place temporarily. Once the whole shield is wound, then other means can be employed to ensure the stability of the windings.

The shield conductor is made of rectangular electrical grade Al, 0.6 in. (1.5 cm) thick and 2.4 in (6 cm) high. A 0.4 in. (1.0 cm) diameter hole is extruded in the conductor on the far end away from the shell. Helium gas at 40 K will be circulated through the coils to supercool them and

reduce their electrical resistance. At the same time, this 40 K surface acts as a thermal barrier between the Helium dewar at 4.2 K and the room temperature vacuum vessel. There will be  $3.35 \times 10^4$  ft. ( $1.024 \times 10^4$  m) of conductor in the shield weighing  $\sim$  25t (22.7 m tons).

The ideal way to wind the shield conductor would be to have a fixed winding station and a rotating magnet as described previously. The conductor would have to pass through rollers which will curve it to the proper curvature commensurate with its location on the toroid. At another point in the station the conductor is wrapped with B cured epoxy glass insulation. Then, by using micarta spacers machined in many different sizes, the conductor will be properly spaced and located on the toroidal shell and attached by means of the welded studs (see lower left corner of Figure VI-2). This process will continue until the whole shield is wound except at the lowest point where the jacks are located. The windings will be added on after the jacks have been removed and the magnet placed on its permanent legs.

From Figure VI-2 it is obvious that some of the windings will have to be displaced from their locations in the region of the legs and at the top where all the vent lines, electrical leads and the other pertinent connections will be made. The effect of this displacement on the shielding ability of the shield will have to be determined.

The problem of splicing conductor together needs to be studied very carefully. Not only electrical integrity has to be maintained but the flow of Helium gas must not be impeded and the splice should be mass-spectrometer tight. Electron beam welding may be the method to use here. Procedures will have to be developed to have the splice X-rayed and leak checked on the spot before the conductor is insulated.

Additional micarta spacers will now have to be added

between turns over the whole shell to secure them against the possibility of moving relative to each other. Once this is done, the whole bundle can be banded and completely wrapped with B cured glass taped into a structure strong enough to withstand the hoop stress developed by a pressure of 75 psi.

At this point the jacks will be lowered, the carriage and rails disassembled, and the magnet supports installed. As mentioned previously, the feet sticking out of the shield windings will have special tapered sockets machined in them. A similar tapered socket will exist in the support leg. To make a flexible support capable of adjusting to the shrinkage of the magnet at cooldown, a rectangular key with rounded ends is placed between the magnet foot and the permanent support as is shown in Figure VI-2. There will be 38 such keys around the machine. A substantial moment can be transmitted through the key to the leg and this will have to be accommodated within the design of the leg. As visualized, the legs will be made of G-10 in order to reduce the heat leak from the ground to the 40 K shield.

The Helium gas manifolds can now be installed and connected to the conductor. The location at which this will be done must obviously be left unwrapped. The manifolds will be tubes  $\sim$  2.5 in. (6 cm) in diameter and will run perpendicular to the conductors as shown in Figure VI-10. There will be a supply and a return manifold located next to each other. Every other conductor will be alternately fed from either side of the manifold. The flow goes in both directions along the shield conductor, proceeds all the way around the torus and exits through the return manifold. The dotted line in Figure VI-10 shows the portion of conductor removed to indicate the direction of flow. It will be noticed that this configuration will always put a cold supply stream next to a warm return stream, such that there will

not be excessively warm or cold regions. The temperature gradients will be small and uniform.

The problem of making connections which necessarily must be electrically insulated is not easy, particularly underneath the magnet. It may be necessary to plan on having a pit underneath the manifolds to make that region accessible by workmen. The connections have been spread apart so that the work will not be excessively crowded. Figure VI-10 illustrates the method rather well. The dark splice in the center of the tubes is the insulated region. One way to make such an insulated section is to start out with a thin walled SS tube, build a G-10 or some other glass epoxy tube around that, then epoxy two aluminum sleeves which are not in mutual electrical contact. The thin wall SS provides the diffusion barrier for the Helium gas and in order to leak, the gas has to diffuse through a lengthy section of a thin glass epoxy tube. Such insulated tubes have been used successfully in the past.

Where the connection is made to the conductor, the insulation will have to be filed away, a hole drilled through to the conductor hole, and then the connector tube welded to it and the joint leak checked. A similar connection is made at the manifold.

Figure VI-2 shows the penetration through the vacuum vessel for supplying and returning the Helium gas. Although it is shown to be located on the side for clarity, it will actually be on the top. This would obviate the necessity of making weld connections on the side through the vacuum chamber. Since the vacuum chamber sections will be dropped from the top, all the connections will be made beforehand.

It will now be necessary to heat the shield in order to cure the glass insulation and allow the whole shield to become a solid fused structure. This can be done by simply energizing the shield at room temperature without cooling.

The last step in building the toroid is to super-insulate it and to surround it with the vacuum vessel. It has been mentioned earlier that the floor of the vacuum vessel is already in place. It will now be necessary to build a reinforcing structure with curved beams to withstand the atmospheric loading. In the flat regions of the vacuum chamber cross braces can be employed for reinforcement. These could be tied to the floor braces as shown in Fig. VI-1. Finally, the vacuum shell which will be 1/8 in. (3.2 mm) SS can be lowered onto the reinforcing structure in sections and welded together. Once the connections for the vent lines, electrical leads, and other feedthroughs are made, the whole chamber will be leak checked.

The energy storage magnet can now start undergoing the testing which will be needed before it can become part of the electrical circuit of the accelerator.

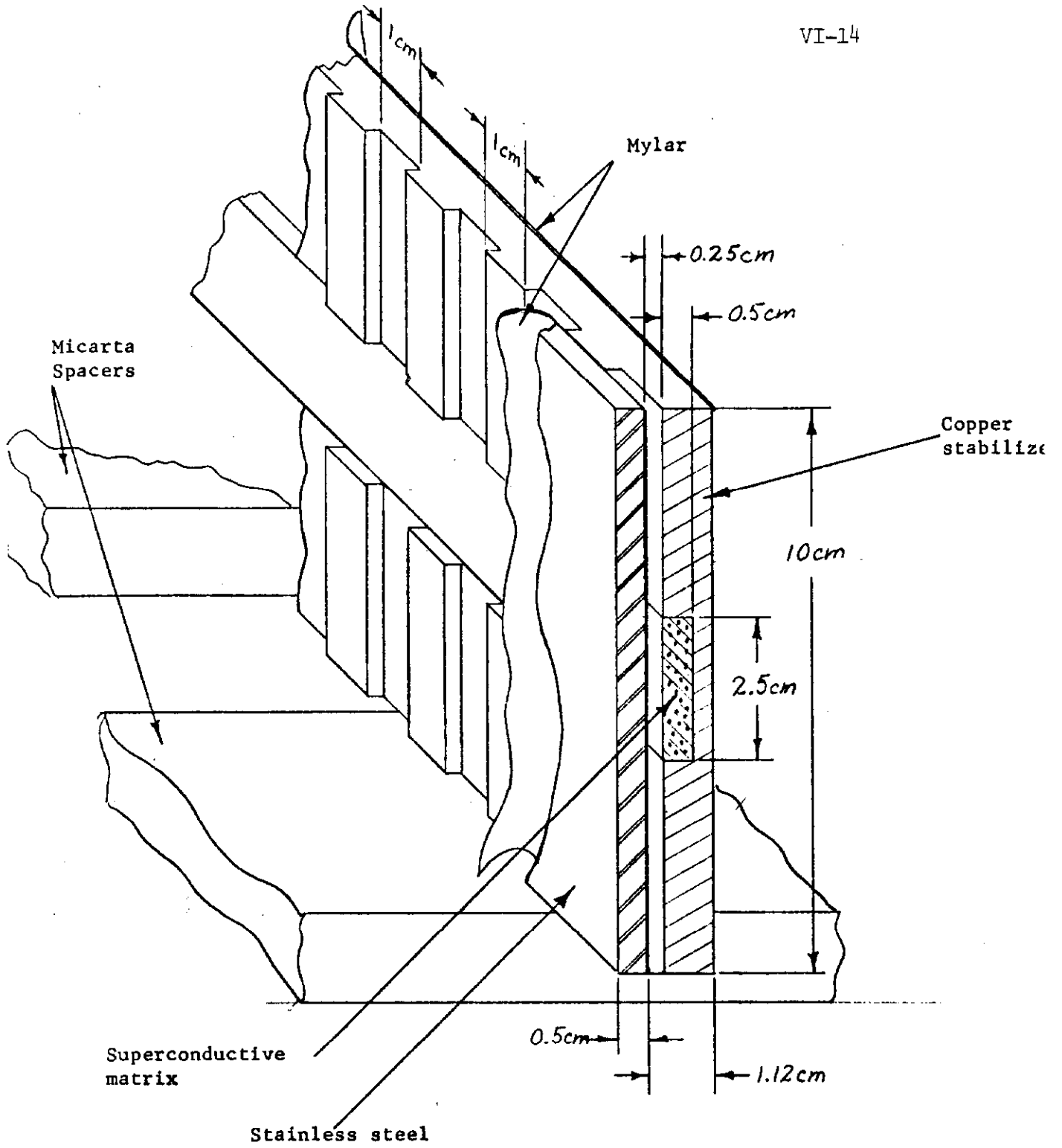
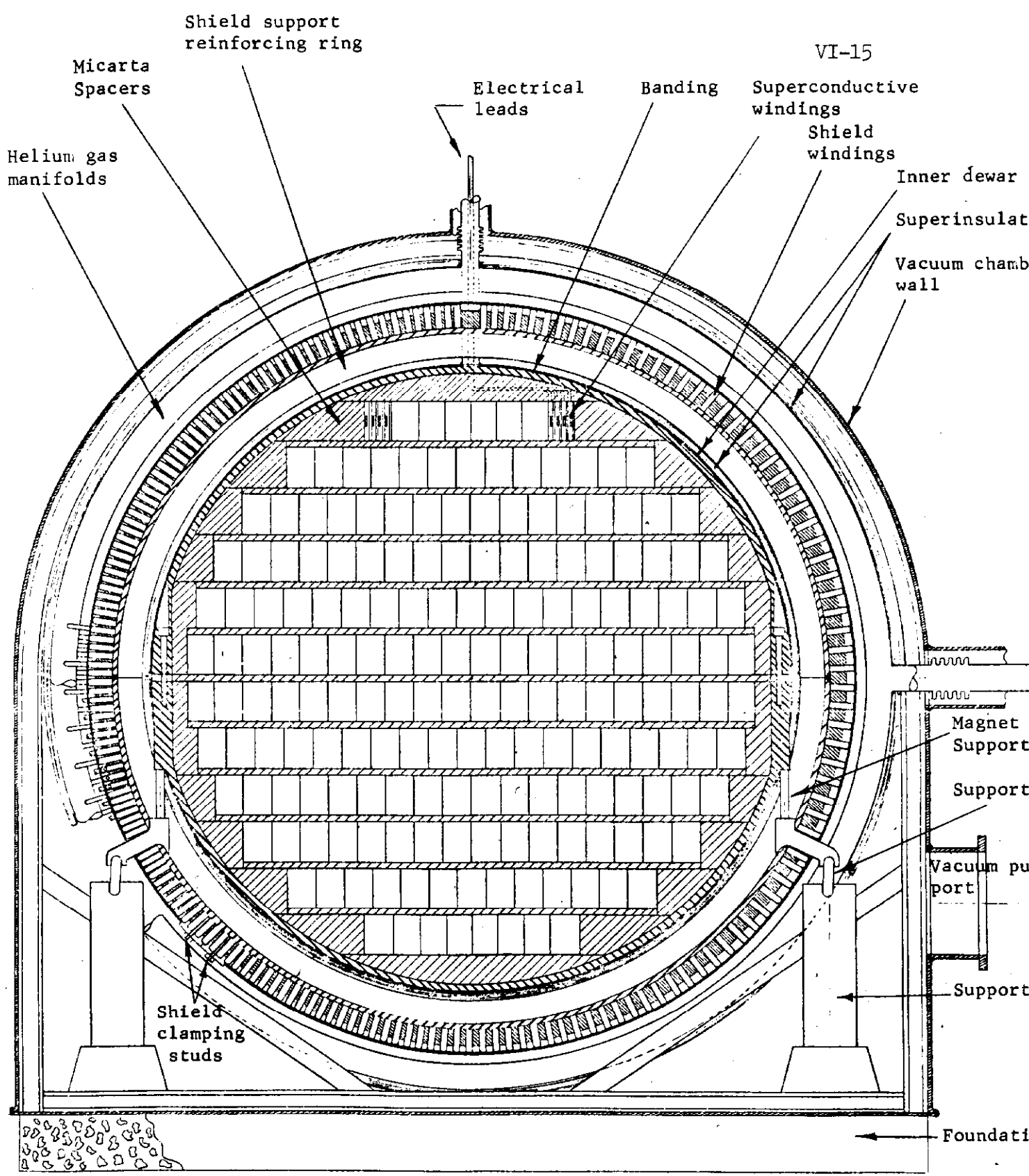


Fig. VI.- 1 CONDUCTOR DETAILS

VI-15



Scale  
 0 10 20 30 40 50 cm.

Fig. VI - 2 OVERALL CROSS-SECTION. N.A.L.-U.W. PULSED ENERGY STORAGE

Direction of rotation

Winding form

Guide post

Winding stations

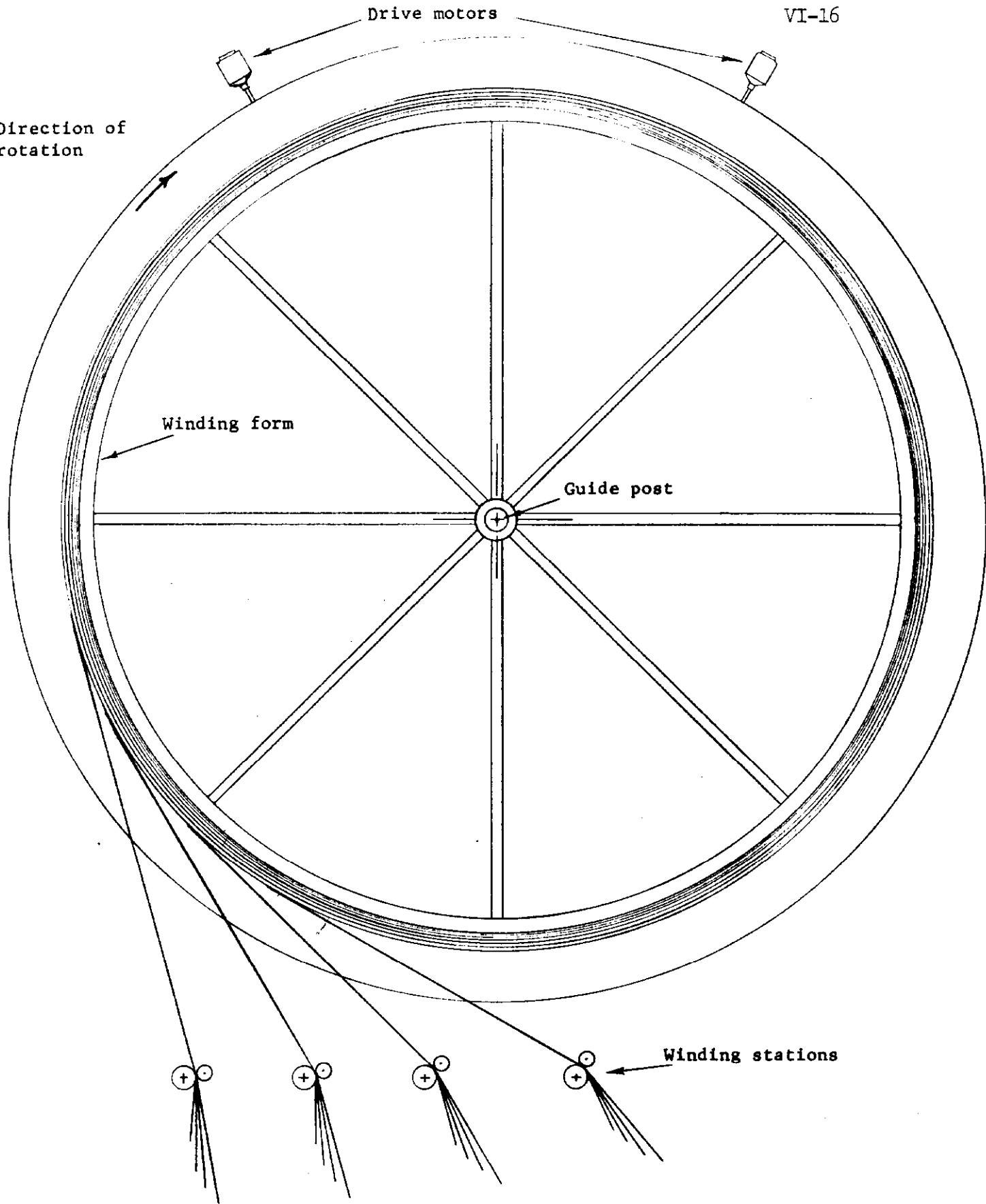
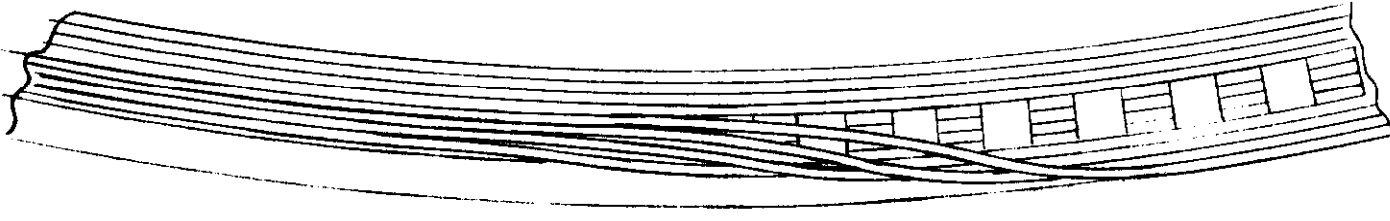
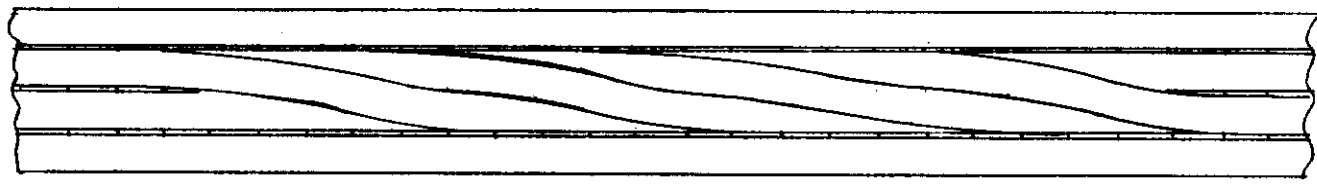


Fig. VI - 3 POSSIBLE WINDING SCHEME- TOP VIEW



(a) Top view



(b) Side view

Fig. VI - 4 CROSS-OVER ELECTRICAL CONNECTION  
BETWEEN LAYERS



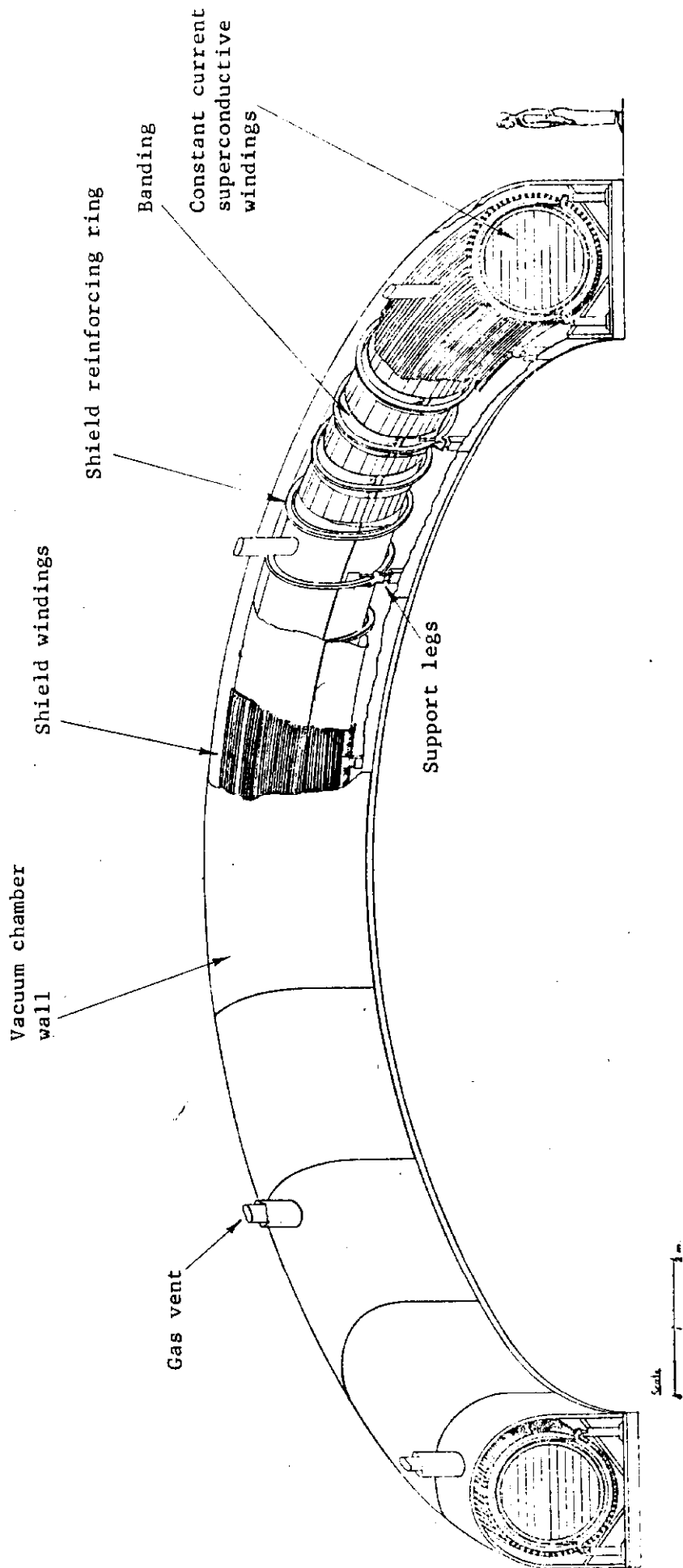
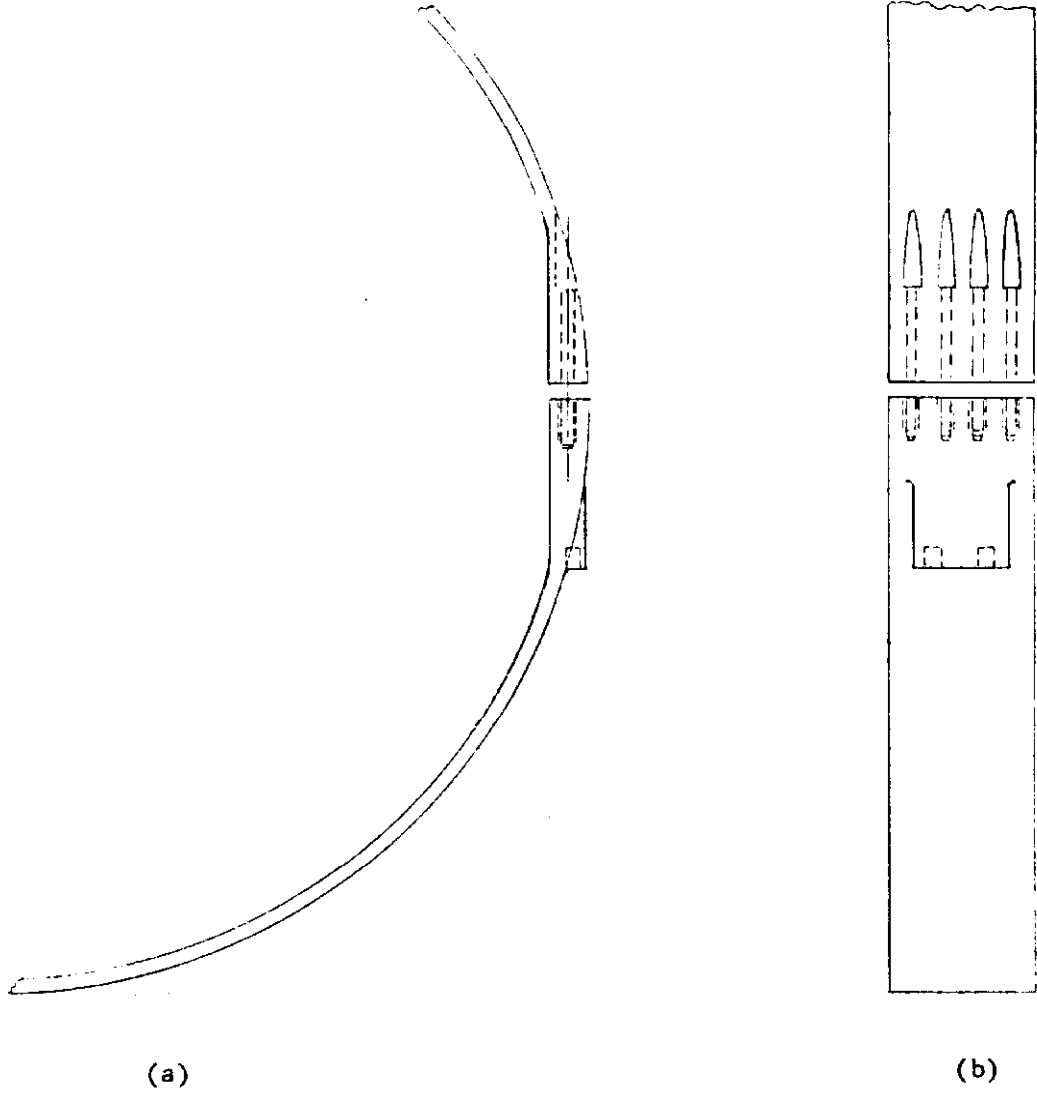
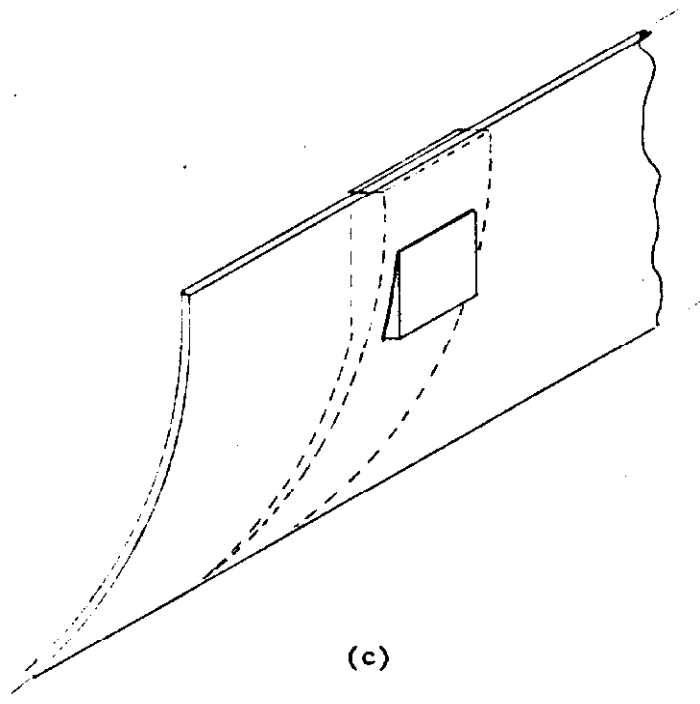


Fig. VI --6 ISOMETRIC VIEW OF N.A.L.-U.W. PULSED ENERGY STORAGE



(a)

(b)



(c)

Fig. VI-7 BANDING DETAIL

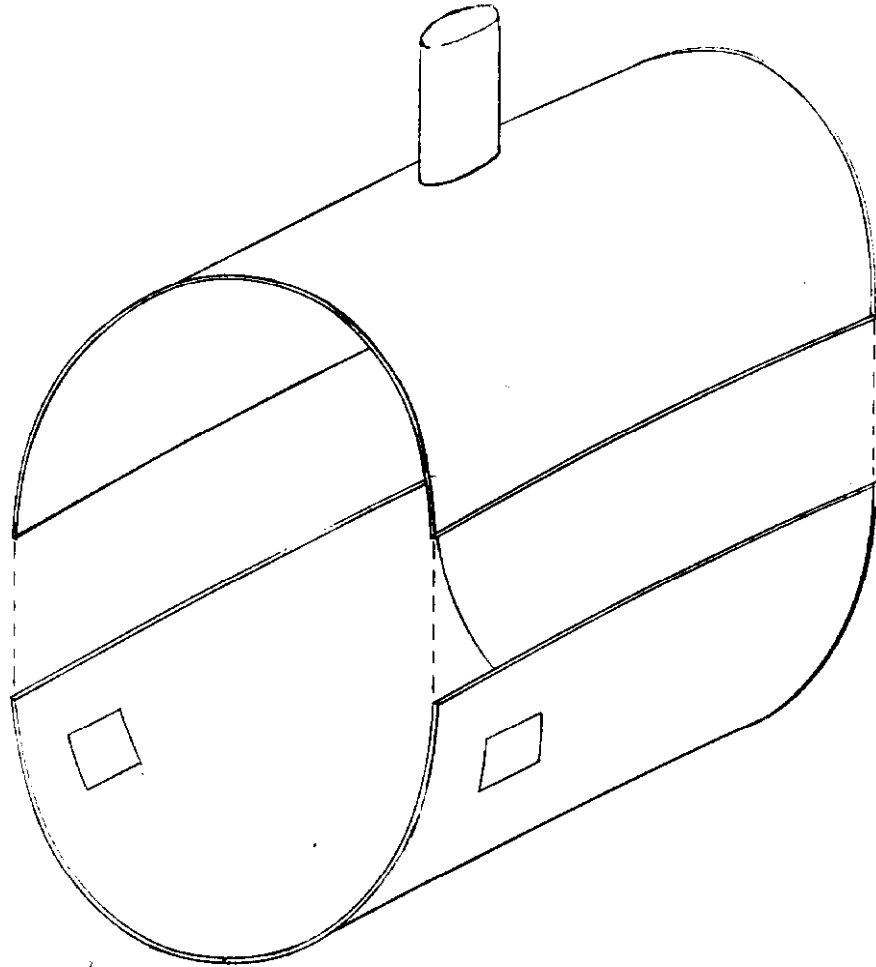
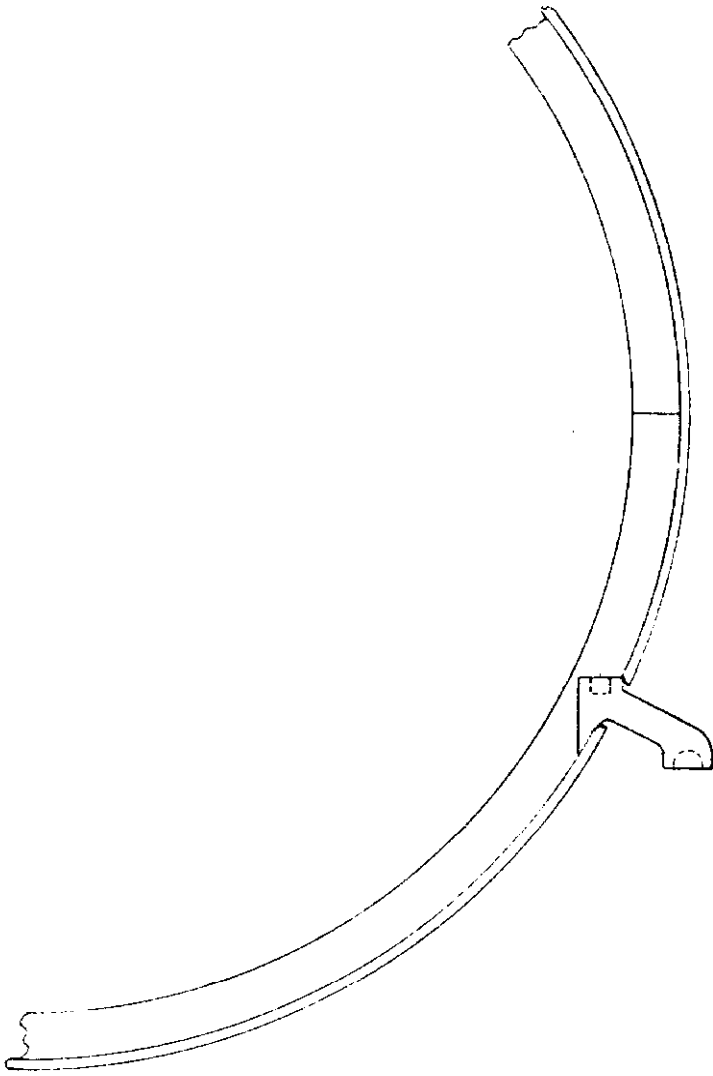
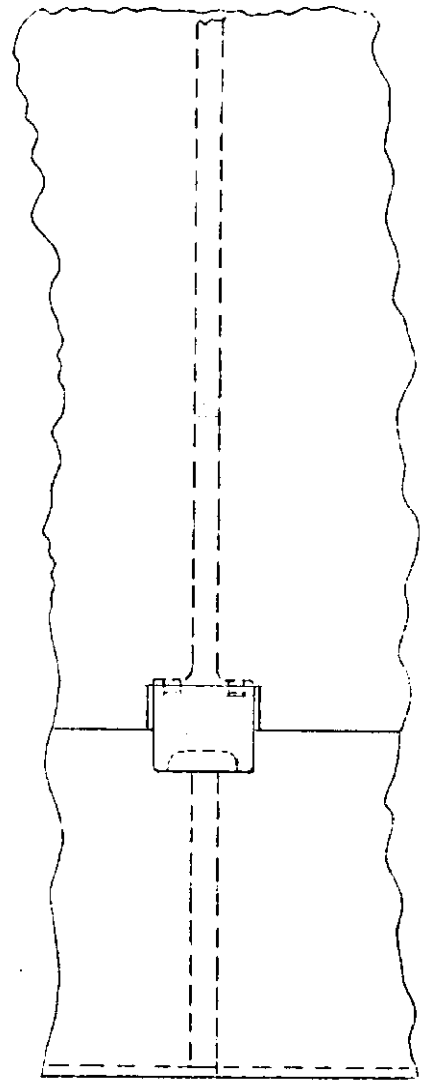


Fig. VI-8 INNER DEWAR SECTION



(a)



(b)

Fig. VI -9 SHIELD SUPPORT REINFORCING RING

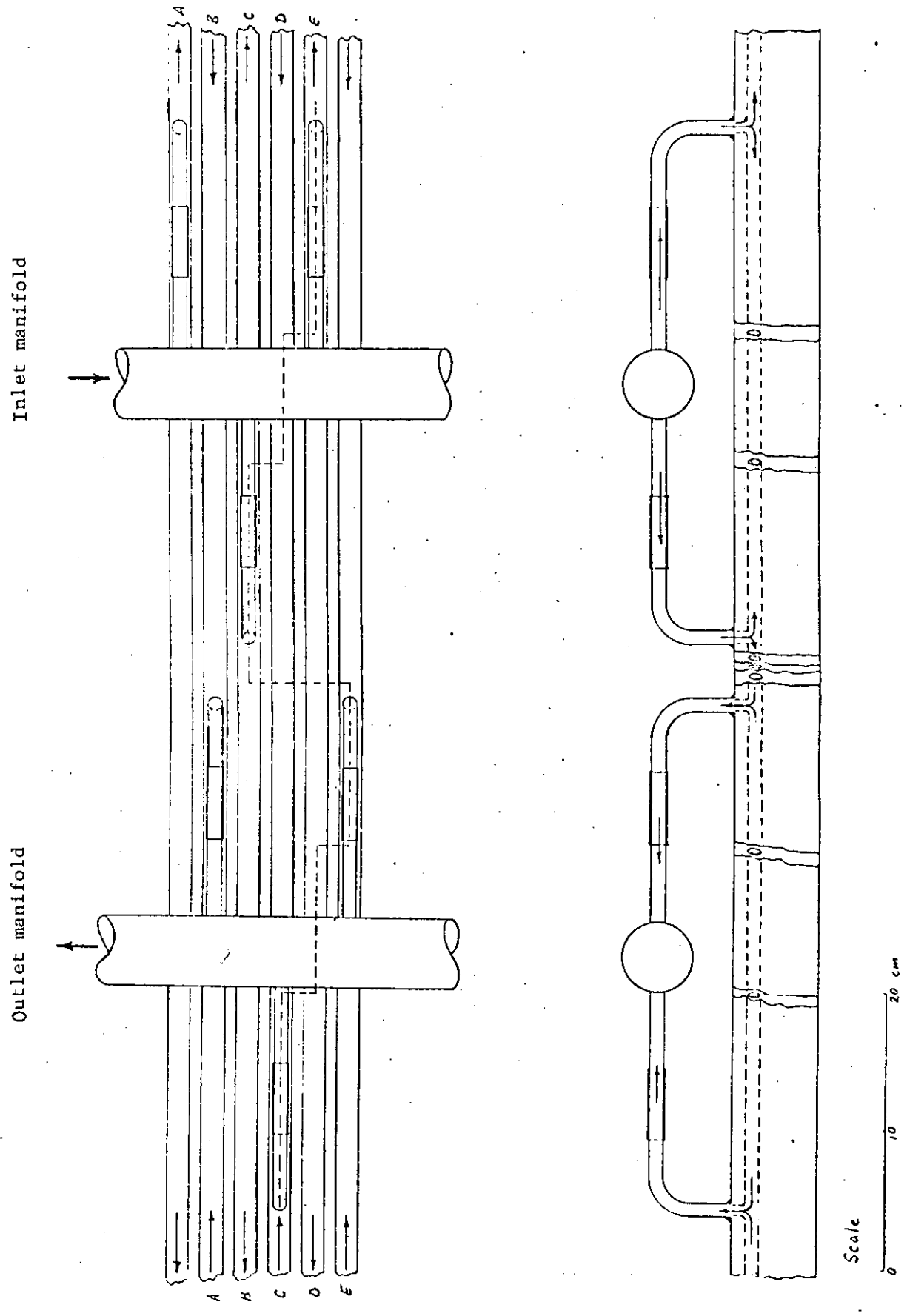


Fig. VI - 10 40° K HELIUM GAS ROUTING SCHEME

APPENDIX VI-A  
POWER SYSTEM SPECIFICATION

The rate of energy transfer to and from the pulsed energy storage inductor will be controlled by a power conversion system. This system will use the technology of the thyristor to control the rate and direction of the power flow between the PES inductor and the AC utility system. This technology is well understood and has been used in many applications. The power supply for the Main Accelerator at FERMILAB is an excellent example of this application. Other examples are the direct current power transmission systems such as the 1440 MW NW-SW Tieline between Oregon and California and the Eel River thyristorized asynchronous tieline.

By setting the phase angle of the voltage in the utility system at which they thyristors are gated on, both the magnitude and direction of the power flow between the inductor and the AC utility system may be controlled.

The direct current side of the power converters will be interconnected in a four-by-four grid network of  $\pm 12.5$  MW, (peak) power supplies with a total peak direct current terminal capacity of  $\pm 200$  MW. The positive polarity represents the converter operating as a rectifier with power flowing towards the AC system while the negative polarity represents power flowing to the AC system and the converter operating in its inverting mode. The connection is shown in Figure VI-A-1. The direct current terminal rating of each converter group will be  $\pm 625, 0$  Volts at 20,000 Amperes. The total connected capacity will be  $+ 2,500, 0$  Volts at 80,000 Amperes. The basic converter circuit which will be used in the power supply will be the three-phase, full-wave bridge with a rated current neutral bypass. This circuit gives six-pulse operation in both the rectify and invert mode of operation. The calculated efficiency for both the rectify and invert modes is greater than 95%.

The power converters are connected to the alternating current distribution system through three-phase transformers. These transformers will have a peak rating of 14.6 MVA and an RMS rating of 7 MVA. As done in the main-ring power supply, the transformers will have a wye connected secondary with an extended delta primary to provide for the proper phasing of the converter groups for 12-pulse operation in the AC system. As indicated in Figure VI-A-1, alternate converters are connected to the AC utility system through a transformer with either a 15-degree angle of advance or retard. The power supplies will be operated at either full rectify or nearly full invert one row at a time until all four rows are energized. With pairs of six-pulse converter groups displaced 30 degrees from each other, the AC utility system will always see twelve-pulse operation. This is desirable to reduce the amplitude of the harmonic currents which would otherwise be in the system. The reactive power in the AC utility system from the system can be reduced by operating the power converter in either full rectify or full invert, or in bypass. Only one set of power supplies at a time will be operated in the intermediate, continuous phase angle mode.

An additional set of thyristors are connected to the direct current terminals of the power supply to provide a bypass for the load current. The reasons for the bypass are twofold:

- 1) Safety. A circuit for the load current is needed in the event of a failure of the AC utility power or a failure in the converter circuit.
- 2) Reduced Power. Operation at reduced power is best achieved by turning on only those power supplies that are needed. All others will be placed in bypass where the terminal voltage will be nearly zero and the inductor will be disconnected from the AC utility system.

### Converter Group

The basic converter group arrangement will be a three-phase, full wave bridge connection (six-pulse operation) with a controlled, neutral connected bypass. The bypass will be rated for full load current. Thyristors will be used in all positions of the converter and bypass, thus offering complete control of the power supply through manipulations of the thyristor gate synchronizing signals in the low-level control circuits.

The 12.5 MW power supply will be built up from 12 parallel connected modules as shown in Figure VI-A-2. Each module contains four sets of series connected thyristors all connected in parallel to the common direct current bus. Three of the series connected sets are used in the bridge circuit while the fourth set is used in the neutral connected bypass. Full current rating of the bypass is achieved by adding four additional modules to the main power bus.

Each module will be connected to the transformer by electrical bus. The impedance provided by this bus can adequately balance the currents in the converter thyristors of the various modules. Current sharing in the bypass thyristors, while more difficult to achieve than in the converter thyristors positions, can be achieved by careful arrangement of the direct current bus and, if necessary, selection of the bypass thyristors according to their conductance. The module also contains amplifiers for the gate drive synchronizing signals.

These modules will be mechanically and electrically identical (except for the use of a higher rated voltage thyristor) to those modules presently used in the main-ring power supply. Much of the low-level control equipment now used in the main-ring power supply can be used directly in the power supply system, thereby reducing the design and construction effort.

The thyristors which would be used are the 50 mm diameter devices which are available in appropriate voltage and current ratings from several domestic manufacturers.

Each converter group will also be equipped with a set of mechanical bypass and disconnect switches to permit routine servicing of the equipment without the necessity of shutting down the entire system.

### Shield Power

A power supply of modest proportions will be included in the shield winding so that the current in the shield current may independently be adjusted to completely cancel out any variations in the current in the superconducting winding that may be introduced during the operating cycle. The maximum current in the shield is expected to be less than 2,500 Amperes at a peak power level of less than 15 kW.

### Operation

The operating parameters of the 12.5 MW power supply and the power system are summarized in Tables VI-A-1 and VI-A-2. These parameters are based on using a 50 mm thyristor in the module with an average current rating of 1,000 Amperes. It is known that higher current devices that are mechanically compatible with the module are being developed. The final choice of devices would be based on cost and availability at the time of construction. Overall economic considerations favor the larger devices.

TABLE VI-A-1  
12.5 MW POWER SUPPLY OPERATING PARAMETERS

Load Current, Amperes	20,000
Rectify Mode (Charge)	
Real Power Input, MW	13.28
Reactive Power, MVAR	6.05
Terminal Voltage	664
Power to Inductor, MW	13.16
Invert Mode (Discharge)	
Real Power Input, MW	12.5
Terminal Voltage	625
Real Power Output, MW	12.36
Reactive Power, MVAR	7.8
AC Line-Line Voltage,	
kV	13.8
Transformer Primary Line Current,	
Amperes (Peak)	611
Amperes (RMS)	305
Transformer Secondary Line - Neutral	
Voltage, Volts	312.3
Transformer Secondary Line Current	
Amperes (Peak)	16,300
Transformer Rating	
Peak MVA	14.6
RMS MVA	7.0
Open Circuit Voltage, Volts	730.5
Number of Modules per Power Supply	12
Power Loss, MW	0.14
Number of Thyristors per Module	8
Number of Thyristors per Power Supply	
Bypass	48
Converter	48

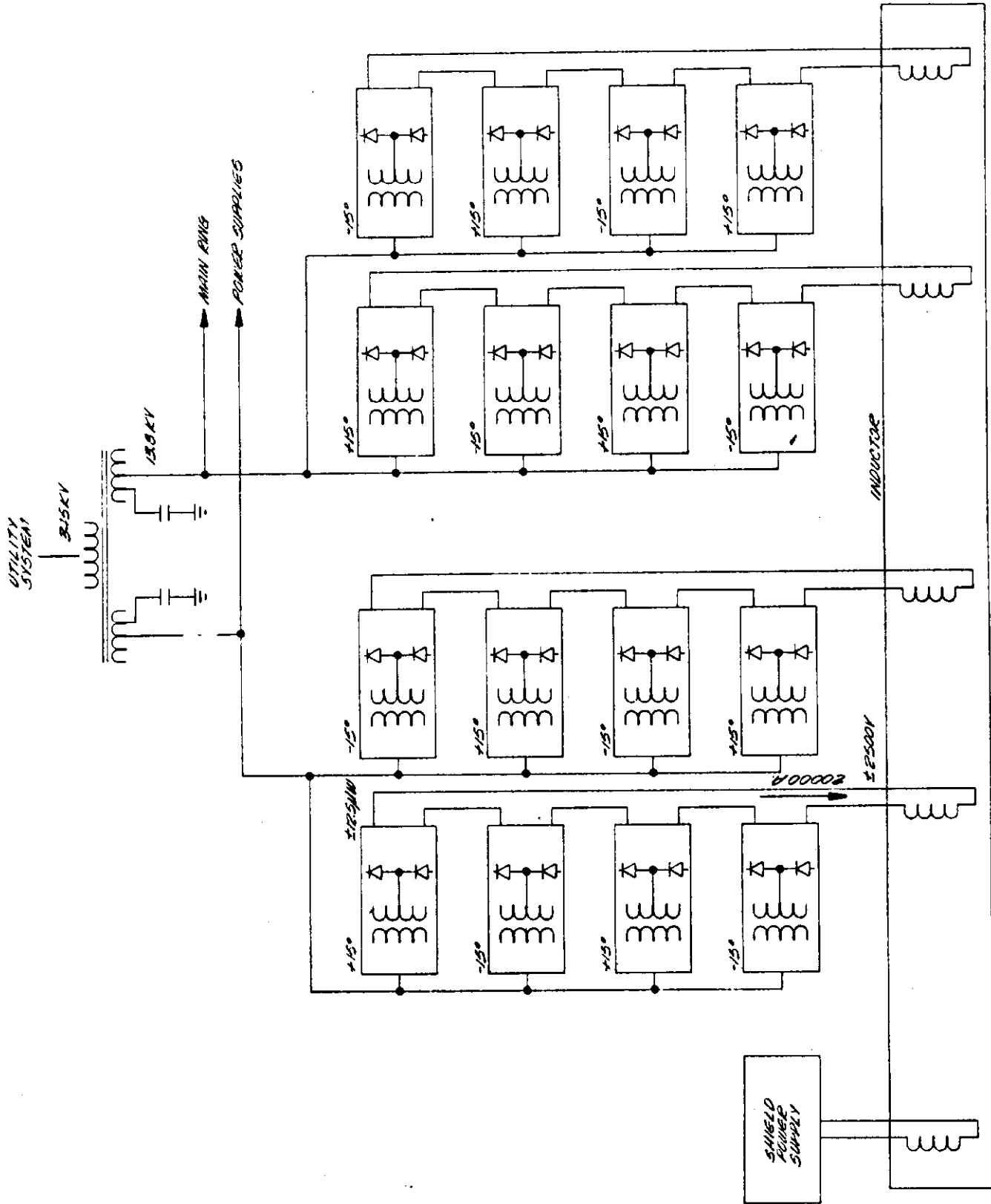
TABLE VI-A-1  
12.5 MW POWER SUPPLY OPERATING PARAMETERS

## Thyristor Operation

	<u>Bypass</u>	<u>Converter</u>
Peak Current, Amperes	833	2,500
Average Current, Amperes	833	833
RMS Current, Amperes	833	1,440
Peak Inverse Voltage, Volts	442	765
Power Loss, Watts	920	1,160

TABLE VI-A-2  
PES SYSTEM OPERATING PARAMETERS

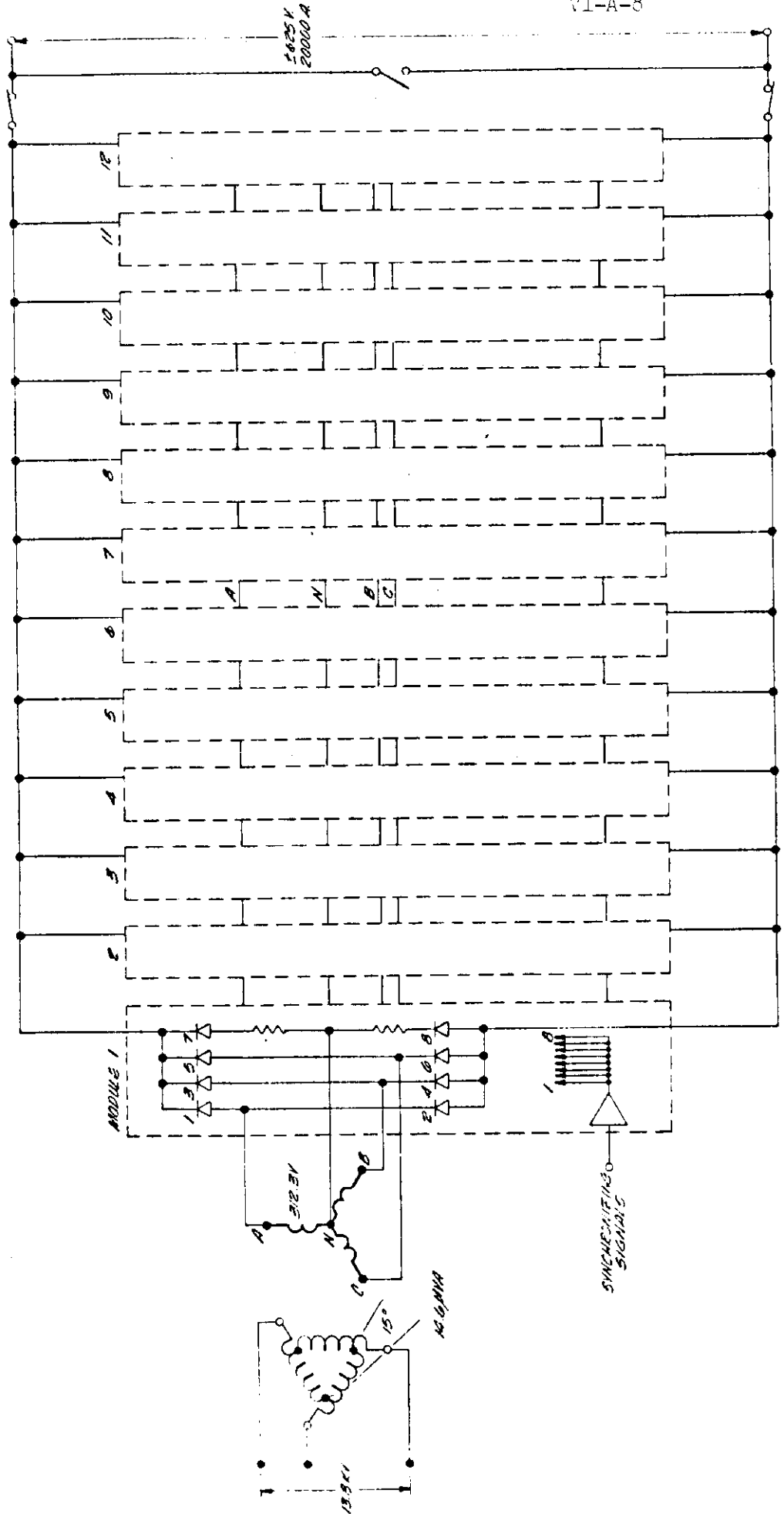
Inductor Terminal Voltage, Volts	
Charge	2632
Discharge	2500
Inductor Current, Amperes	80000
Total Input Power (Charge), MW	212
Total Output Power (Discharge), MW	198
Number of Power Supplies	
Number of Converter Modules	192
Number of Thyristors	1576



PULSED ENERGY STORAGE SYSTEM  
ELECTRICAL NETWORK

Figure VI-A-1

VI-A-8



12-5W CONVERTER

## VII. - CONCLUSIONS

This report describes a system which can be built using present technology at the state of the art. It does not require extensive research and development prior to its implementation. The system is based upon cryogenically stable superconductors and solid state power converters; both of these are employed at NAL, in the 15 foot Bubble chamber and in the main accelerator power supply, respectively. The use of the flux-forcing shield, which has been used for accelerator and plasma devices, allows the accommodation to the short time pulse application. No exotic materials are required for the shield.

Some further overall optimization of the design might lead to a slightly different structure, but we do not expect any major changes to develop. These changes will primarily reflect cost reductions. Major changes in outlook would require major changes in technology, such as improved conductors or refrigeration.

The system described will meet NAL's needs for energy storage in operation of the present system at its highest energy potential. Both the real and reactive power variations for energies up to 500 Gev can be controlled to a level below that anticipated for direct line operation at 200 Gev. The system is surprisingly efficient--approximately 95% of the energy stored per pulse can be returned.

The implementation of this device will play an important role in the development of superconductivity applied to practical use. This is true on a broad scale, but in particular it could be the forerunner of pulsed power systems needed for fusion reactors, and large energy storage inductors used for electrical generating and distribution systems. Specific areas where advances will be made include:

1. Superconducting Magnet Development

The conductor to be employed, although based upon earlier

designs, is a large step toward the high current conductors needed in the future. The system must be designed to operate reliably for a large number of pulses, reflecting the experience of many years of operation of a diurnally varying inductor. Fatigue studies of materials will be useful for future systems.

## 2. Cryogenics and Refrigerator Development

The system will yield experience in several areas including helium pumping, helium leaks and high current leads. It will be possible to make a test of 1.8 K operation, an important step for future systems.

## 3. Operational tests

Since the project is addressed to a real need, it will have to solve all the problems associated with the operation of a large cryogenic system in a power network. Extensive experience about reliability of components and systems will be gained.

In addition, tests for future systems can be made, including tests of dynamic power system stabilization in the local power network. We will be able to operate the device in a wide range of operating conditions and, for example, measure and verify the various A.C. loss mechanisms in the superconductor composite.

## 4. Converter Development

Building upon the experience already gained with the main accelerator power supply, we will test the operation of a large phase controlled converter system. Unique features which will be tested include the higher current (80,000 A), the unusual duty cycle and the control of both real and reactive power.

In addition to direct developmental gains, benefits will be achieved in some unexplored areas. An example is the study of environmental effects of external magnetic fields, on

electrical, mechanical and biological systems. It is not beyond possibility that the device could serve as a bending field for use in some high energy physics experiments.

By 1990, some 10-15% of installed generating capacity in the electric power industry could profitably be in the form of efficient energy storage such as pumped storage hydro, batteries, or superconducting inductors. At the present time this is a \$10 billion market expanding to \$20 billion by 1990. It would seem that 10% of this might be spent on research and development.

We propose that the first step in the superconductive energy storage program be the NAL 1MWh Inductor. This is an excellent step from present experience (0.2 MWh, not pulsed) to the 10,000 MWh sizes needed for electrical power systems. If constructed in a timely manner, it will accelerate and provide invaluable experience and data for large developmental systems to be designed and built elsewhere. Viewed in this light, and the light of projected use of superconducting devices, its cost, which is estimated to be less than \$20 million, seems to be a small but important part of the budget necessary for the implementation of energy storage systems.